A FORCE-SENSING DEVICE FOR ASSISTANCE IN SOFT-TISSUE BALANCING DURING KNEE ARTHROPLASTY

THÈSE N^O 3398 (2005)

PRÉSENTÉE À LA FACULTÉ SCIENCES ET TECHNIQUES DE L'INGÉNIEUR

Institut de production et robotique

SECTION DE MICROTECHNIQUE

ÉCOLE POLYTECHNIQUE FÉDÉRALE DE LAUSANNE

POUR L'OBTENTION DU GRADE DE DOCTEUR ÈS SCIENCES

PAR

Denis CROTTET

ingénieur physicien diplômé EPF
de nationalité suisse et originaire de Portalban (FR)

acceptée sur proposition du jury:

Prof. H. Bleuler, directeur de thèse
Dr L. Dürselen, rapporteur
Prof. L. Nolte, rapporteur
Prof. P. Ryser, rapporteur

Lausanne, EPFL
2005

"If you cannot measure it, you cannot improve it."
Lord William Thomson Kelvin (1824-1907)

Acknowledgements

IV

Contents

Abstract

Nowadays, the large majority of the instrumentation for orthopaedic surgery consists of mechanical tools with varying degrees of complexity. To increase the accuracy and the safety of orthopaedic interventions, sensors and computers were recently introduced in the operating room. Computer Assisted Orthopaedic Surgery (CAOS) uses a navigation system that tracks the movements of surgical instruments in real-time and displays their exact location in relation to the operative area. Such technology improved the quality of orthopaedic arthroplasties, but it is still limited to the measurement of kinematic parameters such as axial alignments, position and angle measurements. In Total Knee Arthroplasty (TKA), the ligament balance, which is crucial for the stability and lifetime of implants, is currently only qualitatively assessed. The goal of this thesis was therefore to demonstrate the importance of intra-operative measurement of musculoskeletal forces through the development of a force-sensing device designed to improve the ligament balancing procedure during TKA.

Three possible device designs were proposed and evaluated using finite element analysis in an iterative optimization process. The final design consists of two sensitive plates, one for each condyle, a tibial base plate and a set of spacers to adapt the device thickness to the patient-specific tibiofemoral gaps. Each sensitive plate is equipped with three deformable bridges instrumented with thick-film piezoresistive sensors, which allow accurate measurements of the amplitude and location of the tibiofemoral contact forces. The net varus-valgus moment is then computed to characterize the ligament imbalance.

Laboratory experiments showed that the device has appropriate accuracy and dynamic range for the intended application. The first experimental trials on a plastic knee joint model and on a cadaver specimen demonstrated the proper *in-situ* functioning of the device. The performance and surgical advantages of the device were then evaluated in an *in-vitro* study including four different experiments: 1) Six knee joints were axially loaded. Com-

1

paring applied and measured compressive forces demonstrated the accuracy and reliability of *in-situ* measurements. 2) To estimate the importance of keeping the patella in its anatomical place during imbalance assessment, the effect of patellar eversion on the mediolateral distribution of tibiofemoral contact forces was measured. One fourth of the patellar load was shifted to the lateral compartment. 3) Assessment of knee stability based on condyle contact forces or varus-valgus moments were compared to the current surgical method (difference of varus-valgus loads causing condyle lift-off). The force-based assessment found to be equivalent to the surgical method while the moment-based technique, which is considered optimal, showed a tendency of lateral imbalance. 4) Finally the effect of minor and major medial collateral ligament releases was biomechanically quantified. Large variation among specimens reflected the difficulty of ligament release and the need for intraoperative force monitoring.

Two clinical trials were carried out to evaluate the device performance in a surgical environment. After the tibial cut, the medial and lateral tibiofemoral gaps ensuring the knee stability were determined from the device measurements and compared to the femoral cuts performed on the basis of standard instrumentation. The agreement between the two approaches was generally good. The only significant difference was measured on the first patient at 90° flexion. At this point, the surgeon also estimated that the knee was not optimally balanced, thus demonstrating the consistency between his perception and the device measurements.

In conclusion, the proposed force-sensing device for assistance in ligament balancing during TKA provides accurate, reliable and useful measurements. In addition to the precise imbalance assessment based on the measurement of forces and moments, important clinical advantages, such as the possibility to keep the patella in its anatomical place during the measurement or the real-time force monitoring during the delicate phase of ligament release, were demonstrated. The encouraging results of the *in-vivo* trial proved the usability of the device in a surgical environment and opens the way for larger clinical studies. The developed device has thus potential to improve the ligament balancing procedure, the consistency of surgery and the lifetime of TKA, illustrating thereby the clinical benefit of measuring forces during orthopaedic surgeries.

Version abrégée

De nos jours, la majeure partie de l'instrumentation pour la chirurgie orthopédique est constituée d'outils mécaniques plus ou moins complexes. Afin d'améliorer la précision et la sécurité de ces interventions, senseurs et ordinateurs ont récemment fait leur apparition en salle d'opération. La chirurgie orthopédique assistée par ordinateur utilise un système de navigation qui suit en temps réel les mouvements des instruments chirurgicaux et affiche leur position exacte par rapport à la zone opérée. Une telle technologie a amélioré la qualité des interventions mais reste malheureusement limitée à la mesure de paramètres cinématiques tels que axes, angles ou positions. Lors d'Arthroplastie Totale du Genou (ATG), l'équilibre ligamentaire, qui est crucial pour la stabilité et la durée de vie des implants, est actuellement évalué uniquement qualitativement à l'aide de manipulations ou d'outils basiques. Le but de cette thèse était donc de montrer l'importance de la mesure intraopératoire des forces musculosquelettiques au travers du développement d'un capteur de force conçu pour améliorer la procédure d'équilibrage ligamentaire lors d'ATG.

Trois designs possibles ont été proposés et évalués en utilisant la méthode des éléments finis au cours d'un processus itératif d'optimisation. Le design final comprend deux plaques sensibles, une pour chaque condyle, une plaque de base tibiale et un set d'écarteurs pour adapter l'épaisseur du capteur à l'espace tibiofémoral du patient. Chaque plaque sensible comprend trois ponts déformables équippés de senseurs piézorésistifs qui permettent de mesurer précisément l'amplitude et la position des forces de contact des condyles fémoraux. Le moment résultant dans les directions varus et valgus est ensuite calculé pour caractériser l'équilibre ligamentaire.

Les expériences en laboratoire ont montré que le capteur a une précision et une plage de mesure appropriées pour l'application envisagée. Les premiers essais sur un modèle en plastique et sur un spécimen cadavérique ont démontré le bon fonctionnement du capteur *in-situ*. Les performances et les

avantages chirurgicaux du capteur ont ensuite été évalués au travers d'une étude *in-vitro* comprenant quatre expériences différentes: 1) Six genoux ont été chargés axialement. La comparaison entre les forces de compression appliquées et mesurées a démontré la précision et la fiabilité des mesures *in-situ*. 2) Afin d'estimer l'importance de garder la rotule à sa place anatomique durant l'évaluation du déséquilibre, l'effet d'une éversion rotulienne sur la distribution mediolatérale des forces de contact a été mesuré : un quart de la force rotulienne est déplacé sur le compartiment latéral. 3) L'évaluation de la stabilité du genou basée sur les forces de contact des condyles ou sur leur moment a été comparée à la méthode chirurgicale actuelle (différence de poids varus ou valgus créant un décollement d'un condyle). L'évaluation basée sur les forces fut équivalente à l'approche chirurgicale alors que celle basée sur les moments, considérée comme optimale, a montré une tendance à un déséquilibre latéral. 4) Finalement, l'effet de relâches ligamentaires mineures ou majeures du ligament collatéral médial a été quantifié biomécaniquement. L'importante variation parmi les spécimens a révélé la difficulté de la relâche ligamentaire et le besoin d'un monitoring intraopératoire des forces.

Deux essais cliniques ont été effectués pour évaluer le fonctionnement du capteur dans un environnement chirurgical. Après la coupe tibiale, les espaces tibiofémoraux médial et latéral assurant la stabilité du genou ont été déterminés selon les mesures du capteur et comparés aux coupes fémorales effectuées sur la base de l'instrumentation habituelle. L'accord entre les deux approches était généralement bon. La seule différence significative a été mesurée sur le premier patient à 90° de flexion. A ce moment, le chirurgien estimait également que le genou n'était pas équilibré de façon optimale, démontrant ainsi la cohérence entre sa perception et les mesures du capteur.

En conclusion, le capteur de force proposé pour l'assistance durant l'équilibrage ligamentaire lors d'ATG fournit des mesures précises, fiables et utiles. En plus d'une évaluation quantitative du déséquilibre basée sur la mesure de forces et de moments, des avantages cliniques importants ont été démontrés, comme par exemple la possibilité de garder la rotule à sa place anatomique ou le monitoring des forces de contact lors de la relâche ligamentaire. Les résultats encourageant de l'essai clinique ont prouvé que le capteur fonctionne parfaitement dans un environnement chirurgical, ouvrant ainsi la voie à de plus larges études cliniques. Le capteur développé a donc montré un potentiel pour améliorer la procédure d'équilibrage ligamentaire, la consistance de la chirurgie et la durée de vie d'une ATG, illustrant ainsi le bénéfice de mesures de forces lors d'opérations orthopédiques.

Chapter 1

Introduction

Orthopaedic surgery, which is the branch of surgery concerned with injuries and disorders of the musculoskeletal system, is an ancient discipline. Archeological traces, such as a prosthesis for a big toe after a healed amputation found on a mummy (circa 1065-650 BC) [1] or the guidelines and reports of surgical cases in the Edwin Smith papyrus (circa 1700 BC) [2], were discovered in Egypt. Other ancient civilizations, such as Greeks or Romans, reported orthopaedic knowledge as well. Various volumes of the important Greek text *Corpus Hippocrates* (circa 430-330 BC) from the name of the famous father of medicine had relevance to orthopaedics. For example, an entire volume is dedicated to joints, where dislocation of the shoulder, knee, hip and elbow joint was described together with the various methods used for reduction. It was nevertheless not before the l2th century that Europe began to awake gradually from its dark ages. Universities and hospitals were being established, human dissection resumed and the great Greek texts were being translated. However, until the l6th century, all developments remained within the shadow cast by Hippocrates. Some of the new techniques introduced at that time were the use of a tourniquet and the ligature for large vessels for amputations or the development of artificial limbs using iron or wood. Modern orthopaedics started only in the early 1900's with the discovery of the X-ray and with the fact that orthopaedics became a specialty in its own. From that point in time the tools for diagnosis, surgical techniques and instrumentation had been continuously improved to the end of obtaining predictable and satisfying outcome of orthopaedic interventions.

Nowadays, the large majority of the instrumentation for orthopaedic surgery consists in more or less complex mechanical tools. Chisels, saws, drillers required to correct or repair bony structure are used in combination with mechanical ancillaries, providing the surgeon with geometrical parameters

such as bone axes, morphologic angulations or distances between bones. To increase the accuracy and the safety of orthopaedic interventions, sensors and computers were recently introduced in the operating room. Computer Assisted Orthopaedic Surgery (CAOS) uses a navigation system that tracks in real-time the movements of the surgical instruments and displays their exact location in relation to the operative area [3]. Such technology enables more precise placement of implants and safer delicate surgical actions, such as the insertion of a pedicle screw in a vertebral body. With the arrival of CAOS systems, surgical instrumentation reached an important turning point and is now experiencing the same natural evolution as the automotive industry during these past decades. Sensors, calculators, automatic control or management are common features in cars nowadays. An Audi A8 for instance contains 45 calculators in its standard version and more than 75 with full options. Even though refractories claimed that this proliferation of electronic components in cars would just increase the risk of break-downs, a large number of new technologies such as airbags, Anti-lock Brake System (ABS), automatic gear change or power-assisted steering have significantly improved the safety and comfort of the end users. According to the first short-term clinical studies, the same benefits can be hoped in the CAOS systems.

However, current navigation systems, although competitive, are mainly limited to the control of geometrical parameters. Stresses in soft-tissue or forces applied by the surgeon are important biomechanical parameters which usually remain unknown. Measurement of forces with smart instrumentation can therefore improve the quality of orthopaedic surgery in three different ways:

1. *Detection of possible damage of healthy tissues.* When the surgeon has no direct access to the operation site, as during minimally invasive surgery, manual guidance of the tools is difficult. Integrating force sensors in the surgical tools can help to detect undesired contact or penetration in healthy tissue. For example, an arthroscope equipped with force sensors can detect contact between its tip and the surrounding tissues [4], thus preventing possible damage of the cartilage. A second example of application is a mechatronic tool for drilling in the osteosynthesis of long bones [5]. In that case, the measurement of the variation of the thrust force experienced by the driller allows determining if the drill bit is in cancellous or cortical bone. When a bone is drilled across, the time of incipient breakthrough on the second cortical wall can thus be detected and the hole completed with minimal protrusion of the drill bit from the bone.

2. *Force monitoring of surgical actions.* While being corrected, cut, rasped, or reshaped, bones experience relatively high stresses. Applying excessive forces on the bony structure can create irreversible damage or give suboptimal outcomes. Instrumenting orthopaedic tools with force sensors can provide useful real-time force-feedback and thereby ensure safe and optimal surgical actions. In the case of correction of scoliosis for example, the realignment of the spine is realized by implanting a rod screwed in the misaligned vertebral bodies. In addition to the axial pull-out strength, the screws are loaded with a force component perpendicular to the screw axis, which may weaken the bone around the head and lower the pull-out force. A high correction force therefore increases the risk of screw pull-out. Instrumented forceps that measure tensile forces in the different segment of the rod can thus be used to maintain constant axial forces in the rod and reduce the transverse force on the vertebral screws [6]. A second example of application could be rasps instrumented with force sensors for the preparation of the femoral cavity in hip arthroplasty. Since there is a direct correlation between the rasping force and the bone density, the measurement of the latter allows the determination of the optimal rasping force. This optimum can then be intraoperatively guaranteed thanks to a monitoring based on the smart rasp measurements, thus avoiding excessive forces that may damage the femur.

3. *Assistance for optimal adjustment of the soft-tissue forces in joint arthroplasty.* Joint arthroplasty is used to treat severe arthrosis and bone deformities. To achieve a satisfying stability and lifetime of the prosthetic joint, the alignment of the bones and the forces experienced by the surrounding soft-tissue must be optimally corrected at the time of the surgery. The intraoperative use of instrumented trial implants or specific force-sensing devices could provide valuable measurements to assist the surgeon in optimally balancing the soft-tissue tensions. Two different applications can be thought for the two most performed joint arthroplasties: an instrumented telescopic neck for Total Hip Arthroplasty (THA) and a force-sensing device for Total Knee Arthroplasty (TKA). One serious problem after THA is dislocation, which is attributed to component malpositioning, soft-tissue imbalance and impingement. An advanced trial implant could allow the medialization and lateralization of the prosthesis and the measurement of the resultant hip force by means of a telescopic neck instrumented with force-sensors. The surrounding soft-tissue such as muscles, fascia, could be more or less stressed by adjusting the length of the neck until the op-

timal resultant hip force is obtained. This procedure may then lead to the proper choice of the prosthetic components, reducing the rate of dislocations in THA. In the knee, the stability of the joint is realized by a complex ligament structure. At the time of arthroplasty, this stability must be reevaluated and, if necessary, corrected to ensure a successful outcome. A force-sensing device that can precisely measure intraoperative mediolateral imbalance of the compressive forces of the knee joint could assist the surgeon in this delicate phase of ligament balancing. This would guarantee an optimal distribution of the compressive forces,leading to an increased lifetime of the prosthetic implants.

The goal of the present work is therefore to demonstrate through an application the importance and benefit of advanced orthopaedic instrumentation providing quantitative knowledge of intraoperative forces. A force-sensing device for improved ligament balancing procedure in knee arthroplasty has been developed and tested. Chapter 2 presents general aspects of the knee joint anatomy and of TKA as well as the specifications of such force-sensing device. The different conceived designs are explained and studied in chapter 3, while the selected sensor technology is described in chapter 4. The calibration method and the evaluation of the intrinsic accuracy of the device is exposed in chapter 5. The result of the *in-situ* evaluation of the device design as well as biomechanical investigations about the effect of ligament releasing can be found in chapter 6. Finally, the possible extension of the developed device to unicompartmental knee arthroplasty is discussed in chapter 8, before concluding this thesis in chapter 9.

Chapter 2

Total knee arthroplasty

2.1   Anatomy of the knee

The knee is the largest and most complex joint in the human body and combines two major joint mechanisms. On one hand, it fulfills the requirements of stability, which allows the transmission of large forces. For example, the knee bears three to four times the body weight during stair climbing. On the other hand, it provides a high degree of flexibility with a range of motion of up to 140° in flexion. The combination of these two functionalities is only possible by a perfect interplay between all the components of the knee.

The knee is indeed a two-joint structure composed of the tibiofemoral and patellofemoral joints [7]. The tibiofemoral joint connects the two longest bones in the human body, namely the femur and the tibia (Fig.2.1). The joint-constructing bone segments are overlaid by cartilage, which protects the bones and ensures free sliding. The absence of bony guidance is compensated by a complex structure of ligaments, which are dense parallel-fibered collagenous tissue. Two collateral ligaments (medial and lateral) limit the mediolateral translation from the tibia with respect to the femur and the so-called abduction-adduction rotation movements. Two cruciate ligaments (anterior and posterior) restrict the translation of the tibia to the femur in anterior and posterior directions. In the tibiofemoral gap are found the lateral and medial menisci, which compensate the bony incongruency and allow compressive forces to be distributed over the entire area of the tibial plateau, thus minimizing the contact stresses.

The patellofemoral joint (Fig.2.2) consists of the femur and the patella, which is a flat bone placed as a cap to the knee. The patella is held by the patellar
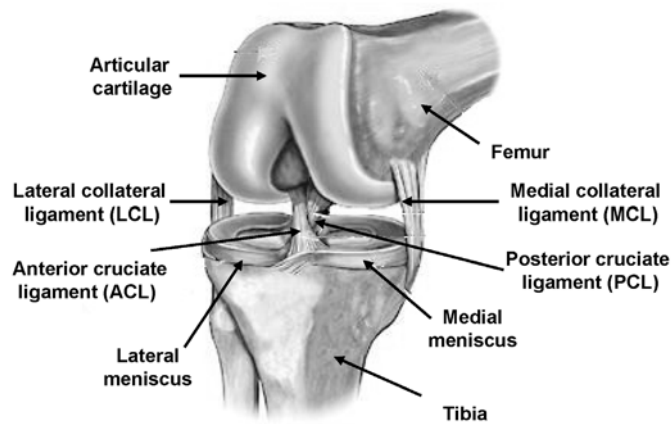
Figure 2.1: Anatomy of the knee

(picture adapted from the anatomy atlas of ADAM, Atlanta, USA)

tendon on the tibial side and by the quadriceps, the most effective active knee stabilizers, on the femoral side. The patellofemoral joint supports the extension of the knee and works as a sagittal stabilizer. The patella is also a protection for the knee in the frontal plane.
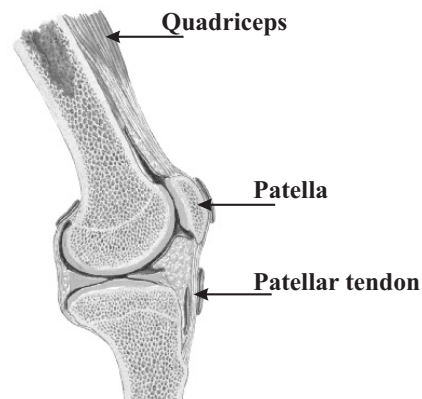
Figure 2.2: Patellofemoral joint

(picture adapted from the anatomy atlas of ADAM, Atlanta, USA)

All these components are the basis of the four degrees of freedom motion of the knee (Fig.2.3). In addition to three rotations (flexion-extension, varus-valgus and rotation), the tibia can perform anterior-posterior translations.

This results in a complex relative motion between the tibia and femur during a gait cycle: the flexion of the knee is accompanied by an external rotation and a posterior sliding of the femur [8]. A detailed description of knee kinematics can be found in [9].
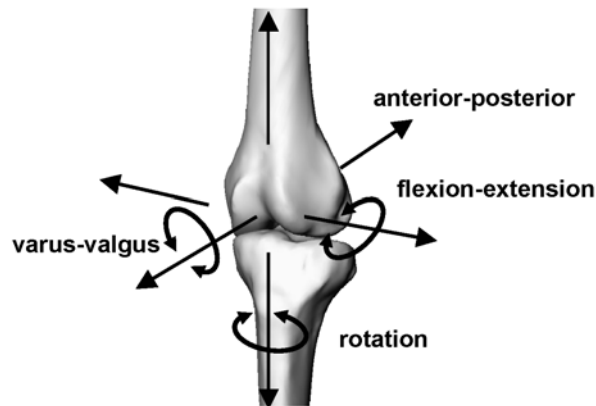
Figure 2.3: Possible motions of the knee

2.2 Total knee arthroplasty

Total Knee Arthroplasty (TKA) is the surgical intervention which consists of replacing a painful, damaged or diseased knee joint with prosthetic components. TKA is usually indicated for patients with end-stage degenerative disease, such as osteoarthrosis.

Even though T. Gluck designed and implanted hinge knee prostheses made of ivory over 100 years ago [11], intensive development of TKA had started by the 1950s. Design limitations in those early days included improper sizing, no provision for replacing the patellofemoral joint, lack of rotational freedom and improper stem fixation. Design of condylar knee replacement and polycentric knees were developed by the 1970s, while the 1980s and 1990s were spent for design improvements, thus allowing: better fixation with or without cement; reduced wear; enhanced kinematics and increased range of motion. The standard modern artificial joint is composed of three parts: metallic femoral and tibial components, which replace the bony structures, and a polyethylene inlay, which plays the role of the removed menisci (Fig.2.4). In the current age of technological advances, reproducing knee kinematics,

minimizing wear and increasing range of motion beyond 125° with proper alignment and stability have become the major goals of TKA [12].
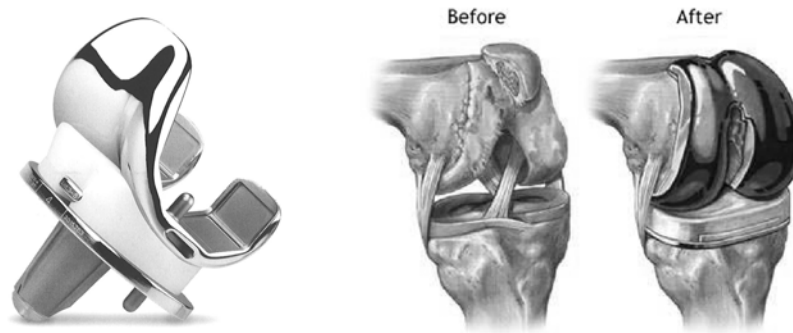
Figure 2.4: Total Knee Arthroplasty

Artificial knee joints are comprised of metallic femoral and tibial components and an inlay that plays the role of the removed menisci. (components picture taken from Zimmer, Warsaw, USA and drawings from Plus Orthopaedics, San Diego, USA)

To obtain a successful TKA, it is essential to produce a neutral mechanical axis from the center of the femoral head through the center of the knee to the center of the ankle by creating a valgus anatomic alignment of the femoral and tibial axes. If the limb alignment is suboptimal, the distribution of the load created by the body weight is not homogeneously distributed and may provoke postoperative complications such as component loosening or fast implant wear. The classic alignment involves the resection of the proximal tibia at a right angle to the long axis of the tibia from an anterior view. This is in contrast to the normal alignment of the articular surface which lies at approximately 4 ° of varus with respect to the tibia's anatomic axis [13] (Fig.2.5). Consequently, more bone is removed from the lateral tibial plateau than from the medial plateau. Accordingly, a larger amount of bone would be resected on the medial posterior femoral condyle than on the lateral in order to create a symmetric, rectangular flexion space, which is essential for proper collateral ligament function. This rotational positioning concept has become known as "external rotation of the femoral component".

In addition to a good tibiofemoral alignment, the stability of the knee joint must be ensured. This involves balancing the medial and lateral ligamentous structures. Medial ligament releases are indicated in a knee arthroplasty in which the patient has varus misalignment, which is the deformity that sur-
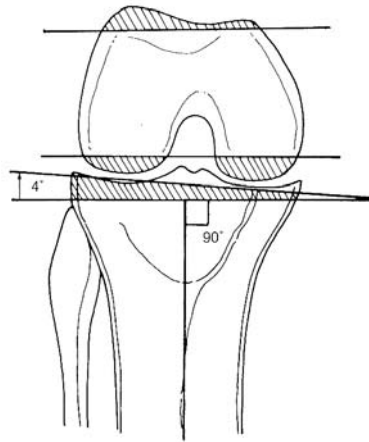
Figure 2.5: Classic bone resection during TKA
(picture taken from [16])

geons encounter most frequently. In case of a valgus knee — rarer but which presents more challenges to the surgeon — the tightest lateral structure is released. Diverse techniques to release ligaments have been reported [14, 15]. Although the approaches can differ among surgeons, a release consists in a partial resection of the fibers constituting the ligament. By doing so, the ligament stiffness is diminished and the tension reduced. This surgical action is of course irreversible and can be used only to reduce tension of tight structures.

Other important concerns in TKA are the preservation of the joint line, the contact line between the tibia and the femur, and the minimization of bone removal. Elevation of the joint line from its anatomic position alters normal ligament function whereas excessive bone resection reduces the stability and limits the chance of a successful revision at a later stage.

At the end of the surgery, i.e. following the bone cuts and the insertion of trial components, the final knee stability is evaluated in flexion and extension. In full extension, three criteria must be met (Fig.2.6):

1. Absolutely full extension without recurvatum or residual flexion contracture

2. Satisfactory valgus anatomic alignment (neutral mechanical axis)

3. Satisfactory varus-valgus stability.

In flexion the knee should feel just slightly more lax than in extension [16].
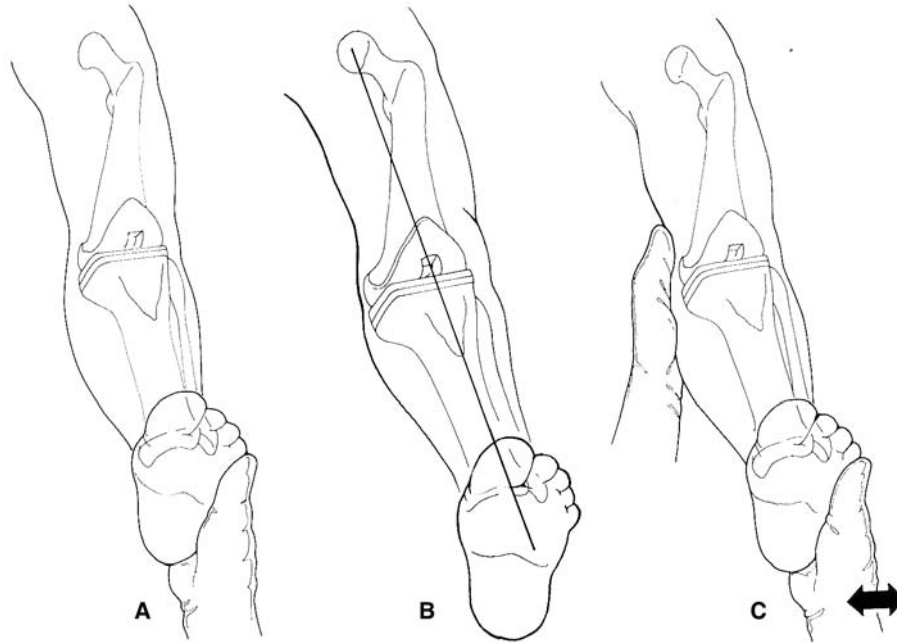
Figure 2.6: Evaluation of the knee in extension with trial components
A: The knee should achieve full extension without recurvatum B: The mechanical axis should be neutral C: Satisfactory varus-valgus stability (picture taken from [16])

To resume, the key points to reach a successful primary knee arthroplasty are establishment of correct mechanical alignment, maintenance of joint stability, preservation of joint line and minimal bone resection [17]. Nevertheless recent analysis showed that failure rates of primary TKA are 9% at 10 years, 16% at 15 years and 22% at 20 years [18]. Common causes of dysfunction after TKA are component loosening and instability. It is nowadays widely accepted that the two surgical factors responsible for these postoperative complications are tibiofemoral misalignment and ligament imbalance [19, 20, 21, 22, 23, 24, 25, 26, 27, 28]. In order to increase the long term success rate of TKA, advanced instrumentation allowing optimal limb alignment and accurate ligament balance must be placed at surgeons' disposal.

2.3 Computer assisted knee surgery

Although the concept of navigating a surgery is over 100 years old, the intensive development of Computer Aided Orthopaedic Surgery (CAOS) started in the early 1990s. Like every surgical navigation system, CAOS consists of three major components: the therapeutic object (the patient), the virtual object (computed tomography, fluoroscopic images or digitized points or curves) and a navigator, a device which links the therapeutic object and the virtual object [29]. Thanks to this navigator, the surgeon always knows the exact location of the tools in the virtual object. Before each crucial step, he can precisely check that the location and orientation of his tool is correct according to his planning and is therefore able to safely and precisely drill or saw the bones.

For example, current surgical knee navigation systems help the surgeon achieve a precise alignment and placement of the prosthetic components. Following the registration of the knee anatomy, the navigation system proposes optimal cuts and component size in order to obtain a neutral mechanical axis of the limb. Postoperative knee kinematics can also be simulated at the time of surgery in order to anticipate what the future range of motion will be and, if necessary, to perform final adjustments. The clinical benefit of such technology has nowadays been extensively reported [30, 31, 32, 33, 34].

Even though good tibiofemoral alignment can be achieved with current CAOS navigation systems, only geometric parameters such as morphologic angulation, depth penetration, etc., are provided. Ligament force imbalance during TKA is still qualitatively assessed by the surgeon through manual trial movements of the limb. Providing an objective and quantitative measurement of the forces acting within the knee could help the surgeon improve the accuracy of the ligament balancing procedure, leading to a potentially longer prosthesis lifetime.

2.4 A force-sensing device for TKA

Various approaches to intraoperatively measure ligament imbalance were reported and are presented below.

Attfield et al. [35] developed an electronic surgical instrument which contains two plates, one being attached to the tibia, the other supporting the femur. The upper plate acts as a mechanical cantilever in the medial-lateral direc-

tion and the ligaments are balanced according to the measured inclination of the cantilever, which depends on the moments applied by the soft tissues. The disadvantage of such an apparatus resides in the size of the handle that prevents the patella from being kept at its anatomical place during the measurement. Undesirable forces are thus generated by the patella tendon and may lead to a non-optimal balancing.

Wallace et al. [36] used a dual-array electronic pressure transducer (Tekscan, Boston, United States). The 10% intrinsic accuracy of the device might be insufficient for such an application and the large number of wires needed for the pressure sensor arrays and the data acquisition requires an arthrotomy through the patellar retinaculum. Similar sensing technology from Novel Electronics, Munich, Germany, was recently used to determine the correlation of intraoperative pressure with postoperative knee kinematics [37, 38].

Knee joint pressure distribution was also measured intraoperatively with Fuji pressure-sensitive films [39], but the accuracy is relatively low and the reading is not available in real-time.

In another development, an implantable tibial tray was instrumented with four load cells and a passive telemetric transmission system [40, 41, 42]. In addition to the long-term post-operative use, it is possible to intraoperatively measure the contact forces of the femoral condyles. Nevertheless, in order to accommodate the load cells, this customized tibial tray is 7.5mm thicker than that of a standard prosthesis, which requires significantly larger bone removal. Davy et al. [43] reported a similar development.

Different designs of calibrated pliers are commercially available for controlled knee distraction. A tensor/balancer device (Stryker Howmedica Osteotonics, Mahwah, United States) was evaluated in 83 consecutive TKAs by Winemaker, who concluded that the device provides an accurate and reproducible way to measure gap differences and angular asymmetry [44]. The BalanSys knee instrument (Mathys LTD Bettlach, Bettlach, Switzerland) is a similar device composed of two calibrated spring tensors that allow medial and lateral force-controlled gap distraction. Finally, an instrumented ligament spreader was combined with the Galileo knee replacement navigation system (PiSystems, Aarau, Switzerland), thus providing a tension/force and a distance measurement as well as information regarding the polyethylene thickness to be selected [45]. Even though the approach is simple and appears efficient, all these devices are encumbering and requires a patellar eversion or subluxation, which can again significantly alter the ligament balance.

Marmignon et al. [46] developed a robotized distraction device, which has a base plate carrying two independent and parallel trays. These trays that support the condyles can be elevated thanks to a jack and a cable applying a force between the central axes or due to two inflatable rubber bladders. The first approach lead to a device not powerful enough (100N maximal force), while in the second, the parallelism of the trays could not be ensured, thus preventing the proper functioning of the device.

To overcome these disadvantages, the optimal force-sensing device for TKA must fulfill the following requirements:

1. Accurate and real-time quantitative measurements to optimally balance the ligament forces

2. Minimal thickness and easy insertion to minimize the tibial resection and avoid any additional surgical actions

3. Adaptable thickness to allow the correction of the tibiofemoral alignment and the compensation for the anatomic variation of each patient

4. Measurements with the patella in its anatomical place to avoid non-anatomical forces due to a patellar eversion or subluxation.

5. Possibility to measure the ligament balance before the femoral cuts. Performing the assessment of the joint stability at an early stage of the TKA procedure offers the possibility to make a better plan for the femoral cuts and the femoral component rotation. The joint line can be more easily preserved and the bone resection minimized. Moreover, strong imbalance that could not be corrected at a later stage with only ligament releases could be rectified at the beginning of the surgery when all the correction means, such as bone cuts, are still at the surgeon's disposal.

Chapter 3

Force-sensing device design

Before designing the device, the biomechanical parameters that characterize the ligament balance must be determined. For that purpose, a simplified biomechanical model of the knee joint is first introduced. Since the design depends as well on the type of sensors selected, several principles of force measurement are then explained. Finally, three possible designs are presented and evaluated using finite element analysis. Basic concepts of mechanics of material necessary to understand the measurement principle of the different designs are recalled in appendix A.

3.1 Simplified biomechanical model

To ensure a stable knee joint and therefore a successful outcome of TKA, it is assumed that the ligament forces must be balanced (c.f. chapter 2). In order to define the relevant parameters characterizing this balance, a simplified model of the knee joint in the coronal plane is used. It considers the collateral ligament forces F_{ML}, F_{LL} and the condyle contact forces acting on the tibia F_{MC}, F_{LC} (Fig.3.1). The cruciate ligaments and the patella tendon are neglected since their effect is mainly limited to the sagittal plane. Although quite simple, this model captures the most important knee balance effects in the coronal plane.

In static conditions, the mechanic equilibrium equations ($\sum_i \vec{F_i} = \vec{0}, \sum_i \vec{M_i} = \vec{0}$) must be satisfied, yielding:

$$\begin{aligned} 0 &= F_{ML} + F_{LL} - F_{MC} - F_{LC} \\ 0 &= x_{ML}F_{ML} - x_{LL}F_{LL} - x_{MC}F_{MC} + x_{LC}F_{LC} \end{aligned} \quad (3.1)$$

where x_i ($i = ML, LL, MC, LC$) are the lever arms of the different forces measured from the origin placed at $L/2$, L being the distance between the
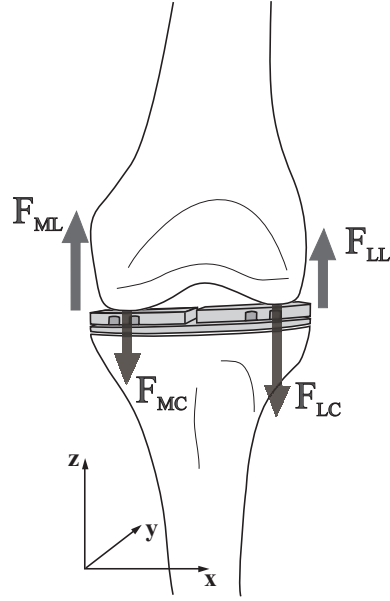
Figure 3.1: Two-dimensional knee joint model

The patella tendon and the cruciate ligaments being mainly effective in the sagittal plane, only the collateral ligament forces (F_{ML}, F_{LL}) and the contact forces (F_{MC}, F_{LC}) are taken into account.

collateral ligaments. The lever arms of the collateral ligaments being $L/2$, equation (3.1) becomes:

$$M_{net} = x_{MC}F_{MC} - x_{LC}F_{LC} = \frac{L}{2}\left(F_{ML} - F_{LL}\right) \qquad (3.2)$$

where M_{net} is the net varus-valgus moment of the contact forces acting on the knee joint. When the tension in the collateral ligaments is equal ($F_{ML} = F_{LL}$), the right side of the equation is zero. Therefore, M_{net} may be regarded as the parameter characterizing the ligament imbalance, and reducing it to zero is equivalent to balancing the ligaments. In conclusion, the device must be able to either measure this net varus-valgus moment or measure parameters that allow its computation.

3.2   Techniques to measure forces

As a force can not be measured directly, its effect on a body, such as the resulting deformation or displacement, must be assessed. For example, the strain experienced at the base of a bending beam is directly proportional to

the force applied at the beam extremity by the well-known flexure formula (c.f. equation (A.22)). Four types of force sensors have been investigated for our application: capacitive, magnetic, inductive sensors and strain gauges.

3.2.1 Capacitive sensors

A capacitor is schematically represented by two conductors separated by a gap. Its capacitance is a function of the area S of the conductors and the gap d:

$$C = \epsilon \frac{S}{d} \,, \tag{3.3}$$

where ϵ is the dielectric constant of the gap. According to equation (3.3) a gap change, which is a relative displacement of the conductors, leads to a variation in the capacitance.

A capacitor connected to an inductor forms a resonant circuit (Fig.3.2). The gain function of such circuit is given by:

$$G(\omega) = \left| \frac{U_o}{U_i} \right| = \left| \frac{Z_C}{Z_C + Z_L} \right| = \left| \frac{1/j\omega C}{1/j\omega C + j\omega L} \right| = \left| \frac{1}{1 - \omega^2 LC} \right| \,,$$

where U_i, U_o are the input and output voltages, ω the pulsation and Z_C, Z_L the complex impedances of the capacitor and inductor respectively. In view of this last expression, the gain amplitude is infinite when $\omega = \sqrt{\frac{1}{LC}}$ or $\nu = \frac{1}{2\pi}\sqrt{\frac{1}{LC}}$, which is called the resonance frequency.
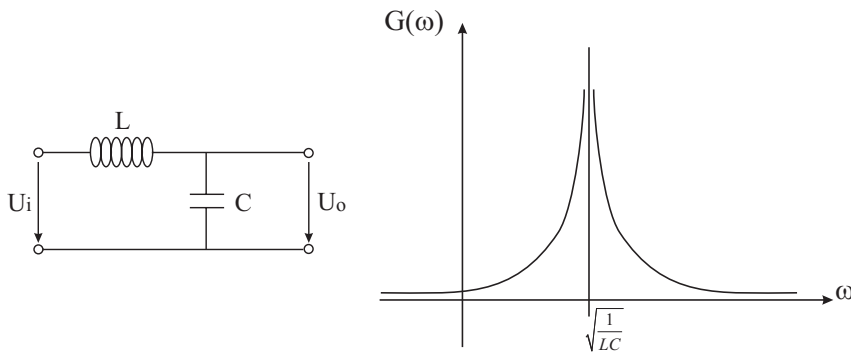
Figure 3.2: LC resonant circuit
The LC circuit scheme and its corresponding Bode diagram

Capacitive sensors can therefore be placed in such a manner that the application of a force makes d or S, and thereby the capacitance C, vary. By integrating the sensor in a resonant circuit, the applied force can be retrieved by measuring the change of the resonance frequency.

3.2.2 Magnetic, inductive sensors

Another possibility to measure forces is to use magnetic or inductive sensors. In both cases, the measurement system is composed of an emitter and a receiver. The emitter generates a magnetic field and is mounted on a part of the sensing device which is deformed by the applied load. The receiver is placed on a fixed reference part and measures the variation of the magnetic field induced by the emitter displacement. Since the emitter position is dependent on the applied load, a direct relationship exists between the magnetic field variation measured by the receiver and the applied load.

The measurement principle of the magnetic and inductive sensors is as follows:

1. **Magnetic sensors**

   - The emitter is a permanent magnet.
   - The receiver is a magnetic field detector based on the Hall effect (Fig.3.3). When a electrical current traverses a metallic plate submerged in a magnetic field, the electrons going through the plate experience a Lorentz force perpendicular to the current direction. A measurable voltage, whose amplitude varies proportionally to that of the magnetic field, appears at its border.
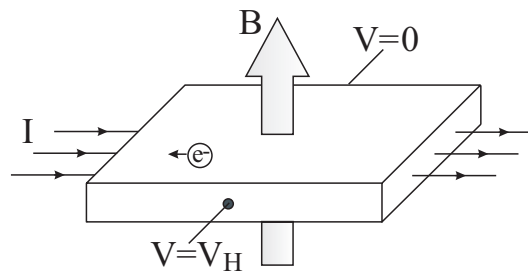
Figure 3.3: Illustration of the Hall effect

When an electrical current (I) traverses a metallic plate submerged in a magnetic field (B), the electrons are deviated and a voltage (V_H) is generated at the borders.

2. **Inductive sensors**

- The emitter is a coil powered by an alternative current, thus generating an oscillating magnetic field.

- The receiver is a coil too, into which the emitted magnetic field induces a current. The amplitude of the induced current varies with the magnetic field amplitude.

3.2.3 Strain gauges

A strain gauge is a device whose electrical resistance varies in proportion to the amount of strain in the device. The most widely used gauge is the bonded metallic strain gauge. The metallic strain gauge consists of a fine wire or, more commonly, metallic foil arranged in a grid pattern. The grid pattern maximizes the amount of wire to strain in the direction parallel to the gauge backing (Fig.3.4). The cross-sectional area of the grid is minimized to reduce the effect of shear strain and Poisson strain (c.f. appendix A). The grid is bonded to a thin backing, which is attached directly to the test specimen. Therefore, the strain experienced by the test specimen is transferred directly to the strain gauge, which responds with a linear change in electrical resistance due to the lengthening or shortening of the metallic foil.
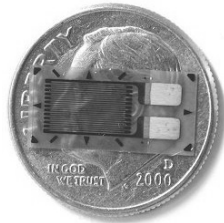
Figure 3.4: Metallic strain gauge
A strain gauge is basically a thin wire arranged in a grid pattern whose resistance
linearly varies with the strain.

Although this low-cost technology gives a large freedom to the designer, a few delicate points such as the bonding and the positioning have to be considered. It is very important that the strain gauge is properly mounted onto the test specimen so that the strain is accurately transferred from the test specimen, through the adhesive and strain gauge backing, to the foil itself. Bad mounting not only affects the measurement sensitivity, but also causes

self-heating problems. Inaccurate positioning, such as bad parallelism, generates deviations by not measuring the desired force, but only its projection on the gauge axis.

Piezoresistive sensors

To overcome the disadvantages of bonded metallic strain gauges, piezoresistive ceramic elements can be used instead (c.f. chapter 4). In addition to a larger gauge factor, which is the ratio between the strain and resistance variation, and a larger resistance, which reduces the self-heating due to the Joule effect, thick-film piezoresistive sensors can be directly deposited on the specimen by screen printing. With such technology, errors due to bad mounting are minimized. Furthermore, the size of piezoresistive sensors are significantly reduced compared to that of standard strain gauges, thus allowing finer designs.

3.2.4   Choice of the measurement principle

Although each of the previously discussed sensor types could be used, thick-film piezoresistive sensors have been chosen for the following reasons:

- The measurement principle is relatively simple.

- The encumbrance is not significant.

- The intrinsic accuracy of the sensor is high.

- It is a low-cost technology.

- The signal conditioning can be ensured with just an amplifier and a filter.

- Standard heat moisture sterilization is possible.

- Biocompatibility can be easily ensured by a final surface coating.

3.3 Definition, evaluation of possible designs

Before describing in details the three designs, the common aspects, such as the perimeter, the different parts composing the device and the material selected are presented.

The three conceived designs were inspired from existing prosthetic components. The perimeter of the device was extracted from a CKS inlay (Biomet, Warsaw, IN, USA). It is 77mm wide and 51mm long, so it is suitable for tibias of medium size. In case of routine clinical use, the device would be available in different scales to cover all the possible knee sizes.

A flat reference surface on the tibial side is required to ensure reliable measurements. Moreover, compressive forces or varus-valgus moments have to be assessed with different knee gaps to comply with the surgical procedure. For these reasons, the device is composed of three distinct parts:

1. *A tibial base plate*, which is fixed by pins on the tibia after a tibial cut and serves as a reference plate.

2. *A sensitive plate*, which measures the moments and which lies on the base plate.

3. *A set of spacers*, which allows measurements at different knee gaps.

Finally, the material used for the sensitive plate has to be:

1. *Biocompatible.* Biocompatibility is the quality of not having toxic or injurious effects on biological systems. There exist different degrees of biocompatibility, depending on the amount of time the material has to be in contact with the human body, especially with bones and bodily fluids. Although the device operates for less than half an hour, implantable material should be used in order to preserve the patient safety in case of accidental release of debris.

2. *Compatible with thick-film technology.* Up to now, the deposition process is controlled for stainless steel based applications. The high curing temperature during deposition limits the choice of material and prevent the usage of metals with better properties for a force-sensing device, such as titanium.

3. *Suitable mechanical properties.* The selected material must have suitable mechanical properties for a force-sensing device, i.e. a large elastic

range and a high ultimate stress. Moreover, as the device is heated
during the sensors curing, it must have these properties in annealed
conditions.

The stainless steel Bioline High-N from Sandvik, Sandviken, Sweden fulfills
the above requirements. It is certified implantable and its mechanical prop-
erties summarized in table 3.1 are perfectly suitable.

Young's modulus	$200 \cdot 10^3$ N/mm^2
Poisson's ratio	0.3
Yield point	430 N/mm^2
Ultimate stress	740 N/mm^2

Table 3.1: Mechanical properties of Sandvik Bioline High-N Annealed

The perimeter, the material and the different parts of the design having been
determined, a detailed description of the three conceived designs is now given.

3.3.1   Design I: opposed bending beams

According to the simplified biomechanical model, the knee stability can be
assessed by comparing the varus-valgus moment of the medial and lateral
condyles. Thus, the first design was inspired by a balance scale: the sensi-
tive plate has the shape of a standard inlay into which two bending beams
reproducing the balance trays are cut (Fig.3.5). According to the flexure
formula (c.f. equation (A.22)), the varus-valgus moments created by the
contact forces are proportional to the stress and strain experienced at the
base of each bending beam, where two piezoresistive sensors are arranged in
a half Wheatstone bridge configuration.
The measurement principle was simulated using Finite Element Modelling
(FEM). 29'680 solid parabolic tetrahedrons with a length parameter of 1.5mm
compose the mesh. A 500N load is applied in the middle of the right side.
The boundary conditions are set so that the device perimeter of the bottom
face is clamped. Fig.3.6 shows the distribution of von Mises stresses (c.f.
equation B.20) in the bottom view of the device. The stresses in the sensi-
tive area are 57N/mm^2.

Two parameters, the radius and the shift between the beginning and the
end of the beam cutout, were optimized to homogenize the stress in the
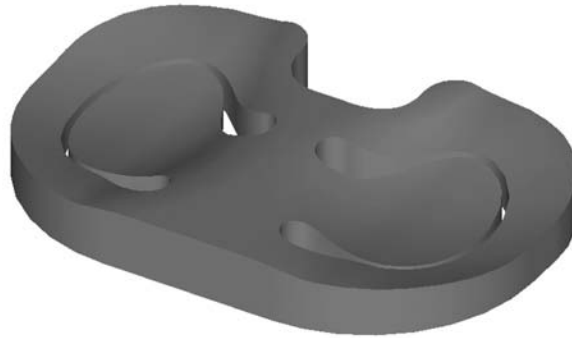
Figure 3.5: 3D model of design I

Two bending beams allow the measurement of the varus-valgus moments of the medial and lateral femoral condyles.

sensitive areas of the device in order to minimize the stress variation along the piezoresistive sensors (Fig.3.7):

1. A small cutout radius generates stress concentrations and a large reduces the beam width, both being able to provide stresses exceeding the material limit. A good indicator of an homogeneous stress distribution is the ratio between the maximal and average stresses. As this ratio this ratio nears 1, the stress distribution becomes more homogeneous. This ratio was therefore calculated by FEM for different cut radii and showed that the optimal radius is 6mm.

2. As the contact point of each condyle is not expected to lie in the center of the beam but rather in the center of the left or right part of the device, the beam rotation axis is not perpendicular to the beam itself. To facilitate the placement of the sensors, which should be on the beam rotation axis where the stress is theoretically maximal, the perpendicularity has to be restored. This can be carried out by imposing a shift between the beginning and the end of the beam cutout. To determine the optimal shift, the stress variations along the axis perpendicular to the beam and going by the point of maximal stress was computed by FEM for different shift amplitudes. The variations are minimal with a shift of 5.6mm.

At first sight, this design seems adequate. The stresses are smoothly distributed in the sensitive area and the ratio of 1.7 between the maximal and average stresses gives a reasonably homogeneous sensitive area. Moreover,
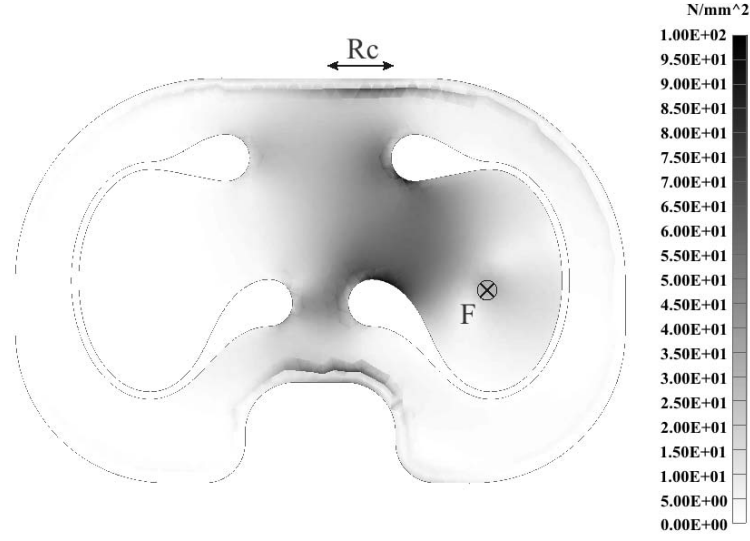
Figure 3.6: FEM of the design I

A 500N load (F) is applied in the middle of the right side

the sensitivity is satisfying and could be easily increased by diminishing the beam thickness. However, an important drawback makes this design unsuitable for our application. The sensitive areas, where the sensors are supposed to measure the varus-valgus moments, are not located at the center of the device but at the base of the bending beam. The distance R_c (Fig.3.6) between a sensitive area and the center of the device is a source of error. When the moments of the contact forces F_1, F_2 measured by each beam are equal:

$$F_2(X_2 - R_c) = F_1(X_1 - R_c)\,, \tag{3.4}$$

X_1, X_2 being the lever arm respective to the device center, the net varus-valgus moment is:

$$M_{net} = F_2X_2 - F_1X_1 \stackrel{(3.4)}{=} (F_2 - F_1)R_c\,. \tag{3.5}$$

R_c being 10mm and supposing that the measured varus-valgus moment of each contact force is 1440Nmm with respective forces of 80N and 120N, and respective lever arms of 28mm and 22mm, M_{net} is 400Nmm. This means a 8% error relative to the sum of the effective lateral and medial varus-valgus moments. In practice, additional experimental errors will affect the device accuracy, thus bringing the final measurement error surely above 10%. To overcome this problem, the location and amplitude of the femoral contact forces have to be measured separately.

Figure 3.7: Design optimization

The radius and the shift between the beginning and end of the cutouts were optimized to have maximal homogeneous stress areas

3.3.2   Design II: open load cell

To measure the amplitude and location of the femoral contact forces, three measurement points per condyle are necessary. The simplest way to realize that is to have a defined medial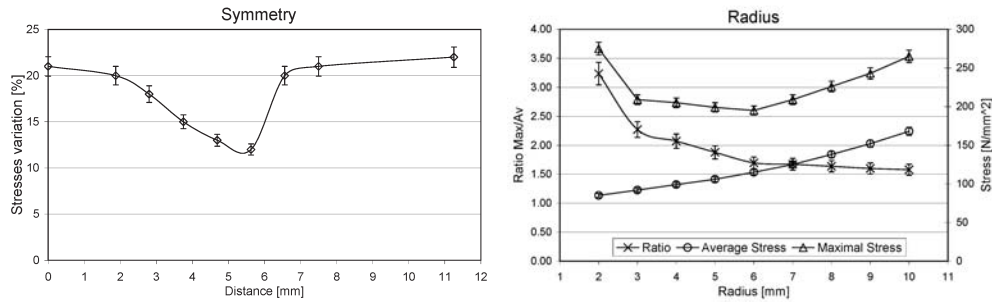 and lateral contact area attached to a frame by three deformable bridges (Fig.3.8). When the device is loaded, the sum of the stresses experienced by the three bridges is proportional to the amplitude of the applied force whereas the ratio determines its location. To perform correctly, however, such a device needs a large and strong frame, rigid enough to absorb and homogeneously distribute the load. The room being restricted in our application, this condition can not be ensured and the measurements could depend on the location of the contact points between the frame and the tibial base plate. For a good accuracy and reliability of the measurements, the contact points between the plates must be mechanically well defined. Therefore, two sensitive plates and two sets of three balls are used to avoid statically indeterminate conditions.

The thickness of the sensitive plates is 3mm. The contact areas have an internal diameter of 19mm. The bridges are 4mm wide to leave enough space for the electrical connections, as well as 5mm long and 1mm thick to be sensitive enough to the deformations. The large contours at the bridge extremities avoid stress concentrations. Two piezoresistive sensors are placed at each side of each bridge, with two working in compression and two in tension. A full Wheatstone bridge can thereby be used, increasing the measurement sensitivity and avoiding temperature drift. To prevent the femoral condyles from being damaged by the cuts, a plastic hat could be placed on the top of the sensitive plates.
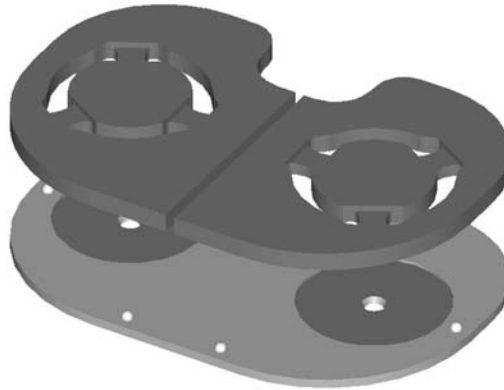
Figure 3.8: 3D model of the design II
A circular contact area is attached to the frame of the device by three deformable
bridges, thus allowing the measurement of the amplitude and the location of the
compressive forces.

The measurement principle is simulated by FEM analyses for one single sensitive plate (Fig.3.9). The mesh is composed by 28'596 solid parabolic tetrahedrons with a length parameter of 1.5mm. The boundary conditions are set so the ball seats are clamped. A 500N load is applied once at the center and once shifted by half of the radius of the sensitive area to exemplify the determination of the contact point.

These FEM analyses demonstrate the suitable sensitivity of the device. With a 500N centered load, each bridge experiences stress of $120N/mm^2$. When the load is not centered, the closest bridges from the application point undergo almost twice more stress ($160N/mm^2$) than the most distant ($70N/mm^2$). With a relative difference of 8%, the sum of the stress in both situations ($360N/mm^2$ and $390N/mm^2$) can be considered equivalent in compliance with the fact that the amplitude of the applied load is the same.

Despite the apparent suitability, this design has two major problems. Firstly, the sensitive area is too limited. According to [8] the rollback of the lateral condyle is about 10mm for a 0-90° flexion and 22mm for a 0-120° flexion. Although these movements can hold in the contact areas, there is no significant safety margin. Moreover, the device is intended for use with pathological knees where deviations from this standard can be expected. Secondly, the contact with the balls can be a source of error. In practice, friction between
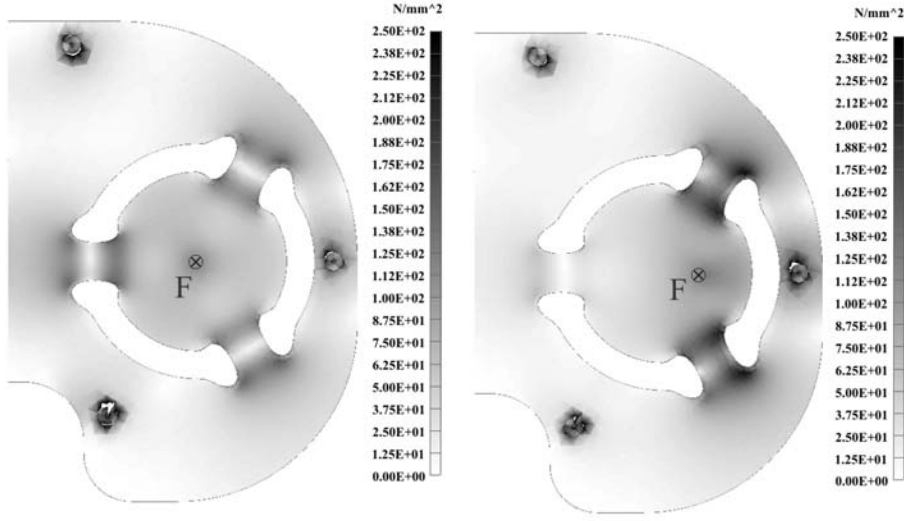
Figure 3.9: FEM of the design II

A 500N load applied once at the center, once shifted to the right, shows the sensitivity as
well as the functioning

the balls and the base plate generates moments in the bridges which have
not been taken into account so far. The friction force is proportional to the
reaction force (F) which creates the moment in the bridge. Therefore, the
ratio between the moment that has to be measured and the moment due to
friction is given by:

$$\frac{\mu F d_1}{F d_2} = \frac{\mu d_1}{d_2} \, . \tag{3.6}$$

The lever arm of the friction moment (d_1) is equivalent to the device thick-
ness, i.e. 3mm. The distance between a bridge and the closest contact point
varies from 10mm to 20mm (d_2). A typical metal-to-metal friction coefficient
(μ) being 0.2, the friction moment in a bridge corresponds to 3% to 6% of
the effective moment. The device having six bridges, the total measurement
error due to friction is definitely not acceptable. To further optimize the de-
sign, the contact area must be increased and the disturbances due to friction
moment minimized.

3.3.3 Design III: integrated bridges

To maximize the contact area, the three bridges needed to measure the lo-
cation and the amplitude of the femoral contact forces must be shifted to

the device border (Fig.3.10). The bridges are 4mm wide and 4mm long to
have enough room for the sensors and their connections and 1mm thick to
ensure a good sensitivity. The bridge cutouts have been optimized by FEM
in order to suppress stress concentrations while keeping a sufficiently large
contact area. The fillet under the bridges has a 1mm radius, which follows
the empirical rule stating that a fillet as large as the bridge thickness allows
avoiding stress concentrations. A ball is inserted in each pillar extremity to
ensure mechanically well defined contact points between the tibial base plate
and the sensitive plates. Moreover, since these balls allow rotations, torsion
is avoided and the bridges undergo pure bending.
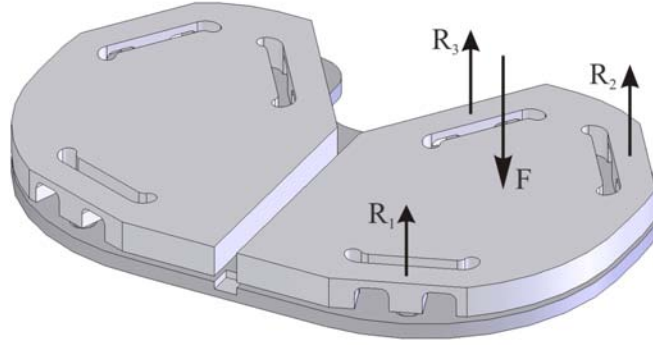
Figure 3.10: 3D model of design III

The three bridges are placed at the device border to maximize the sensitive area and a
symmetrical bridge is used to minimize error due to friction moments. When a load F is
applied on the device, three reaction forces R_i ($i = 1$, 2, 3), whose amplitude depend on
the amplitude and location of the original load, are generated. The deformation of each
bridge due to a single reaction force is then measured.

The measurement principle is as follows: when a load $\vec{F}$ is applied in the
sensitive area, three reaction forces $\vec{R}_1$, $\vec{R}_2$ and $\vec{R}_3$ are generated at the
bridge pillars. The amplitude of those reaction forces is directly related
to the location and amplitude of the applied load through the equilibrium
equations:

$$\sum_i \vec{R}_i + \vec{F} = 0$$

$$\sum_i \vec{X}_i \wedge \vec{R}_i + \vec{X} \wedge \vec{F} = 0 \,, \tag{3.7}$$

where $\vec{X}_i$, $i = 1, 2, 3$ are the respective lever arms. As all the forces are

perpendicular to the plate surface, the previous vectorial equations come down to three independent scalar equations:

$$
\begin{aligned}
x_1 R_1 + x_2 R_2 + x_3 R_3 - xF &= 0 \\
y_1 R_1 + y_2 R_2 + y_3 R_3 - yF &= 0 \\
R_1 + R_2 + R_3 - F &= 0,
\end{aligned}
\tag{3.8}
$$

which can be solved for F, x, y.

$$
\begin{aligned}
F &= R_1 + R_2 + R_3 \\
x &= \frac{x_1 R_1 + x_2 R_2 + x_3 R_3}{R_1 + R_2 + R_3} \\
y &= \frac{y_1 R_1 + y_2 R_2 + y_3 R_3}{R_1 + R_2 + R_3}
\end{aligned}
\tag{3.9}
$$

Due to the difference of rigidity between the bridges and the rest of the sensitive plates, each bridge is deformed by the reaction force experienced by its own pillar. Everything occurs as if each bridge was laterally clamped and a single force applied at its center. In such situation, one compression and one tension domain appears at each side of the bridge pillar (Fig.3.11). The amplitude of the reaction forces can be measured with four piezoresistive sensors placed at these specific locations (c.f. appendix A) and arranged in a full Wheatstone bridge. The location and amplitude of the applied load can then be calculated thanks to equation (3.9).
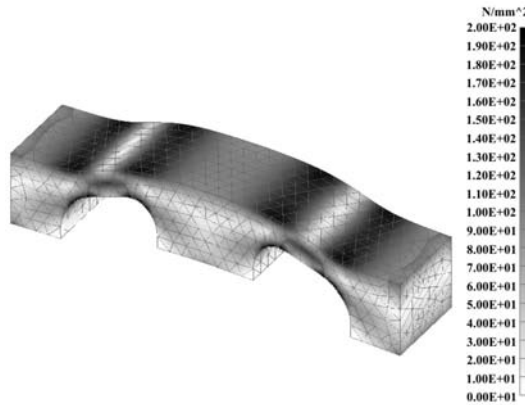
Figure 3.11: Deformation of a single bridge
The sides of the bridge are clamped and a load is applied at the center. Two compression and tension areas appear at each side of the pillar.

With this design, the contact area is defined by a triangle, whose edges are located at the pillar centers. This triangle has a base of 22mm and a height of 36mm, which is much larger than with the open load cell design. Another advantage of such a bridge configuration is the self-compensation of error due to friction moments. As the effect of friction has the same amplitude but an opposite sign at each side of a single bridge, it is electronically cancelled out by the Wheatstone bridge.

Fig.3.12 is a typical simulation by FEM of the device performance. 28'735 solid parabolic tetrahedrons with a length parameter of 1mm compose the mesh. The boundary conditions are set so the pillar extremities allow rotations but not translations. A 500N load is applied once centered and once posteriorly shifted to illustrate the measurement principle. The maximal compressive von Mises stress is $150N/mm^2$ and the maximal tensile stress is $210N/mm^2$ when the load is centered. This asymmetry comes from the overall bending of the sensitive plate, which is added on the bridges, thus decreasing the compression and increasing the tension stresses. However, this asymmetry is not a problem in practice since contributions equal in amplitude and sign cancel each other due to the full Wheatstone bridge configuration.

Figure 3.12: FEM of the design III

A 500N load applied once at the center, once posteriorly shifted, shows the sensitivity as well as the working principle

Finally particular attention must be paid to the balls: a very small ball diameter creates huge contact pressure which can tear the tibial base plate. The hertzian theory is therefore used to verify that the selected mate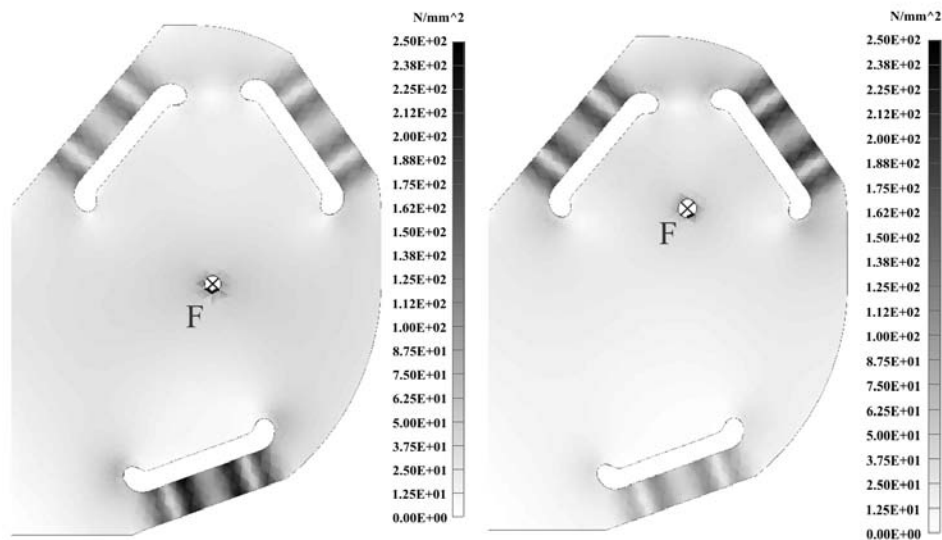rial and geometry support the loads involved in this application. From appendix B, it is known that the maximal pressure of a sphere in a spherical seat is given by

$$P_{max} = \frac{1}{\pi} \sqrt[3]{\frac{6}{\pi^2} \frac{F}{(K_1 + K_2)^2} \frac{(R_1 - R_2)^2}{R_1^2 R_2^2}}, \tag{3.10}$$

$$K_i = \frac{1 - \nu_i^2}{\pi E_i} \qquad i = 1, 2.$$

E is the Young's modulus, ν the Poisson's ratio, i indexes the two bodies, F the load, R_1 and R_2 the radius of the ball and its seat. From this maximal contact pressure, the corresponding effective stress or von Mises stress, which can be compared to the material specifications given by the manufacturer, can be calculated using the relationship (c.f. appendix B):

$$\sigma_{eff}^{max} = 0.6 P_{max}. \tag{3.11}$$

Since the Sandvik High-N stainless steel would not support the contact pressure, titanium has been chosen for its biocompatibility and its relatively low Young's modulus (c.f. Table 3.2), which decreases the maximal pressure according to equation (3.10).

Young's modulus	$114 \cdot 10^3$ N/mm^2
Poisson's ratio	0.34
Yield point	870 N/mm^2
Ultimate stress	950 N/mm^2

Table 3.2: Mechanical properties of Titanium Grade 5 ELI

The diameter of the balls is 3mm and corresponds to the largest diameter allowing press-fit in the pillars. The seat in the base plate is 3.5mm and follows from a trade off between the pressure amplitude and the manufacturing precision. On one hand, the seat diameter should be as close to the ball diameter as possible to maximize the contact area and therefore minimize the contact pressure. On the other hand, it should be large to minimize the errors induced by the manufacturing accuracy: a shift between the balls and the seat location would lead to reaction forces not parallel to the pillars,

thus inducing measurement errors. As the selected steel balls are normally used in ball bearings and can support a pressure as large as $4'200N/mm^2$ before reaching their yield point, only the titanium plate has to be inspected. With the numerical values presented above, the $870N/mm^2$ yield point of titanium is reached with a load of 270N: more than half of the maximal load can be supported by a single pillar without yielding, which is sufficiently safe.

In conclusion, this design fulfills the requirements and shows important decisive advantages:

- Accurate measurement of force amplitude and location

- Mechanical decoupling between the medial and lateral sides

- Maximal contact area

- Minimal parasite effects (temperature drift, friction moments)

- Small size and thickness

- Possibility to keep the patella at its anatomical place during the measurement

- Sterilizable

This last design has therefore been considered as optimal and a series of prototypes were built.

Extension of the sensitive area

Although the sensitive area has been maximized, the contact points of the femoral condyles can be located close to the lateral device borders due to deformities or unusual anatomy. Such cases would be out of the sensitive area and therefore not measurable. In addition to this, the sensitive plate should be fastened to the base plate in order to avoid lift-off during manipulations or in absence of compressive forces.

To address these two issues, a fixation mechanism was developed (Fig.3.13). It has a T-shape whose pillar is screwed to the base plate and whose arms cover the posterior medial bridge of each sensitive plate. A screw with a spherical head placed at each arm's extremity allows the bridges to be fixed. The spherical screw head enables rotations, thus avoiding torsion in the bridge. With this system, the posterior medial bridge can measure vertical reaction forces in both directions, which allows the measurement of contact
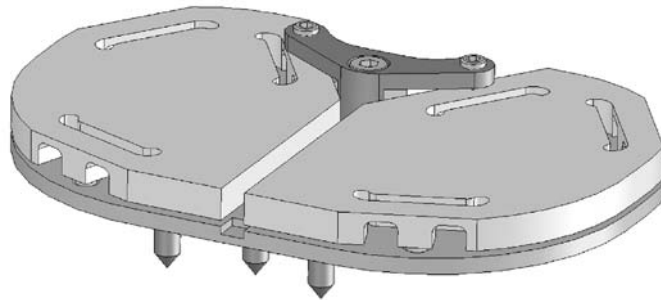
Figure 3.13: Fixation mechanism

A T-shape mechanical part allows the posterior medial bridge of each sensitive plate to be fastened to the tibial base plate.

forces located close to the lateral edge of the device. The same calibration model can be used since the only change is the sign of the output voltage reflecting the direction of the reaction force. In addition to extending the sensitive area, this fixation mechanism enables the sensitive plates to be rigidly fastened to the tibial base plate. Thus, the different parts constituting the device can be introduced as one piece into the knee, which improves the ergonomics of the device.

Spacers

As previously mentioned, a set of medial and lateral spacers are needed to adapt the device thickness to the patient-specific tibiofemoral gaps. From the engineer's point of view, the best solution would be to intercalate spacers between the tibial base plate and the sensitive plates. By doing so, the femoral condyles are directly in contact with the sensitive plates, thus ensuring an optimal output signal. However, this solution would significantly diminish the device ergonomics since the fixation mechanism would need to be replaced each time a thicker spacer is used. To overcome this disadvantage, spacers should be placed on the top of the sensitive plates. Particular attention must therefore be paid to the shape of the spacers and the material used to keep accurate measurements.

Thin adaptor spacers (2mm) are placed directly on the top of the sensitive plates to ensure a correct transmission of applied loads to the sensitive area (Fig.3.14). Medial, lateral and posterior cutouts allow accommodating the wires and the fixation mechanism. The bottom surface follows the contour of the sensitive area to enable the deformation of the sensitive plates. If these

adaptor spacers would lie on the bridges, applied loads would be withstood
by the reaction forces in the bridge pillars without producing any beam de-
formation. Two rectangular extrusions designed to fit in the sensitive plate
cutouts avoid rotations and translations of the spacer. Finally, the top sur-
face has an anterior elliptical extrusion which serves as an attachment point
for the additional block spacers (Fig.3.14). These latter have thicknesses
ranging from 1mm to 10mm. A posterior cutout allows accommodating the
fixation mechanism and a bottom anterior conical hole enables the block
spacers to be plugged into the adaptor spacers.

(a) Top view   (b) Bottom view
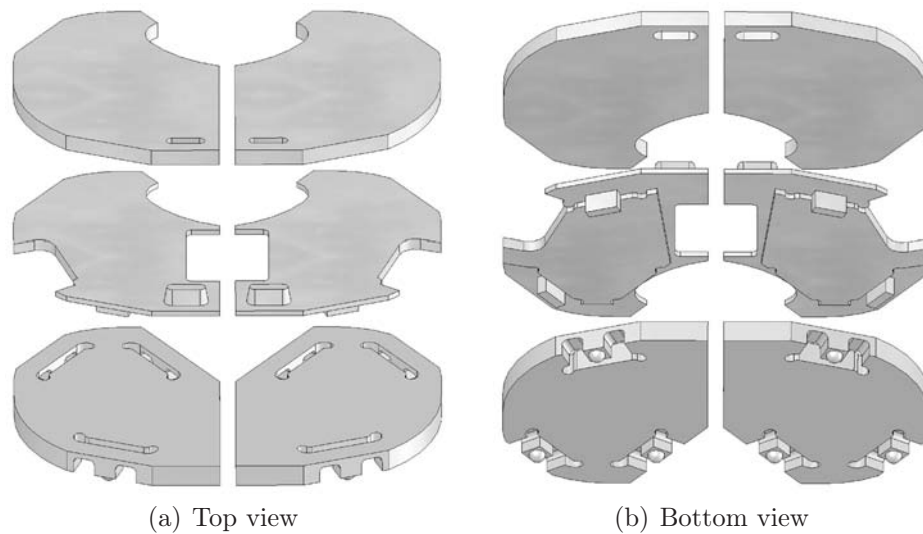
Figure 3.14: Spacers

Thin adaptor spacers, onto which block spacers of different thicknesses can then be
plugged, are used to ensure a correct transmission of applied loads to the sensitive area.

The reliability of the load transmission through the spacers depend not only
on the geometry but also on the material used. To ensure an optimal se-
lection, the contact pressure distribution at the bottom surface of a spacer
was analyzed by FEM for different materials. The model consisted of a 5mm
thick spacer placed on a single sensitive plate. The contact condition was
carried out by a penalty method. The meshes of the spacer and the sensitive
plate were composed by 5931 and 4927 tetrahedron elements respectively,
with a length parameter of 1mm. A 100N vertical force was applied to the
top of the spacer, at the center of the sensitive area. The contact pressure
distribution was then calculated for four different materials: stainless steel,
aluminium, and polyethylene with a 10GPa or 1GPa Young modulus.

(a) Stainless steel

(b) Aluminium

(c) PE 10GPa

(d) PE 1GPa

Figure 3.15: Spacers made of different materials

Pressure distribution at the bottom surface of spacers made of stainless steel, aluminium, or polyethylene with a Young modulus of 10GPa and 1GPa.

The results are that hard materials, such as stainless steel or aluminium, hardly deform and the main contact points are located at the border of the contact area (Fig.3.15). This situation should be avoided since high stress concentrations would be generated close to the measurement bridges. With softer material, such as polyeth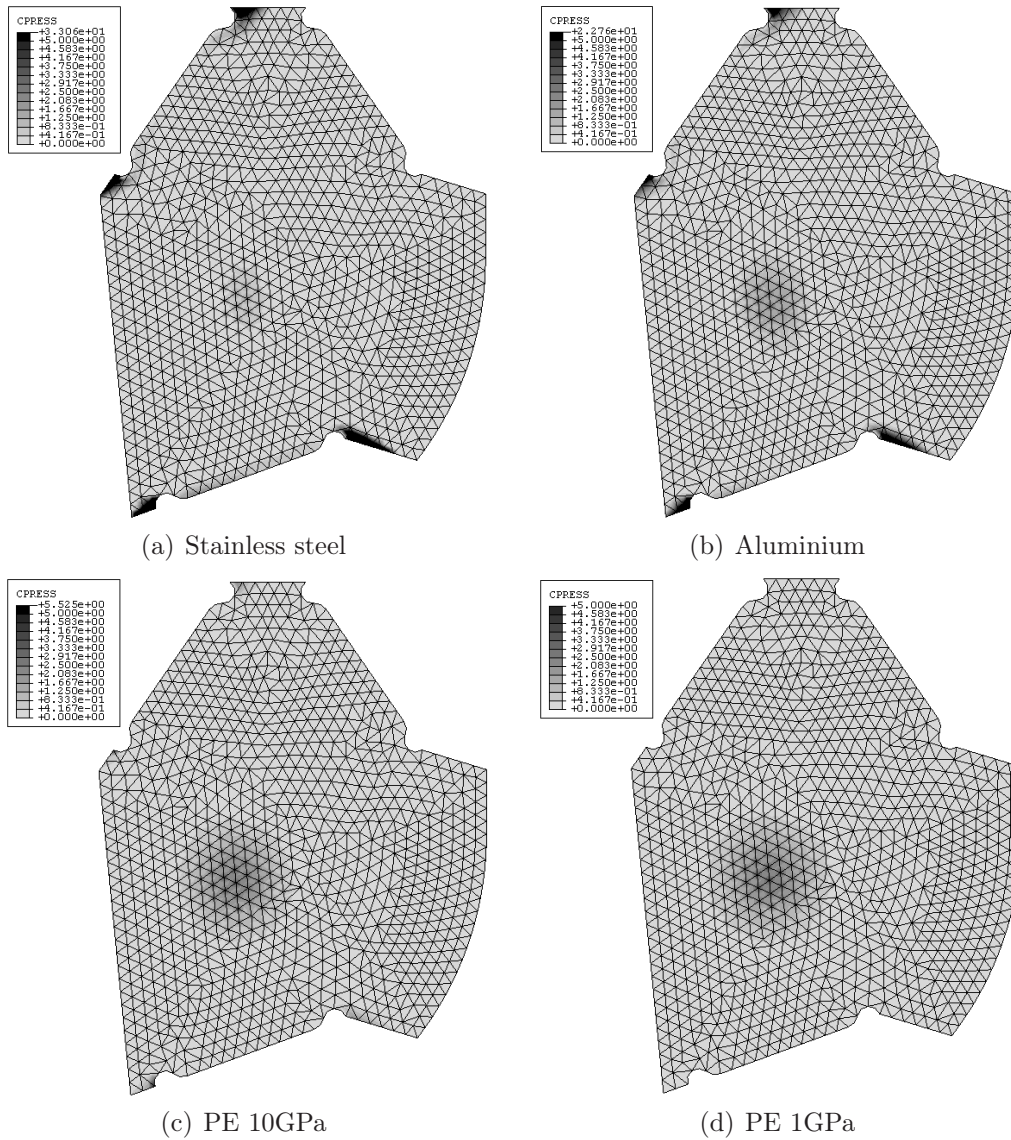ylene, the spacer deformation is much larger. Thus, a circular contact area, whose center corresponds to the point of application of the load, can be observed and the pressure concentrations close to the bridges disappear. Spacers must consequently be made of polyethylene or other biocompatible materials with similar mechanical properties.
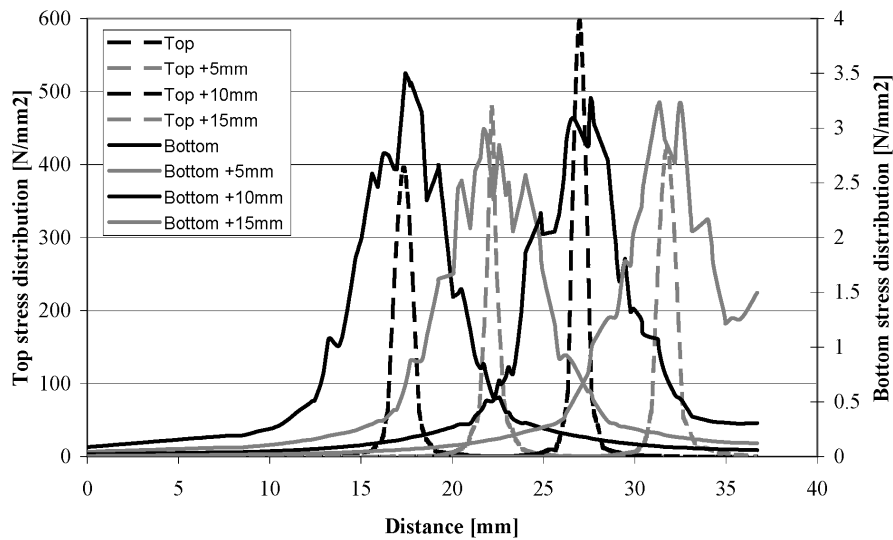
Figure 3.16: Variation of stress distribution

Comparison between the top and bottom surface stress distribution when the applied load is being laterally shifted.

Finally the issue of accuracy loss due to spacers must be addressed. The precision of the force amplitude measurement should not be affected since the device provides an integral measurement, which is by definition independent on the force distribution. However, one may imagine that intercalating spacers between the femoral condyles and the sensitive plates can reduce the accuracy of the force location measurement. As the force-sensing device measures the location of the gravity center of applied loads, accuracy loss for the position measurement should not happen as long as the gravity centers of the stress distributions on the top and bottom surfaces of the spacers are the same. To verify that, the stress distributions were compared for a

100N load being shifted from the center to the border of the sensitive area by steps of 5mm. For each step, the gravity center calculated by the FEM software was identical for the top and bottom stress distributions. Fig.3.16 also demonstrates this equivalence in a graphical way: the symmetry center of the stress variation along a horizontal axis is the same for both distributions. Therefore, no accuracy loss due to the intercalation of spacers should be expected.

To conclude this chapter, the design of the complete device is shown in an exploded three-dimensional view (Fig.3.17).

Figure 3.17: Complete device
Exploded three-dimensional view of the complete device

Chapter 4

Thick-film piezoresistive sensors

4.1 Piezoresistive effect

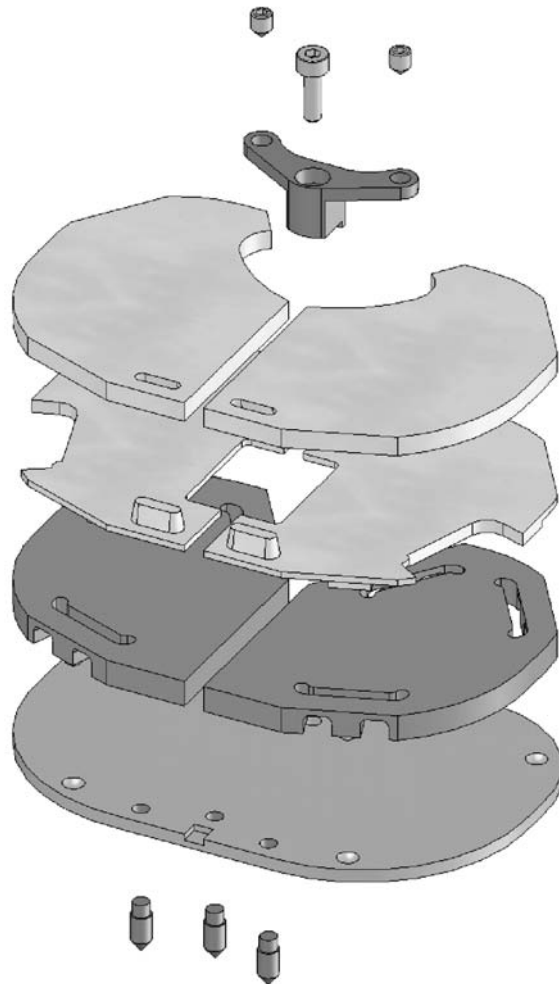By definition, piezoresistive sensors are elements whose resistance varies in response to a mechanical stimulation. They can therefore be considered as strain gauges, akin to metallic gauges, whose principle has been shortly explained in section 3.2.3. A more elaborate technique is nevertheless used in order to obtain a higher strain sensitivity as well as a good quality of the gauge bond to the substrate, usually a source of difficulties and errors with foil gauges. A thick-film piezoresistive bridge, directly screen-printed and fired onto the steel substrate, was used. The sensing thick-film resistors are typically composed of 85% of glass ($PbO - SiO_2 - B_2O_3 - Al_2O_3$) and 15% of conductive oxide particles (RuO_2 and $Pb_2Ru_2O_6$). After sintering, the resistor material consists of an insulating glass matrix, in which the conductive particles form a percolating network. Charge transport between adjacent particles is governed by tunnelling through a very thin (ca. 1nm) insulating layer. The interparticle resistance depends directly on the average distance d separating two charged particles. Therefore, when the sensor is strained, the average distance d is modified and the resistance varies accordingly. The tunnelling effect and the local strain inhomogeneity [48, 49] account for the relatively high sensitivity ("gauge factor") of thick-film resistors, ca. 12 vs. ca. 2 for metal gauges.

A thick-film sensing bridge on steel requires at least three different materials: the insulating dielectric, the conductor and the piezoresistor. Usually, a fourth protective glassy layer is applied over the circuit to improve chemical and electrical stability.

4.2   Thick-film technology

To produce thick-film sensors, the screen printing technique is used, whereby the thick-film materials, formulated in paste form (active material, binder, solvent and additives), are printed onto the substrate through a screen which defines the pattern. A typical thick-film screen is a fine metallic mesh mounted on a frame and coated by a photosensitive emulsion. The electronic pattern is printed on a transparent page and transferred to the thick-film screen by an ultraviolet light exposition. The screen, which has now open and closed areas defining the desired pattern (Fig.4.1(a)), is mounted on a screen-printing machine at a distance of about 0.5mm from the substrate. A squeegee pushes the thick-film paste over the screen, and thereby dispenses a well-defined amount of paste onto the areas of the substrate defined by the screen (Fig.4.1(b)). The paste is then dried at 150°C to eliminate the solvents, allowing further printing operations. After printing and drying one or several layers, the thick-film materials are fired in an oven, using a temperature profile having typically a ten-minute plateau at 850°C (Fig.4.1(c), 4.1(d)). Note that the thick-film process is not only used with piezoresistive elements but also in a wide range of applications involving piezoelectric, capacitive, photovoltaic, thermal, magnetic or chemical sensors [50, 51].

Thick-film piezoresistive sensors are usually printed on ceramic substrates such as alumina, due to their thermal stability and chemical inertness [52]. However, the use of ceramic substrate has several limitations such as a poor machinability, the incapacity of withstanding high strain or the brittle nature of ceramic. In the nineties, stainless steel was successfully used as a substrate [53, 54, 55], thus opening the way to more robust and precise metal-based applications. Current developments are focused on reducing the firing temperature of thick-film pastes to allow employing substrates with excellent mechanical properties, such as titanium [56], while examining the effect of the substrate (thermal and chemical properties) on the resistive and piezoresistive behavior [57, 58, 59].

4.3   Mechanical properties

A current drawback of thick-film technology on steel is the high required firing temperature (850°C), which is not compatible with most steel strengthening mechanisms such as cold work, martensitic transformation or precipitation hardening. Therefore, a nitrogen-containing biocompatible austenitic stainless steel was used: Sandvik Hi-N, where the nitrogen content imparts a

(a) Thick-film screen

(b) Paste deposition

(c) Oven
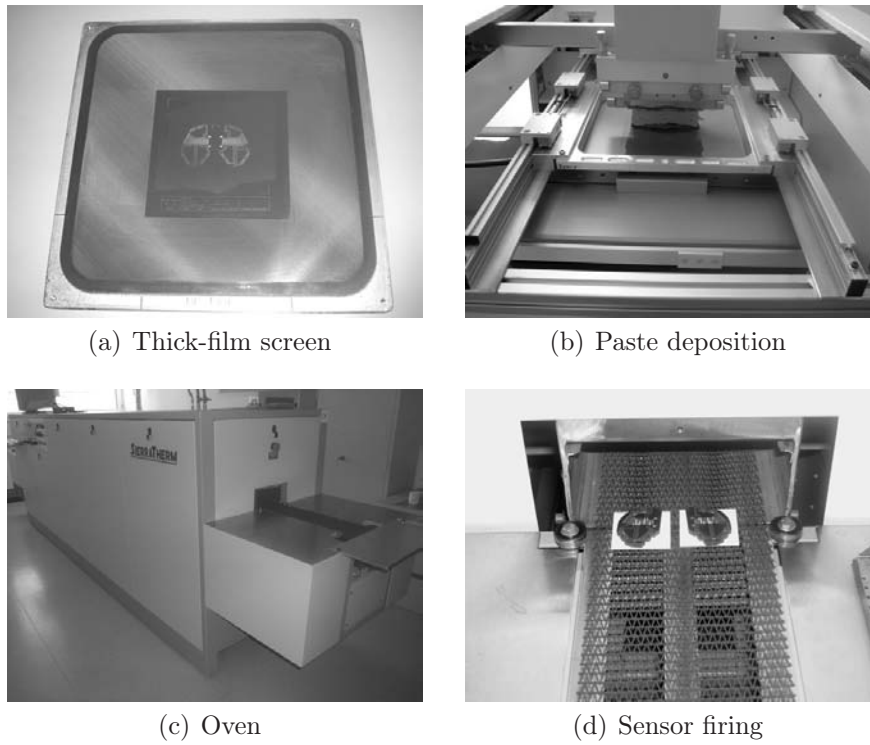
(d) Sensor firing

Figure 4.1: Screen printing process

considerable solution strengthening effect, which is not affected by the thick-film firing process. To test the compatibility between the selected steel and the thick-film piezoresistive sensors, deformable membranes have been manufactured (Fig.4.2(a)). Such pressure sensor is a reference device for material characterization of the Laboratoire de Production Microtechnique, EPF Lausanne, Switzerland, the collaborative institute in charge of the production of the sensors.

Different pressure magnitudes were applied stepwise on the membrane generating radial stresses (σ_r) up to 600MPa. The relative signal drift reported in figure 4.2(b) is lower than 0.1% for all the applied stresses. The softer stainless steel DIN 1.4435, from which is branched off the biocompatible steel DIN 1.4441 used for numerous surgical tools such as scalpels, pliers or chisels, has standard mechanical properties and is presented in the diagram for comparison. The obtained result demonstrates the proper functioning of the device and therefore the compatibility of the technique with the selected stainless steel.

(a) Deformable membrane

(b) Signal drift

Figure 4.2: Deformable membranes

4.4   Custom low-temperature dielectric

Due to the high coefficient of thermal expansion (CTE) of the austenitic Sandvik Hi-N steel ($16.5 \ 10^{-6}/°C$), delamination due to thermal mismatch with the thick-film l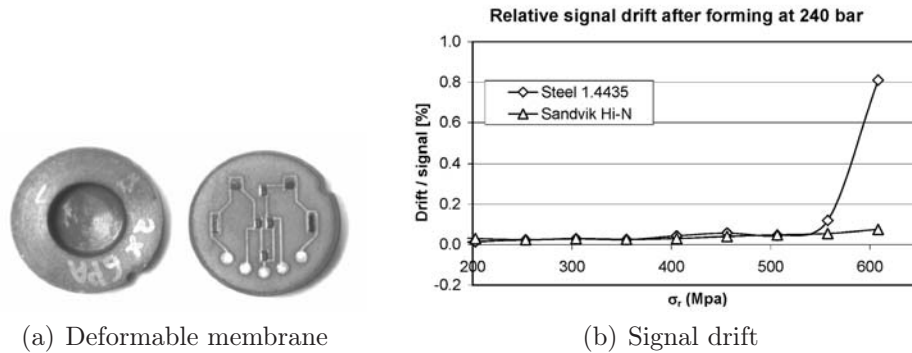ayers may occur during the cooling phase following firing. Extensive problems were not observed on the simple membranes described in the previous section, which only comprise a dielectric - conductor - piezoresistor sequence, although local chipping at the edges of the printed dielectric layer indicated extensive compressive stresses. Our force-sensing device, however, is more complex than the membranes and requires additional dielectric and conductor layers to allow electric cross-overs. The resulting stress build-up proved fatal to the devices: extensive spallation in the thick-film circuits occurred in these cross-over zones.

Therefore, cross-overs were made with different materials: a commercial low-firing fritted silver conductor, together with a special low-stress dielectric developed at EPFL. This low-firing dielectric consists of a dispersion of alumina powder in a low-melting lead borosilicate glass having a high CTE. The high CTE, together with the low softening temperature, results in very little additional stresses being developed in the cross-overs: no spallation was observed with the new materials. One must note that the present state of thick-film technology does not allow the use of these materials for the main insulating dielectric layer between the steel and the sensor circuit.

Chapter 5

Calibration and intrinsic accuracy

5.1 Calibration method

The calibration of a sensitive plate consists in establishing the numerical relationship which converts the three measured voltages (M_1, M_2, M_3) into the corresponding location (x, y) and amplitude (F) of the applied force. The calibration model results directly from equation (3.9), which describes the measurement principle of the device, and is expressed by:

$$
\begin{aligned}
F &= C_{11}M_1 + C_{12}M_2 + C_{13}M_3 \\
x &= \frac{C_{21}x_1C_{11}M_1 + C_{22}x_2C_{12}M_2 + C_{23}x_3C_{13}M_3}{C_{11}M_1 + C_{12}M_2 + C_{13}M_3} \\
y &= \frac{C_{31}y_1C_{11}M_1 + C_{32}y_2C_{12}M_2 + C_{33}y_3C_{13}M_3}{C_{11}M_1 + C_{12}M_2 + C_{13}M_3} .
\end{aligned}
\qquad (5.1)
$$

The three first calibration coefficients (C_{11}, C_{12}, C_{13}) correspond to the proportionality factor existing between the output voltage and the reaction force amplitude of each bridge. The six last coefficients quantify the deviation of the experimental reality from the theoretical model in the x (C_{21}, C_{22}, C_{23}) and y (C_{31}, C_{32}, C_{33}) directions. In an ideal case, they should be 1.

To determine these nine coefficients, 16 points of measurements are used: four loads evenly distributed in the range 0-500N and four locations evenly distributed on the sensitive area. As the determination of the six last calibration coefficients depends on the three first, the computation based on a least square method is performed in two steps. Table 5.1 shows an example of a typical calibration matrix. As the most important deviation of the six last coefficients from the ideal value of 1 is 5% only, the calibration model is

considered correct and appropriate.

4.757	4.508	4.580
1.009	1.007	1.006
1.048	0.998	1.000

Table 5.1: Example of a calibration matrix

5.2   Intrinsic accuracy

The intrinsic accuracy of the device was evaluated by loading the sensitive area with 18 weights ranging from 0N to 500N, applied at 20 different locations evenly distributed (Fig.5.1). The positioning of the tip of the mechanism supporting the weights was controlled by a micrometer table (Fig.5.2). For each location, the different weights were applied incrementally.
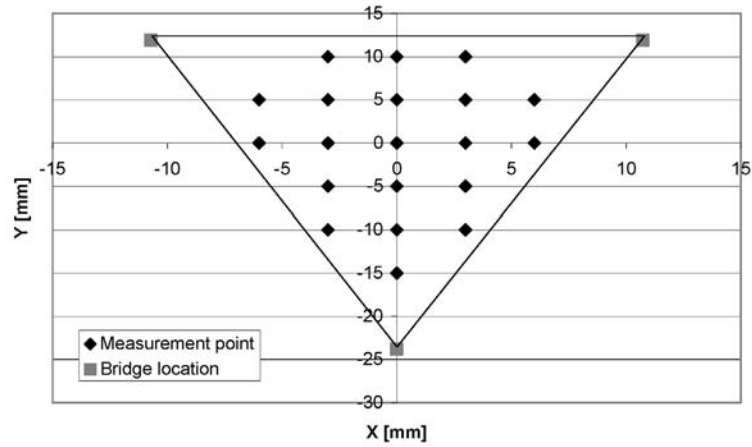
Figure 5.1: Measurement points for the accuracy study

Figure 5.3 compares the measured force amplitudes and applied weights. The close-to-one slope (1.0009) and confidence parameter (1) of the linear regression validates the measurement principle and demonstrates the absence of systematic errors. The absolute difference between the measured and applied loads and locations are shown in the figures 5.4(a), 5.4(b) and 5.4(c). The maximum force amplitude and location error among the 360 measurements were 2.6N and 0.8mm, whereas the mean absolute errors were 0.7N
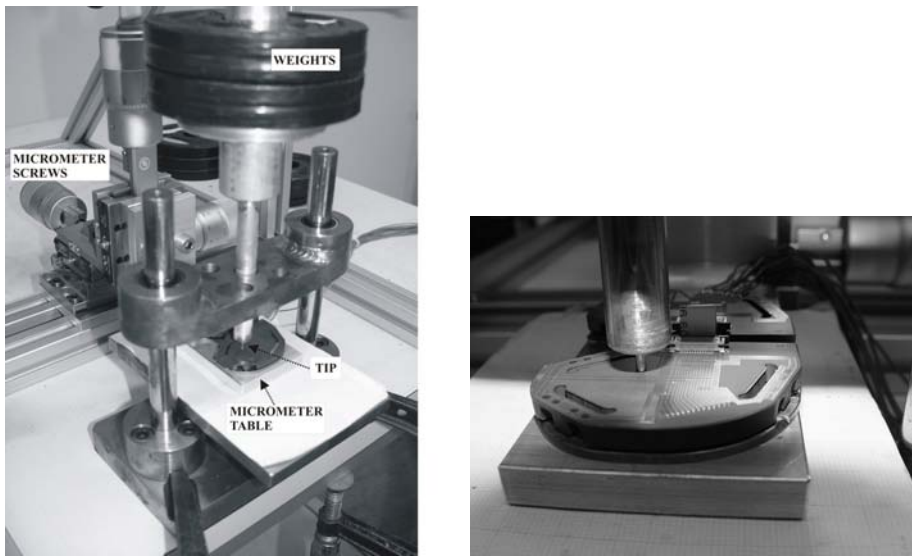
Figure 5.2: Set-up used for the accuracy study

and 0.3mm respectively. Note that the location measurement error decreases with increasing load. Since the location computation is based on a ratio between the bridge voltages, the larger each voltage is, the better defined is the ratio. The error of the applied weights (0.01N) and locations (0.001m) being

Figure 5.3: Force amplitude vs applied weight

negligible, the measured deviations characterize the intrinsic accuracy. The device thus offers an 0.5% full scale accuracy for the force amplitude measurement and a submillimeter accuracy for the force location. Such accuracy is comparable to that of various commercial force-sensing devices based on strain gauge technology and can be considered as excellent.
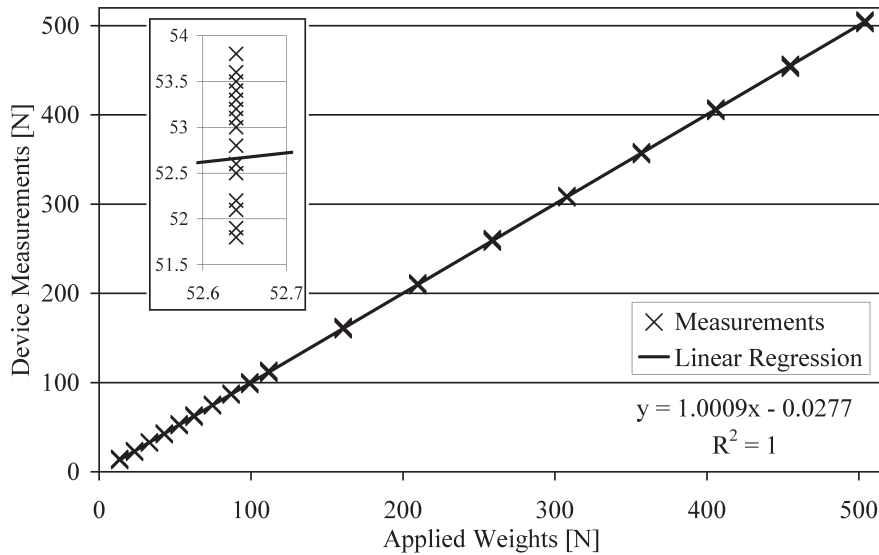
Since the passive compression forces of a human knee joint are expected to be below 100N, a specific calibration can be performed to decrease the force amplitude measurement error in this range. The coefficients obtained from the calibration of the same prototype with four loads ranging from 0N to 100N instead of 0N to 500N are summarized in table 5.2 and are consistent with their equivalent in table 5.1. Furthermore, the coefficients characterizing the deviation from the calibration model are again very close to the ideal value of 1, thus confirming the soundness of the calibration procedure.

4.796	4.568	4.465
1.024	1.008	1.004
1.037	1.001	1.000

Table 5.2: Calibration matrix for the range 0-100N

Figures 5.5(a), 5.5(b), 5.5(c) show the absolute difference between the measured and applied loads and locations with the new calibration. This time, the maximum force amplitude and location error were 5.6N and 0.8mm, whereas the mean absolute errors were 1.0N and 0.3mm respectively. As expected, the location measurement errors were not affected by the new calibration while the force amplitude error decreased in the range 0-100N and increased in the range 100-500N. However, the mean force amplitude error remains comparable to that previously computed, thus demonstrating that changing the calibration range amounts to redistributing the total error. With a maximal measurement error of 1.5N in the range 0-100N, the measurement accuracy of the force amplitude is below 2%, which is suitable for the intended application.
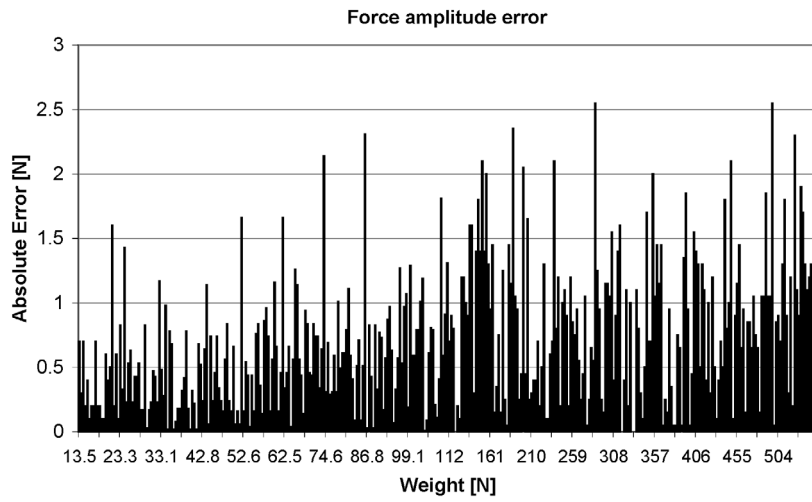
(a) Absolute force error
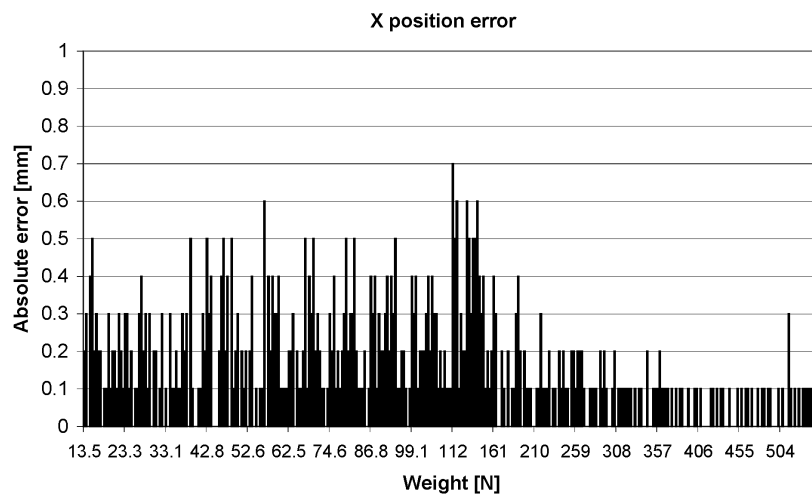
(b) Absolute x location error
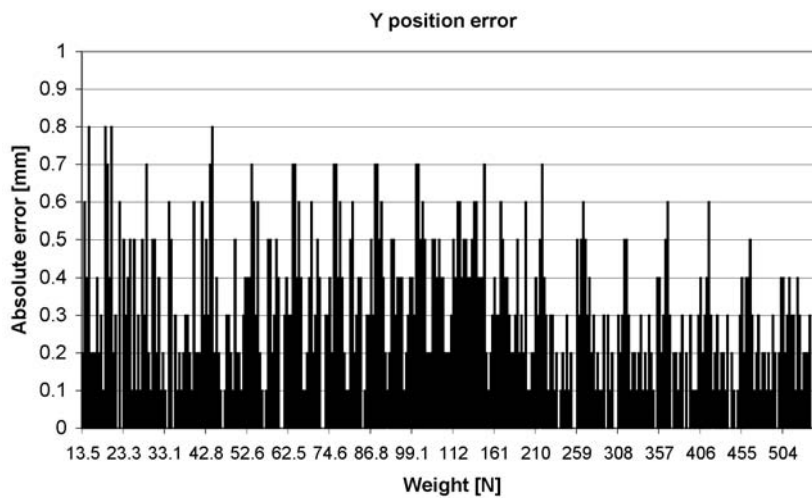
(c) Absolute y location error

Figure 5.4: Measurement errors with a calibration in the range 0-500N

(a) Absolute force error

(b) Absolute x location error

(c) Absolute y location error

Figure 5.5: Measurement errors with a calibration in the range 0-100N

5.3 Accuracy in the extended sensitive area

To verify the proper device functioning in the extended sensitive area created by the fixation mechanism (c.f. section 3.3.3), the intrinsic accuracy was also evaluated close to the lateral edge. The same experimental set-up as in the previous section was used. The device was loaded with 9 weights ranging from 0N to 100N applied at 15 different locati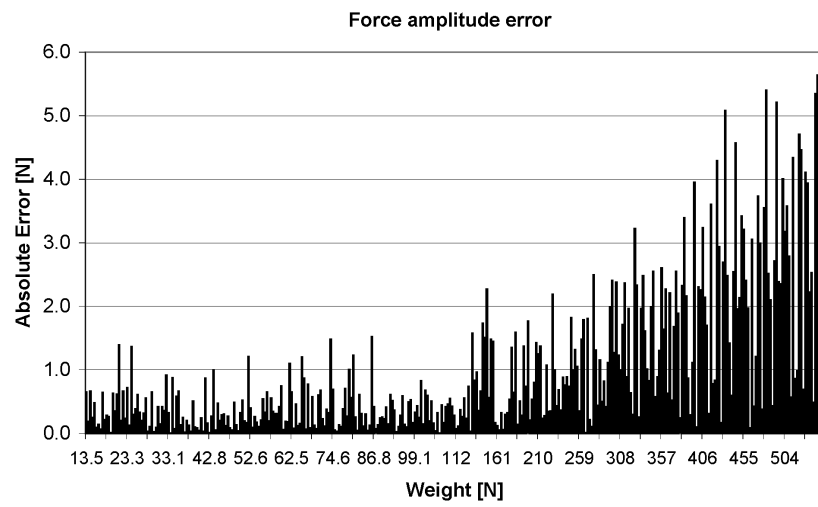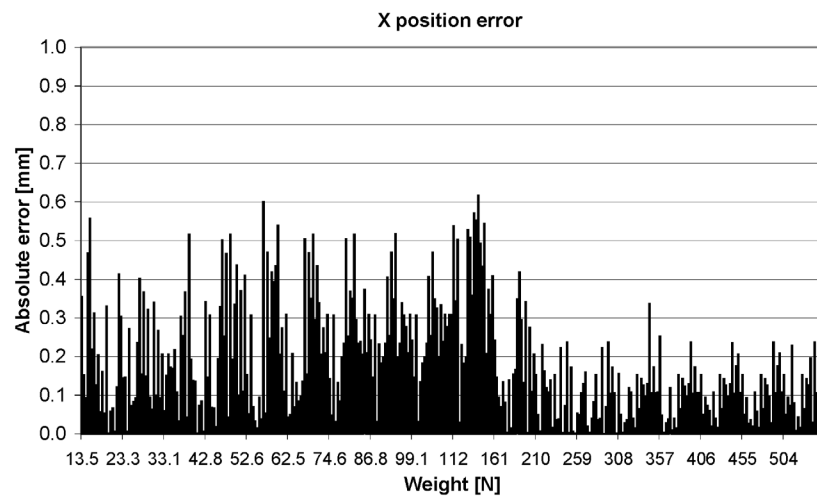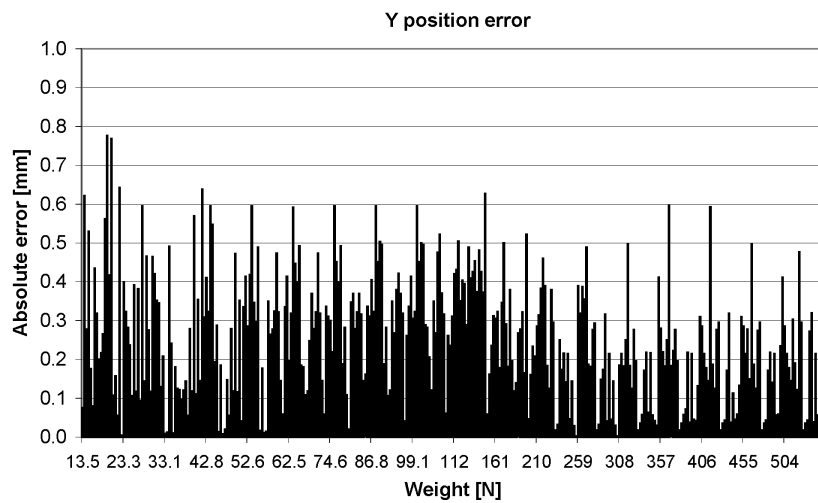ons evenly distributed in the extended sensitive area. Figures 5.6(a), 5.6(b), 5.6(c) show the absolute difference between measured and applied loads and locations. The maximal force amplitude and location errors were 1.8N and 1.2mm, whereas the mean absolute errors were 0.5N and 0.3mm respectively. With three values greater than or equal to 1mm, the accuracy of the location measurement is slightly diminished. However, these errors were observed only with small weights, i.e. at low output voltage, and did not affect the average measurement error. It can thus be concluded that the accuracy close to the edge of the device is equivalent to that in the center.

5.4 Accuracy with spacers

In section 3.3.3, where the design of the spacers is presented, it has been concluded that the measurement accuracy is theoretically not affected by the use of spacers placed on the top of the device. To verify that conclusion in practise, the device was loaded with four weights ranging from 0N to 100N, applied at five different locations, without spacer and with spacers of 5mm and 10mm thickness. The maximal error, i.e. the maximal absolute difference between the measured and applied loads, was determined for each measurement condition. Fig.5.7 shows that the use of spacers slightly increased the measurement error, which can be due to imperfect manufacturing or border effects creating an asymmetric load distribution around the point of application. However, with maximal errors of 1.4N and 1.1mm, the accuracy is still very satisfying and the ergonomic benefit of these top spacers are more important than the measured loss of accuracy.

5.5 Calibration and autoclave sterilization

Finally, the influence of sterilization on the calibration had to be evaluated. The device was loaded again with four weights ranging from 0N to 100N applied at five different locations before and after steam sterilization (121°, 100% humidity, 20min.). No difference in measurement errors was found (Fig.5.8), thus demonstrating the autoclavability of the device.
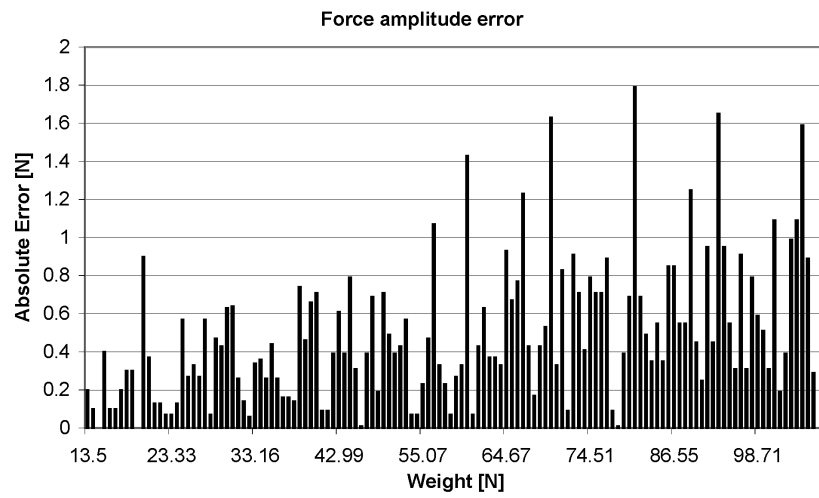
(a) Absolute force error
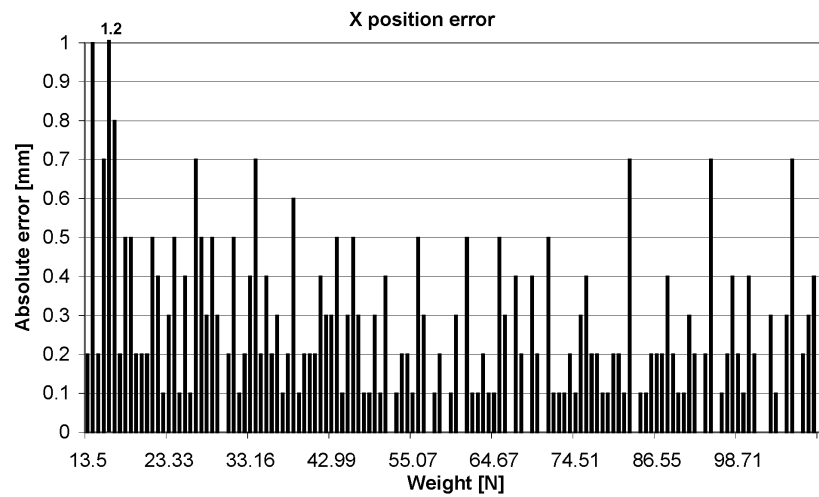
(b) Absolute x location error
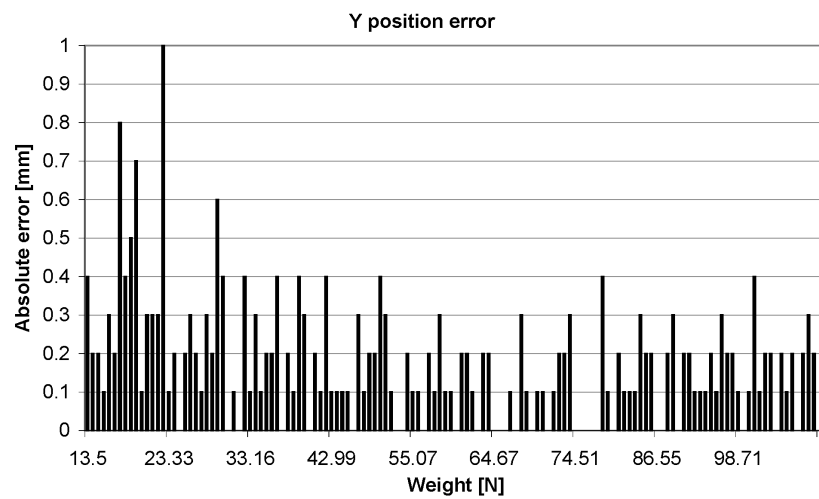
(c) Absolute y location error

Figure 5.6: Measurement errors in the extended sensitive area
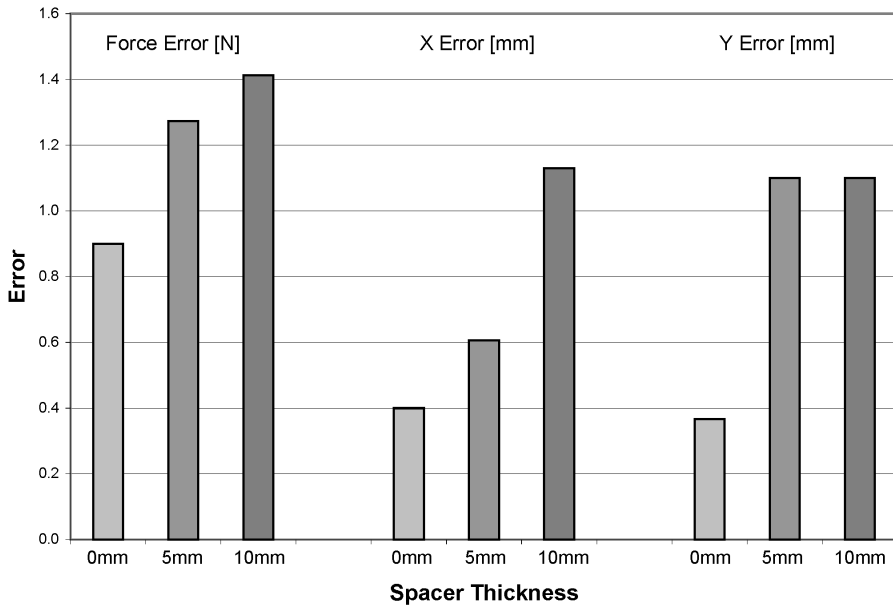
Figure 5.7: Accuracy loss due to spacers
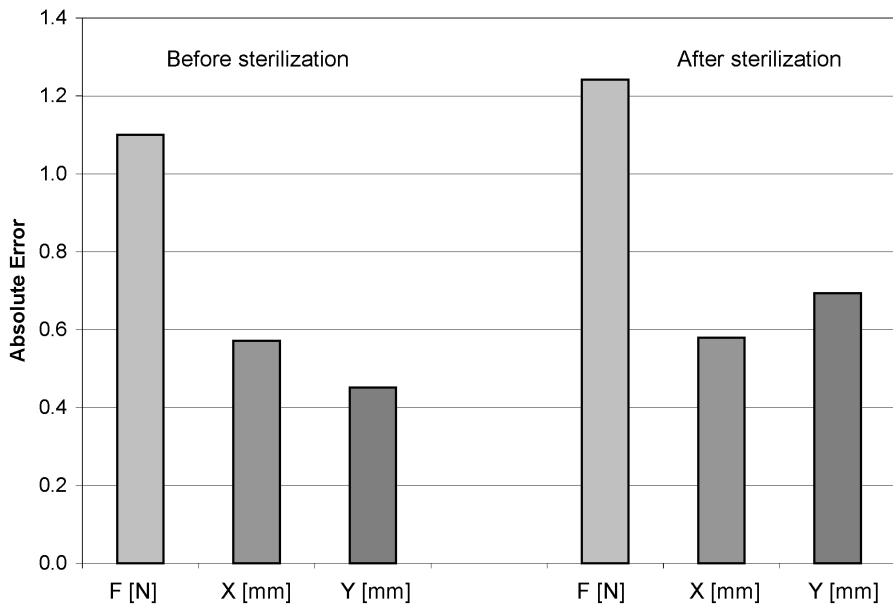
Figure 5.8: Influence of sterilization on the calibration

5.6   Plastic deformation

For safety purposes, the largest load the device can bear without being irreversibly damaged — that means the load causing a plastic deformation, a calibration loss and therefore a wrong diagnosis — had to be experimentally determined. To evaluate this effective elasticity limit, the force-sensing device was loaded with a series of forces ranging from 500N to 2000N by steps of 250N. These forces were applied at the gravity center of a sensitive plate by a 12cm diameter tip driven by a hydraulic testing machine, a 858 Bionix from MTS Systems Corporation, Eden Prairie, USA (Fig.5.9). For each step, the nominal force was reached with an average loading speed of 15N/s and was then sustained for 5s before releasing.
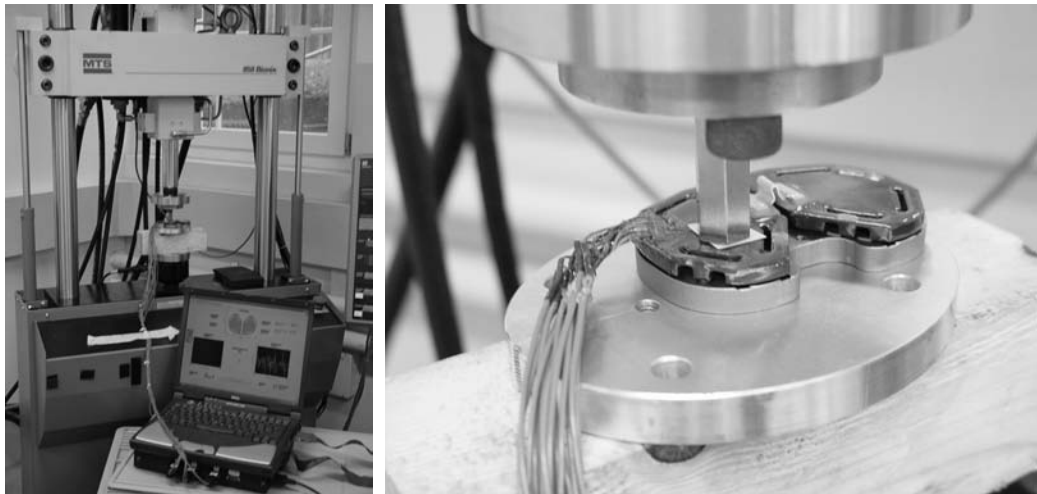
Figure 5.9: Set-up used for the plastic deformation test

Fig.5.10 compares the force amplitude measured by the load cell of the testing machine and by the device, while Fig.5.11 shows the signal drift, which corresponds to the difference between both. The device signal significantly deviated from the ideal elastic behavior with forces over 1500N. Considering the measurement range of the device (0-500N), the safety factor is 3, which is sufficient according to empirical designing rules.
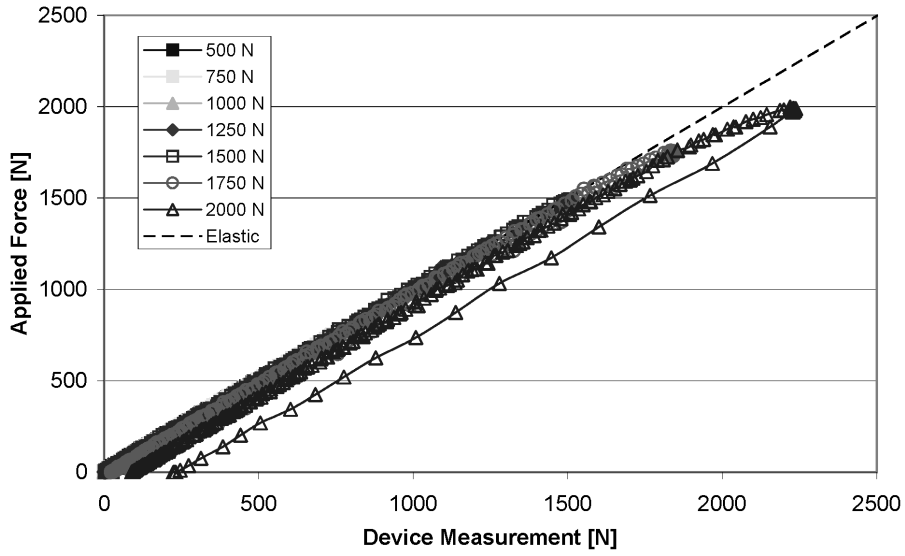
Figure 5.10: Comparison of MTS forces and device measurements
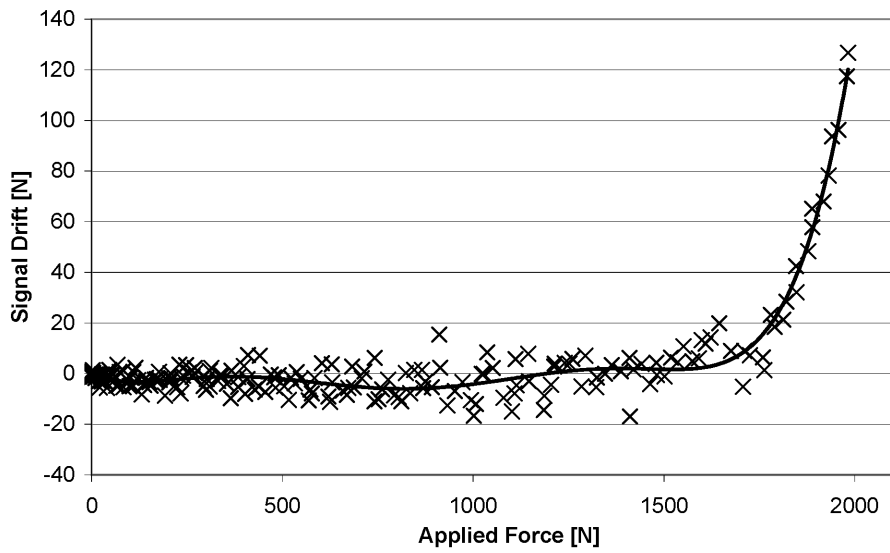
Figure 5.11: Signal drift during plastic deformation

In summary, the theoretical measurement principle was validated by the calibration procedure and the obtained coefficients. Furthermore, the 0.5% full scale accuracy and the safety factor of 3 meet the current industrial standards and makes the device reliable. The accuracy in the extended sensitive area and with the use of spacers is slightly reduced in practise, but still very satisfying for the application. Finally, autoclave sterilization does not influence the calibration. The device design has therefore been validated and the evaluation of its ability to help the surgeon in ligament balancing is now assessed with *in-vitro* studies.

Chapter 6

In-vitro study

Three different types of experiments were performed in order to validate the device design and to evaluate the biomechanical influence of different surgical actions, such as a patellar eversion or a ligament release, on the ligament balance.

6.1 Control experiment with a plastic model

To assess the suitability of the device for the purpose of ligament balancing, the prototype was introduced in a plastic knee joint equipped with adjustable springs. These latter simulated the collateral ligaments and the adjusting-screws of the side mechanisms allowed varying the spring tension (Fig.6.1). To validate that the varus-valgus moment measurements provided by our device agree with defined imbalances, different spring tensions representing ten levels of medial and lateral imbalance were applied. According to laws of mechanics, it exists a linear relationship between these spring tensions and the net varus-valgus moments of the tibiofemoral contact forces and the corresponding proportionality factor is the lever arm of the spring forces.

The expected linear relationship between the measured net varus-valgus moment of the contact forces and the spring tensions was experimentally verified (Fig.6.2). Furthermore, the measured proportionality factor (46mm) corresponded to the real lever arm (52mm) with a relative error of 13%. This deviation is due to the cumulative effect of the intrinsic accuracy of the device, the adjustment uncertainty of the spring tension and the play in the mechanical fixation of the springs. The agreement between the theoretical expectations and the effective measurements demonstrates the device suitability for imbalance characterization in a well-controllable environment.
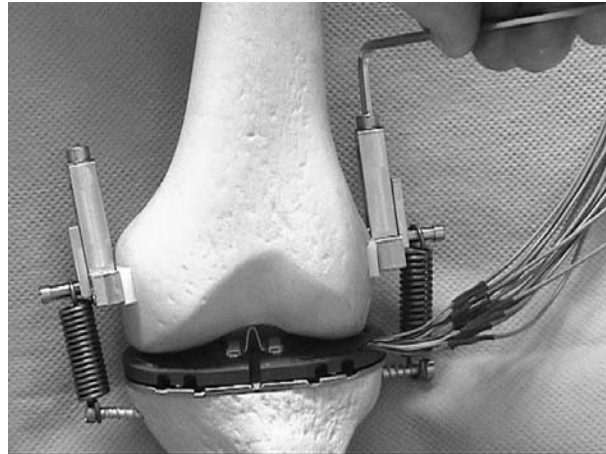
Figure 6.1: Plastic knee joint model

Adjustable springs simulated the collateral ligaments and the adjusting-screws of the side mechanisms allowed varying the spring tension
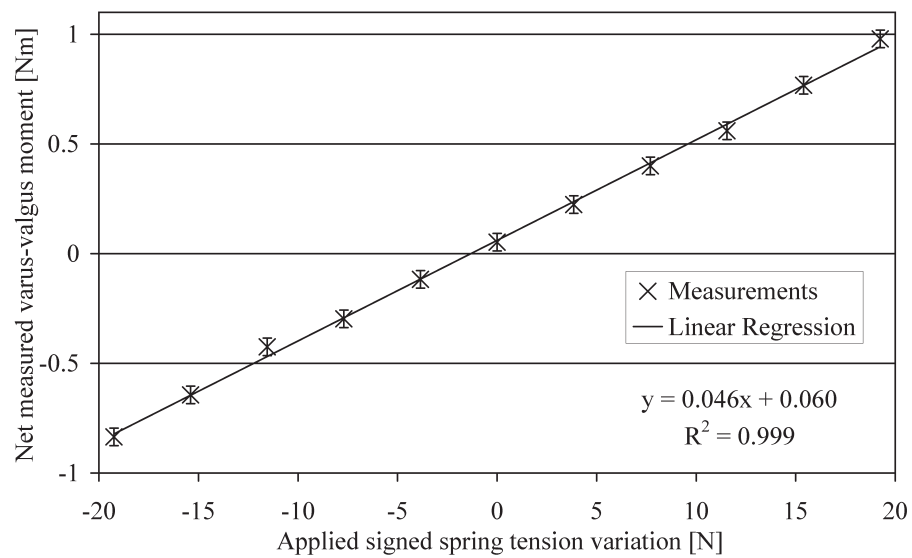
Figure 6.2: Imposed imbalances and measured varus-valgus moments

The expected linear relationship between the measured net varus-valgus moment of the contact forces and the spring tensions was experimentally verified

6.2 In-vitro trials

In order to verify the suitability of the range of measurement of the device and the consistency between the measurements and the surgeon's perception, the prototype was tested in two cadaver specimens.

In the first experiment, the device was installed in the knee gap after a tibial cut of about 6mm. The medial and lateral femoral contact forces and the net varus-valgus moment were measured during a ligament release procedure. When no external forces were applied, the measured contact forces ranged from 40N to 70N. When the surgeon manually applied varus-valgus loads comparable to those that would be applied during a standard TKA, the maximal contact force reached 350-400N. Thus, the measurement range of the device (0-500N) is appropriate. The surgeon then performed a medial ligament release guided by the device measurements until the net varus-valgus moment was reduced from an initial imbalance of 1.25Nm to 0.15Nm. The obtained ligament balance was qualitatively consistent with the surgeon's perception of a "balanced knee".

In the second *in-vitro* trial, the tibiofemoral forces and moments were measured in a balanced and imbalanced condition. Furthermore, five 90° knee flexions were performed with two different degrees of ligament balance, which were realized using a) a 3mm lateral and medial spacers and b) a 6mm lateral spacer and a 3mm medial spacer. According to the surgeon's judgment the second condition was better balanced than the first. In the balanced knee condition, a lateral and a medial force amplitude of 24N and 22N were measured. The relative difference of the respective varus-valgus moments was 6%. In the imbalanced condition, the lateral and medial force amplitudes were 36N and 9N, and the relative difference of the respective varus-valgus moments was 60%. These results indicate that device measurements reflect the surgeon's perception. The averaged forces and moments measured during the flexion experiments are shown in Fig.6.3. In agreement to the surgeon's opinion, the second condition exhibits a relative varus-valgus moment significantly closer to 0.

In conclusion, the range of measurement of the device is suitable and the measurements provided are in agreement with the surgeon's perception.
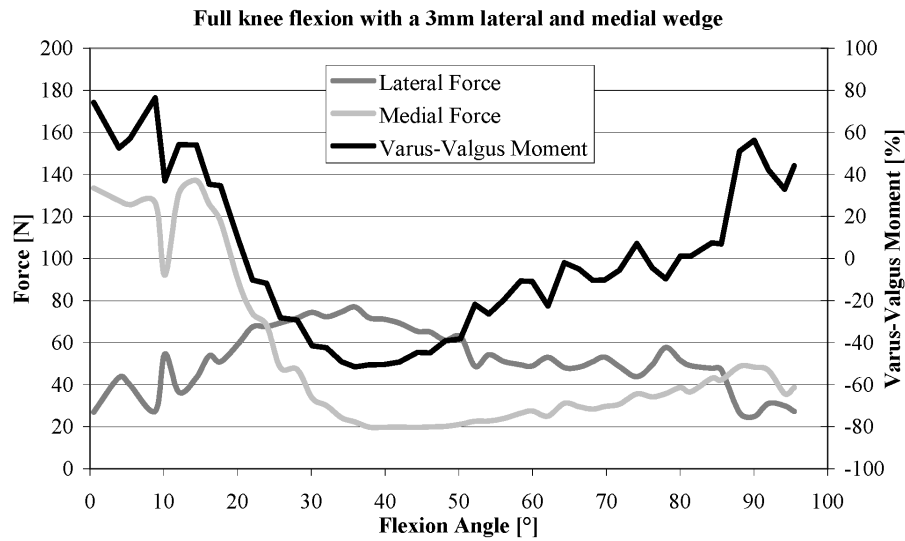
(a) Imbalanced
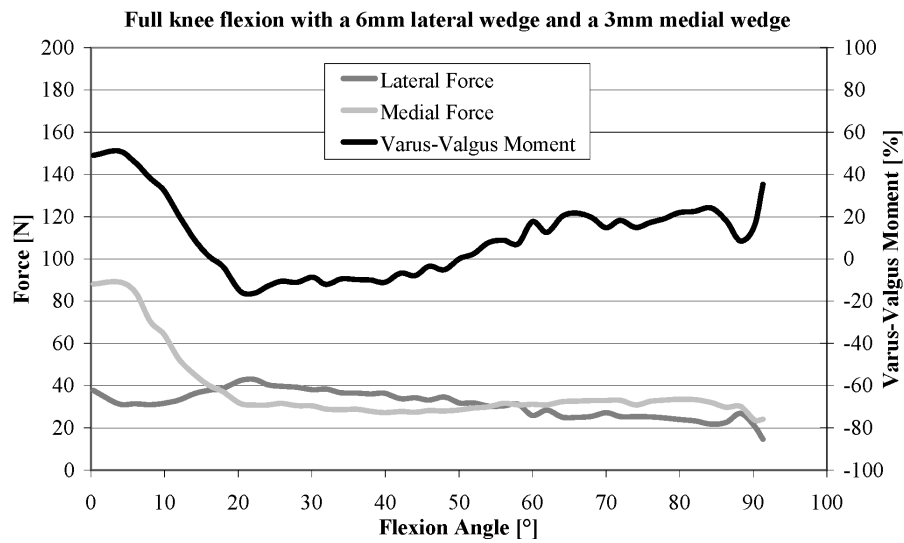
(b) Better balanced

Figure 6.3: Contact forces and moments during knee flexion

Tibiofemoral contact forces and varus-valgus moment during 90° knee flexions with two different degrees of ligament balance

6.3   In-situ evaluation

Following these promising preliminary experiments, a complete *in-vitro* study was carried out. The three primary goals were:

1. To evaluate the *in-situ* functioning and potential clinical advantages of the novel force-sensing device.

2. To identify the biomechanical parameter that the surgeon intraoperatively assesses during ligament balancing. Each measurement system described in section 2.4 and aimed at providing a quantitative measurement of the ligament imbalance measures a different biomechanical parameter: Winemaker [44] measures extension gaps, Morris et al. [41] compressive forces, Takahashi et al. [39] and Wallace et al. [36] pressure and finally Attfield et al. [35] angular deviations of a scale-like device. This indicates that there is no standard interpretation of what the surgeon intuitively calls ligament balancing in biomechanical terms.

3. To quantify the effect of collateral ligament release in terms of forces. Even though ligament release is a commonly used surgical action to correct imbalance, its biomechanical effect in terms of knee joint forces is poorly documented.

6.3.1   Method

The force-sensing device was tested in six human cadaver knees from donors with an average age of 82 years (63 to 90). The surgical preparation of each specimen consisted of the two first steps of TKA, i.e. accessing the joint with a medial parapatellar approach followed by the resection of the tibial plateau. The force-sensing device was then introduced (Fig.6.4) and the specimen mounted on a knee joint loading apparatus (Fig.6.5) previously described by Dürselen at al. [60]. This machine provides all the degrees of freedom needed for unconstrained knee motion and allows the monitoring of the relative angular position between the femur and tibia. Compression loads and varus-valgus moments can be applied by using a system of weights and pulleys. Additionally, quadriceps forces can be simulated by loading the patellar tendon with weights.

To validate the *in-situ* measurement of forces, the knee joint was first loaded in full extension with axial compressive weights ranging from 1kg to 15kg. The sum of the medial and lateral contact forces measured by the device,

(a) Before insertion   (b) Insertion

(c) After insertion
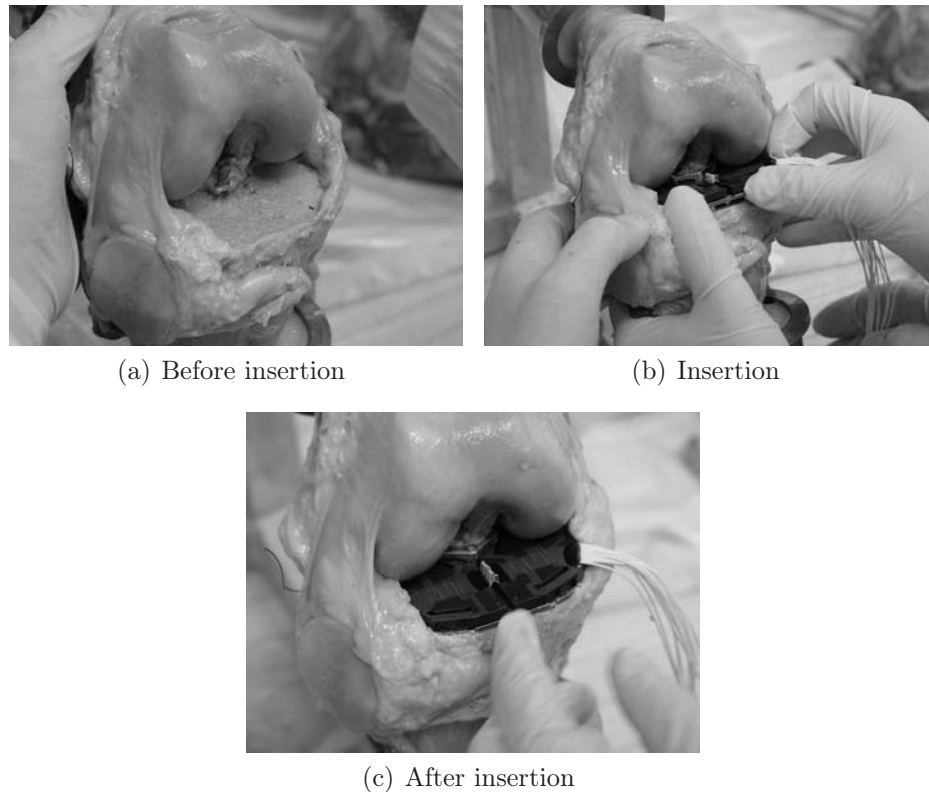
Figure 6.4: Device insertion

The insertion of the device into a knee joint is fast and easy. The elapsed between the
first and last picture was 1min.28s.

i.e. the total force transmitted through the tibiofemoral joint, was then com-
pared to the applied loads.

Since the possibility of having the patella in its anatomical place during the
measurement is claimed to be a major advantage, the effect of a patellar
eversion on the mediolateral distribution of the contact forces was evaluated.
The patellar tendon was loaded with weights ranging from 1kg to 5kg at 0°,
30°, 60° and 90° flexion with and without a patellar eversion. The relative
amounts of the applied load going through the medial and lateral compart-
ments of the knee joint were measured and compared for each position and
each condition (patella everted or not). As part of the load applied on the
patella tendon was transmitted parallelly to the tibial plateau, the measure-
ments were normalized by the perpendicular component to ensure compa-
rable data. The sum of the relative medially and laterally transferred loads
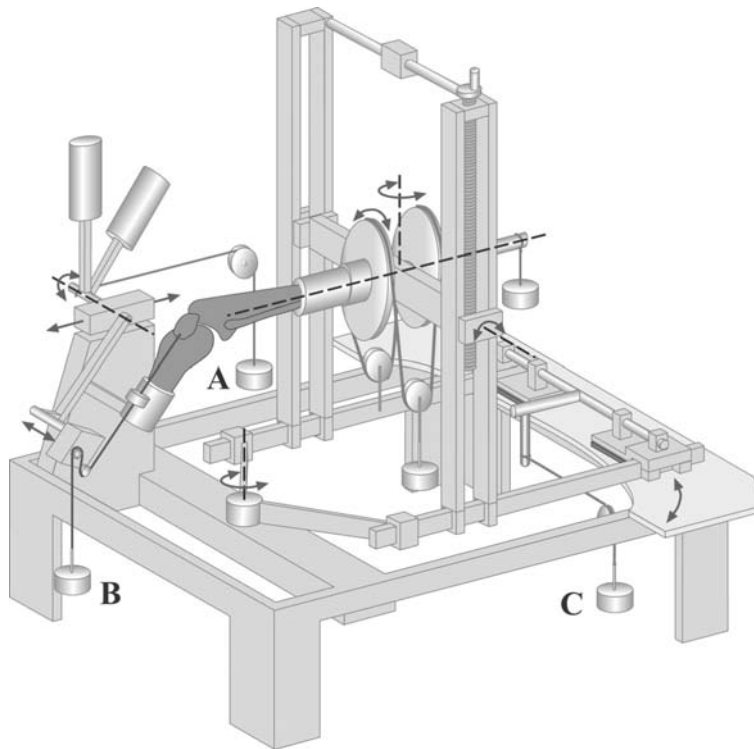
Figure 6.5: Knee joint loading apparatus

The arrows indicate the degrees of freedom of the machine, which allows unconstrained knee motion. Compression loading (A), quadriceps force simulation (B) or varus-valgus loading (C) can be carried out with a system of weights and pulleys.

then corresponds to 100%. The statistical significance was determined with a sign test for paired samples (Matlab, MathWorks Inc, Natick, United States).

The second part of the study aimed at identifying the biomechanical parameter that the surgeon assesses during ligament balancing. Intraoperatively, the surgeon manually compares the varus and valgus forces that must be applied at the ankle to create a lateral or medial condyle lift-off. With a simplified two-dimensional model (Fig.6.6), it can be theoretically demonstrated that this corresponds to a balancing of the medial and lateral condyle contact forces. The model considers the five major forces involved in the varus-valgus stability: the medial and lateral collateral ligament forces (F_{ML}, F_{LL}), the medial and lateral contact forces (F_{MC}, F_{LC}) and an external varus force (F_{EX}). The center of rotation, which in Fig.6.6 corresponds to the contact point of the medial condyle, is taken as the reference for the computation of

moments. In this model, bones are considered as rigid bodies and ligaments as springs, thus implying that ligament forces can be assumed constant at a given flexion angle as long as both condyles are in contact with the tibia. The tension in a spring-ligament would vary only when the joint starts to open, i.e. when one condyle lifts off.
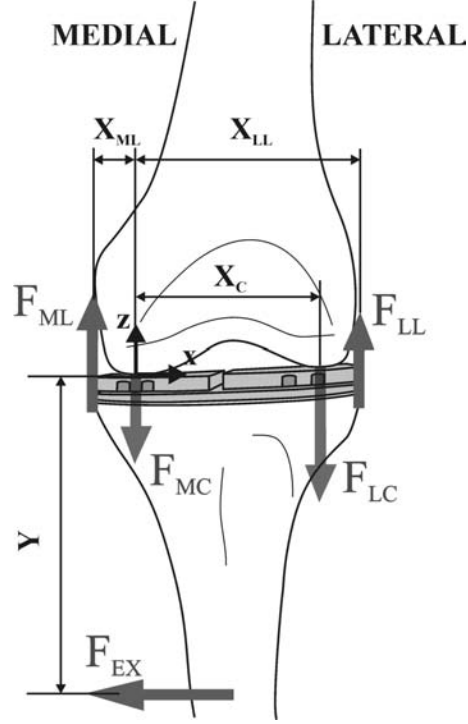
Figure 6.6: Varus-valgus loading model

A simplified two-dimensional biomechanical model of a knee joint experiencing varus or valgus load to create a lateral or medial condyle lift-off. The five major forces involved in the varus-valgus stability, which are the collateral ligament forces (F_{ML}, F_{LL}), the contact forces (F_{MC}, F_{LC}) and the external force (F_{EX}), are taken into account.

The equilibrium condition for the moments yields:

$$X_{ML} \cdot F_{ML} - X_{LL} \cdot F_{LL} + X_C \cdot F_{LC} + Y \cdot F_{EX} = 0 \qquad (6.1)$$

The resultant ligament moment M_{LIG} is:

$$M_{LIG} = X_{ML} \cdot F_{ML} - X_{LL} \cdot F_{LL} \qquad (6.2)$$

The contact force F_{LC} depends on the applied force F_{EX}:

$$F_{LC} = F_{LC}(F_{EX}) \qquad (6.3)$$

The combination of equations (6.1), (6.2), and (6.3) can then be written as:

$$M_{LIG} + X_C \cdot F_{LC}(F_{EX} + Y \cdot F_{EX} = 0) \tag{6.4}$$

When there is no external force applied ($F_{EX} = 0$), equation (6.4) gives:

$$M_{LIG} = -X_C \cdot F_{LC}(0) \tag{6.5}$$

When there is a varus load ($F_{EX} = F_{varus}$) that generates a lateral condyle lift-off ($F_{LC} = 0$), equation (6.4) gives:

$$M_{LIG} = -Y \cdot F_{varus} \tag{6.6}$$

The relationship between the varus load required for a condyle lift-off and the initial lateral contact force can be deducted from equations (6.5) and (6.6):

$$F_{varus} = \frac{X_C}{Y} F_{LC}(0) \tag{6.7}$$

The same approach can be adopted for the case of a valgus load and a medial condyle lift-off:

$$F_{valgus} = \frac{X_C}{Y} F_{MC}(0) \tag{6.8}$$

With equation (6.7) and (6.8) it can finally be concluded that the relative difference of the forces required for a condyle lift-off is equal to the difference of the contact forces:

$$Relative\,Imbalance = \frac{F_{varus} - F_{valgus}}{F_{varus} + F_{valgus}} = \frac{F_{LC}(0) - F_{MC}(0)}{F_{LC}(0) + F_{MC}(0)} \tag{6.9}$$

In order to experimentally validate this equivalence as well as to compare this approach to the device measurements, the relative imbalance was assessed on the basis of three different parameters: 1) the weights required for a condyle lift-off, 2) the contact forces and 3) the varus-valgus moments. The knee joint was therefore loaded with varus and valgus forces with weights increasing from 0kg to 1kg. If the condyle lift-off was not achieved before 1kg, larger weights were used. Since during the surgery the ligament imbalance is assessed in full extension and in 90° flexion, the experiment was performed in both positions.

In the third step, the biomechanical effect of medial collateral ligament releases was quantitatively evaluated. With interarticular spacers applying stress to the ligaments, a minor followed by a major medial collateral ligament release was performed with the knee in full extension. The medial and

lateral contact forces were recorded after each surgical action and compared to the initial value. In order to quantify the effect of the ligament release on the tibiofemoral alignment, the variation of the varus-valgus angle resulting from the releases was measured as well. Finally, the initial and ultimate contact forces were measured at 0°, 30°, 60° and 90° flexion to evaluate the effect of ligament releases throughout the knee flexion.

6.3.2   Results

All the curves obtained during the compression loading experiment were highly linear ($r^2 = 1.00$) and the measured slopes ranged between 0.96 and 1.03, thus being very close to the ideal value of 1 (Fig.6.7). The average difference between the applied and measured compressive force was 1.8N. Thus, the *in-situ* force measurements are accurate and repeatable.
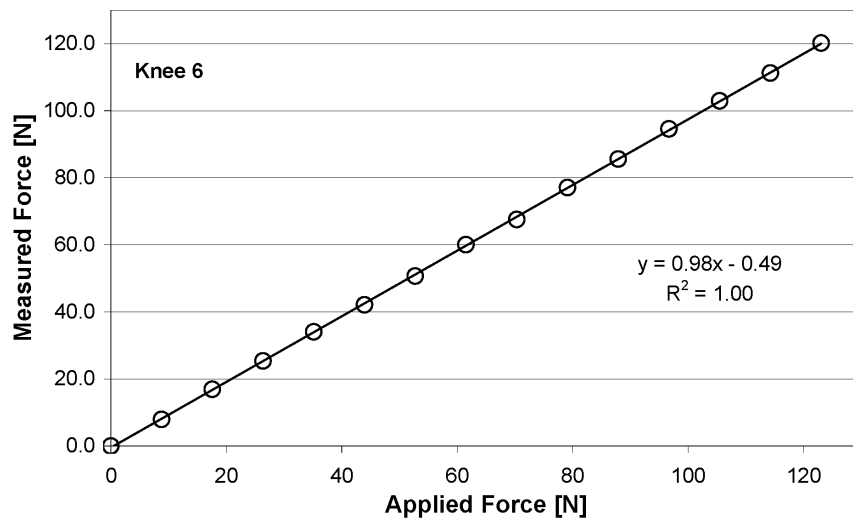
(a) Example of compression loading

	knee 1	knee 2	knee 3	knee 4	knee 5	knee 6
slope	1.03	0.98	1.03	0.96	1.00	0.98
y-intercept	-1.2	-1	-0.2	-1	0.3	-0.5

(b) Linear regression parameters

Figure 6.7: Compression loading experiment
a) Comparison between the measured and applied forces during the compression loading experiment for one specimen. b) Parameters obtained from the linear regressions, which demonstrate the accuracy and reliability of the *in-situ* force measurement.

In the patellar load distribution experiment, the relative amounts of the applied load going through the medial and lateral compartment of the knee joint were measured. The mediolateral load distribution did not vary considerably with knee flexion (standard deviations ranged from 3% to 8%), therefore the laterally transferred loads were averaged over the different knee positions. The mediolateral distribution of the patellar load was significantly different (p=0.03) when the patella was in its anatomical place or not: one fourth of the patellar load was shifted from the medial to the lateral side with a patellar eversion (Fig.6.8). Additionally, it can be noted that the patella in its anatomical place already influenced the mediolateral distribution of the contact forces since the average laterally transferred load was 62% without a patellar eversion.
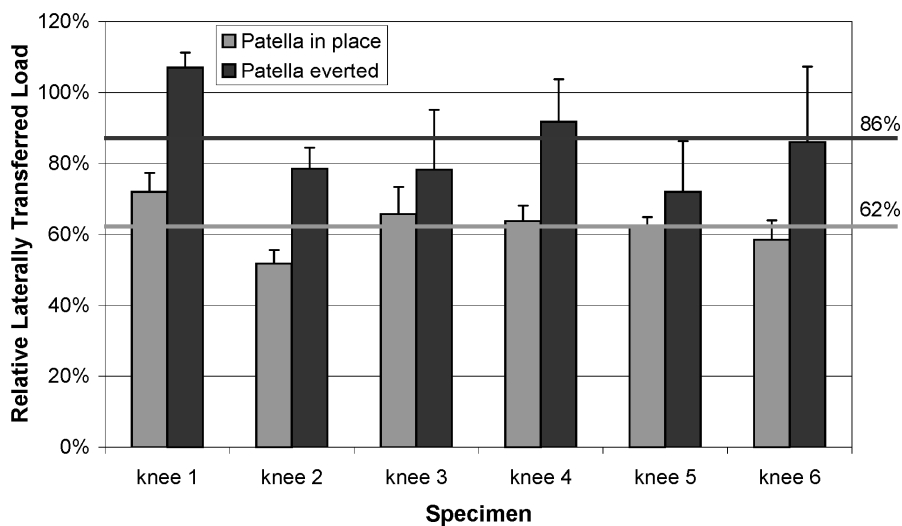
Figure 6.8: Effect of patellar eversion

Relative laterally transferred loads during the patellar load distribution experiment, showing that the patellar eversion significantly affected the mediolateral distribution of the contact forces. The grey and black horizontal lines correspond to the average loads with the patella respectively in place or everted.

A typical curve obtained during a varus-valgus loading (Fig.6.9) presents
three distinct areas: 1) the lateral condyle is in contact; 2) both condyles
are in contact; 3) the medial condyle is in contact. In each area, a linear
relationship between the applied and measured varus-valgus moments was
found. The slope was lower in the situation where only one condyle was in
contact than where both were.
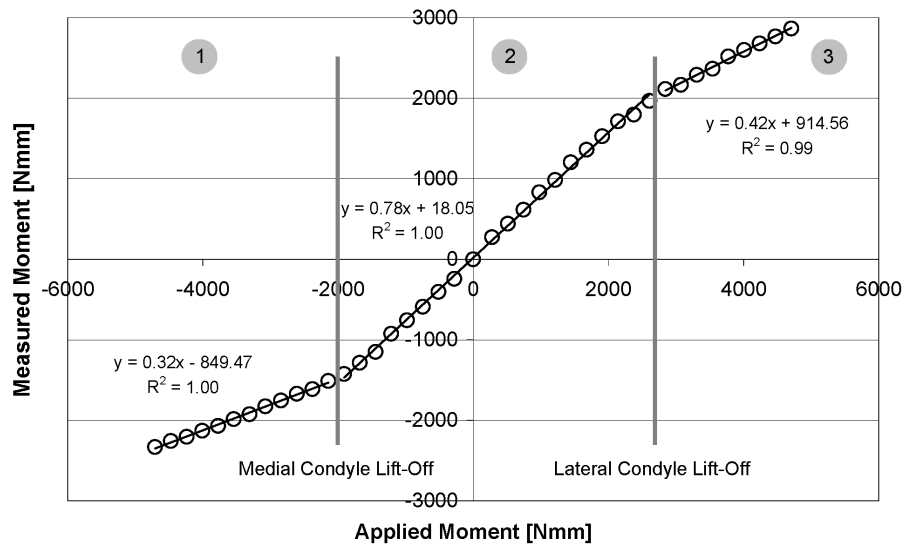
Figure 6.9: Varus-valgus loading experiment

Comparison between the applied and measured moments during varus-valgus loading,
where three different situations can be distinguished: 1. the lateral condyle is in contact;
2. both condyles are in contact; 3. the medial condyle is in contact. Each area presents a
specific linear relationship and the difference of the slopes expresses the different
contribution of the collateral ligaments in the situations where only one or both condyles
are in contact.

Based on these measurements, the varus and valgus weights causing a condyle
lift-off were determined to compute the normalized imbalance expressed in
equation (6.9). By definition, a positive/negative value is related to a lat-
eral/medial imbalance. The normalized imbalance based on the measurement
of contact forces or varus-valgus moments was computed in the same way.
The three approaches to assess the knee stability gave consistent diagnosis for
the majority of the specimens (Fig.6.10). Taken the weight-based assessment
as a reference (Fig.6.11), the force-based assessment has an average difference
of 0%, thus demonstrating the expected equivalence of the two approaches.

However, the moment-based assessment shows a tendency for lateral imbalance. Even though the average difference was small (6%), large differences were found in some cases, such as in the third knee. Similar results were obtained for the measurements performed in 90° flexion but with an average difference of imbalance of -4% and 7% respectively for the force-based and moment-based assessments. The statistical significance, which was again determined with a sign test for paired samples, was achieved at 90° flexion (p=0.03), but not in full extension (p=0.38).
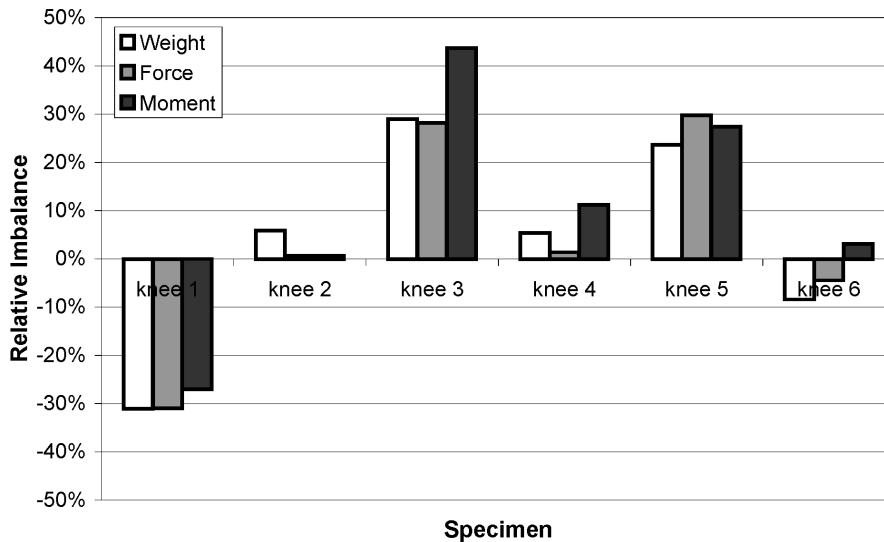
Figure 6.10: Comparison of imbalance assessment

Assessment of the relative ligament imbalance based on three different parameters: 1. the varus or valgus weights causing a condyle lift-off, 2. the contact forces and 3. the varus-valgus moments. The diagnosis given by the three methods were consistent.
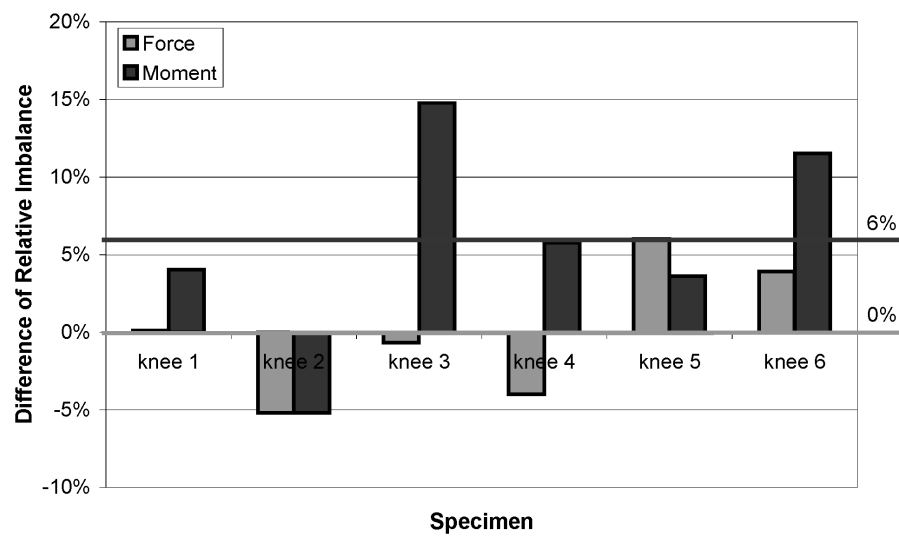
Figure 6.11: Difference of imbalance
The weight-based approach, which corresponds to the current surgical approach, is taken
as a reference. On average, the force-based approach was equivalent (0%) while the
moment-based approach showed a slight lateral imbalance (6%).

Finally, the minor and major medial ligament releases reduced the medial contact force in full extension by 20% and 46% on average (Fig.6.12). The large standard deviations, 19% and 25%, demonstrated the high variability of the biomechanical effect of a ligament release among the specimens. The lateral contact force was just slightly influenced by the medial ligament releases (Fig.6.13), since an average increase of 9%, which is only one fifth of the reduction on the medial side, was measured. For all specimens, the variation of the varus-valgus angle was below 0.2°, which is not clinically relevant. This indicates that the ligament release did not substantially modify the tibiofemoral mechanical axis. Finally, the effect of ligament releases varied strongly along knee flexion, being less relevant at 30° and 60° than in full extension or 90° flexion (Fig.6.14).
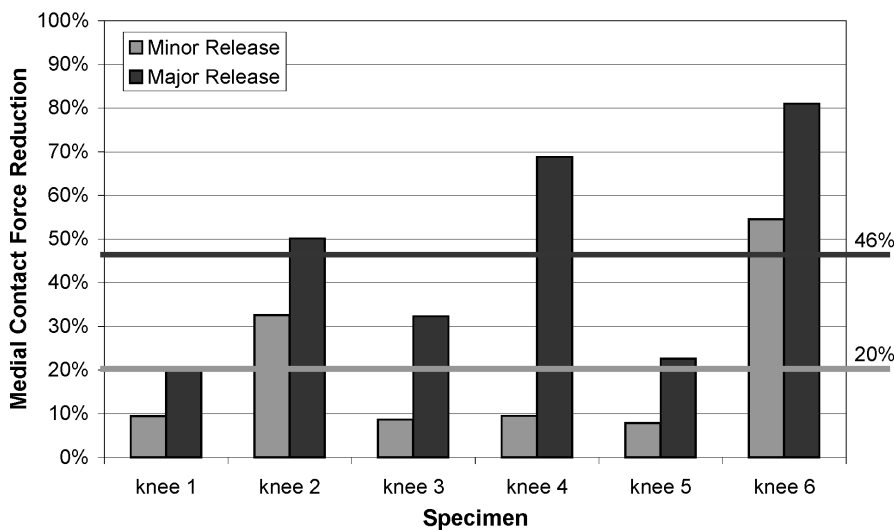
Figure 6.12: Medial contact force reduction

Relative reduction of the medial contact forces following a minor and a major medial collateral ligament release. The grey and black horizontal lines show the average force reduction due to a minor and a major release respectively.
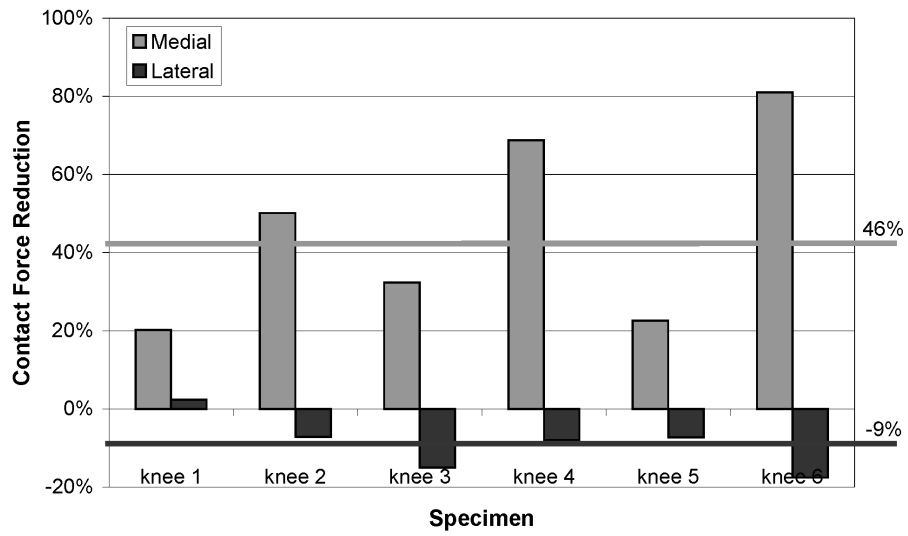
Figure 6.13: Lateral contact force increase

With an average increase (9%) equivalent to a fifth of the medial force reduction (46%),
the influence of a medial ligament release on the lateral contact force was minor.
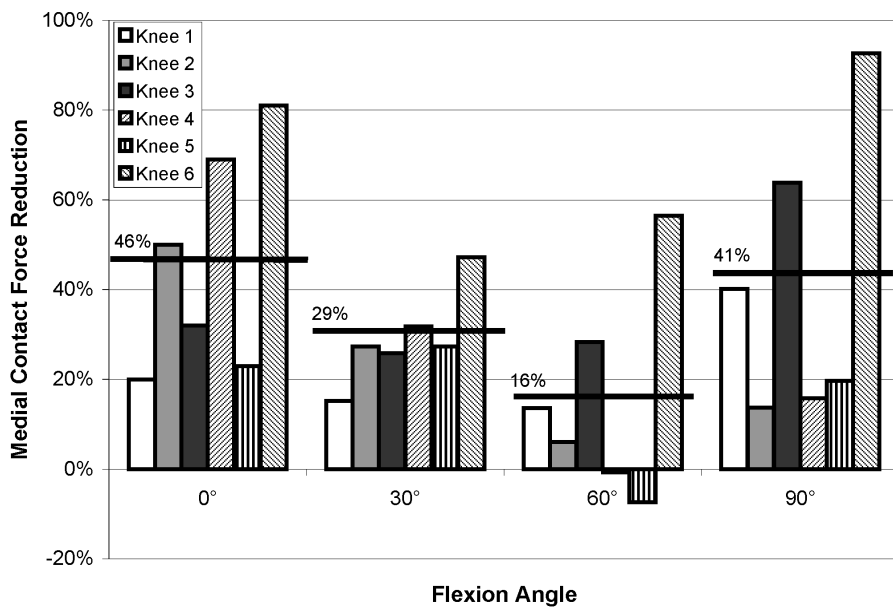
Figure 6.14: Effect of ligament release throughout flexion

The release was less effective at 30° and 60° flexion than in full extension or 90° flexion.
The black horizontal lines correspond to the average values at the different positions.

6.3.3 Discussion

The performance and the clinical advantages of the force-sensing device for improved ligament balancing procedure in TKA was evaluated with six cadaver knees and four different experiments: compression loading to validate the device measurements, patella loading to demonstrate the advantage of keeping the patella in its anatomical place during the measurement, varus-valgus loading to compare the device measurements to the current surgical approach and finally ligament releasing to quantify its biomechanical effect in terms of forces.

The very good agreement between applied and measured tibiofemoral contact forces during the compression loading experiment proved the accuracy and reliability of the *in-situ* device measurements.

The advantage of having the patella in its anatomical place during the measurement was shown by the significant influence of the patellar eversion on the mediolateral distribution of the condyle contact forces. One fourth of the patellar load was shifted to the lateral compartment with a patellar eversion. Although the influence of patellar eversion on the mediolateral force distribution is intuitive, it is the first time according to the authors' knowledge that the effect is quantified in terms of forces. Only one recent study [61] compared the influence of the patellar eversion and subluxation to the physiological situation in terms of angular variation. With a given interarticular load of 150N for the medial and lateral side, the patellar eversion increased the leg axis by 2.9° valgus. Although a quantitative comparison to the present study is not possible, the measured effects are qualitatively consistent. Finally, the fact that the patella in its anatomical place already influenced the mediolateral distribution of the contact forces could be due to a non-symmetrical contact area between the patella and the femoral trochlea or due to the medial incision of the knee joint.

The shape of the curves obtained during the varus-valgus loading experiment can be biomechanically explained. When the joint opens after condyle lift-off, the lateral or medial collateral ligament bears a relevant part of the applied load. Since this part is not measured by the device, it therefore appears as a drop in the slope. The difference of the slopes between the areas 1 and 3 also demonstrates that the lateral and medial ligaments can have different stiffness. The determination of the weight causing a medial or lateral condyle lift-off allowed the comparison of the current surgical approach to assess the knee instability to the approach based on the measurement of the contact

forces or varus-valgus moments. Overall, the three methods gave consistent results. Weight-based imbalance assessment was equivalent to force-based, as expected by the simplified two-dimensional model. Moment-based imbalance assessment, which is assumed to be the optimal approach, showed a tendency of lateral imbalance. This can be anatomically explained by the fact that the medial condyle is smaller than the lateral [62] and consequently has its contact point closer to the center of the joint. It should also be noted that this cadaver model does not take into account any arthritic deformities, which knees selected for TKA would have. Bone deformities can significantly shift the condyle contact points and thereby further increase the difference between the force-based and moment-based imbalance assessment. In such cases, measuring not only the contact forces but also the varus-valgus moments is an undeniable advantage.

On average, the minor and major medial collateral ligament releases substantially reduced the medial contact force (20% and 46% respectively). The large variation among the specimens illustrates the difficulty of ligament release. An intraoperative force monitoring during this delicate surgical action could provide further support to ensure an accurate, patient-specific adjustment of the ligament tensions. The increase of the lateral force after the major medial ligament release was only a fifth of the decrease on the medial side. Consequently, in the case of a small ligament imbalance requiring only a minor force reduction, the effect of the ligament release on the opposite side of the surgical action can be neglected. The ligament releases had also negligible effect on the tibiofemoral alignment. As ligament release can be considered as a change of the ligament stiffness without modification of the ligament length, the medial and lateral knee gaps, and consequently the tibiofemoral alignment, are not affected. It is in opposition to the gap-based approach where the contact forces are kept constant with a distraction device such as in the studies reported by Krackow et al. [63], Mihalko et al. [64] or Baldini et al. [65]. In these cases, diminishing the ligament stiffness with a ligament release alters the tibiofemoral gap due to constrain on the force amplitude. Both methods, force-based and gap-based, are conceptually different. While the former measures directly the contact forces determinant for the component wear, the latter is limited by the complex force-displacement relationship of ligaments, which moreover is not necessarily identical on the medial and lateral side. A well balanced distribution of medial and lateral contact forces avoids overload of one compartment and thus premature wear. Finally, a variation of the effect of ligament releases along knee flexion was observed. A different arrangement of the ligament fibers in the different positions could explain this variation. This again exemplifies the complexity of

ligament balancing and the importance of an intraoperative force monitoring.

In conclusion, the device worked correctly under realistic conditions of use. In addition to the accurate imbalance assessment based on the measurement of forces and moments, important clinical advantages, such as the possibility to keep the patella in its anatomical place during the measurement or the real-time force monitoring during the delicate phase of ligament release, were demonstrated. The proposed device has thus shown potential to improve the ligament balancing procedure and the lifetime of TKA.

Chapter 7

Clinical trials

7.1 Safety requirements

Before testing the device *in-vivo*, a risk analysis must be performed. Three kinds of risks can be identified:

1. Mechanical risks

   - Damage to healthy tissues
   - Rupture of the device

2. Chemical risks

   - Contamination with toxic substances
   - Infection

3. Electrical risks

   - Electromagnetic disturbances
   - Electric shocks

Since the shape of the device was designed to follow the contours of the tibial plateau, surrounding soft tissue is expected to be unaffected by insertion or use of the device. Furthermore, the plasticity test showed that the device stays in the elastic range with forces up to 1'500N. It is therefore expected that the force required to break the device is well over the maximum *in-vivo* load, thus making an *in-situ* rupture of the device impossible. Consequently, complications due to mechanical problems are very unlikely.

All the metallic parts constituting the device are made of biocompatible stainless steel or titanium. The wires have an insulation of teflon, a chemically inert material. All the connectors used are certified for medical applications. Therefore, the only possibility of chemical contamination comes from the exposed circuitry, piezoresistive sensors and soldering tabs. However, the parylene coating ensures a full chemical barrier and prevents toxic exposure to these parts. Finally, a standard sterilization procedure is adopted to minimize risks of infection.

With a power supply of 5V DC, the device should not disturb any other surgical device through electromagnetic interferences. Nevertheless, particular attention must be paid to potential electric shocks. The device has to comply with the general requirements of the standard for medical electrical equipment [66]. The two most important requirements are: a) a galvanic separation that prevents direct connection between the electric network and the patient and b) a patient leakage current that must not exceed $10\mu A$ in normal condition and $50\mu A$ in single fault condition. Although the parylene coating provides a good electric isolation (3500V DC and 2500V AC), a special signal conditioning unit has been produced to further ensure the patient safety in a fault condition (Fig.7.1).
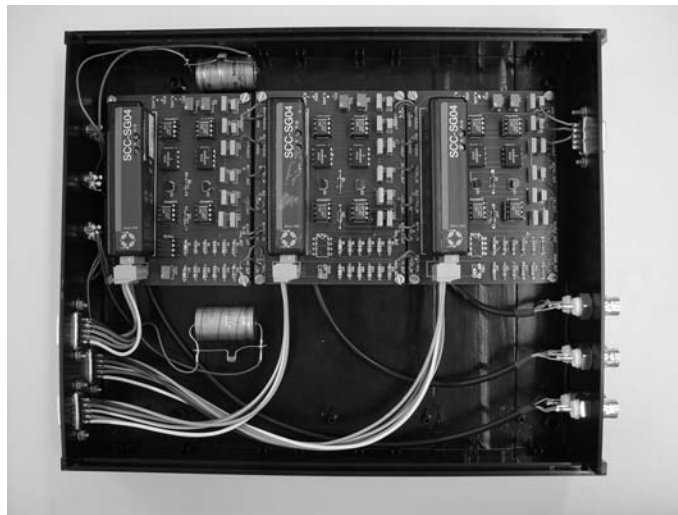
Figure 7.1: Custom signal conditioning unit

The principle for the electric isolation of the patient is schematically explained in Fig.7.2. The signal conditioning unit is powered by a power sup-

ply certified to provide a galvanic separation and to ensure a patient leakage current lower than 10μA. A standard industrial amplifier for strain gauge applications is then used to power the Wheatstone bridge and to amplify its output. Finally, the electrical signal goes through an optical decoupling that prevents uncontrolled currents coming from the computer from harming the patient. The main component of this electronic circuit, which is shown in details in Fig.7.3, is an optocoupler. This device has two diodes ; one that emits light to convert the input voltage into a luminous flux and a second that receives this light and converts it back into a voltage output. This way, the information contained in the electrical signal is transmitted without any electrical contact between the patient and the data acquisition computer.
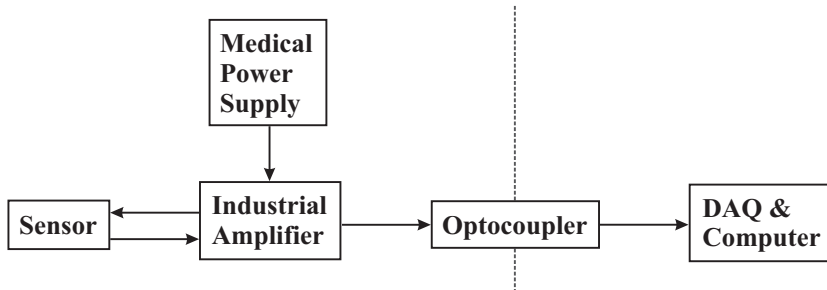
Figure 7.2: Patient isolation principle
The medical power supply complies with the medical standard and therefore can be in direct contact with the patient. The optical decoupling prevents uncontrolled external current from harming the patient.
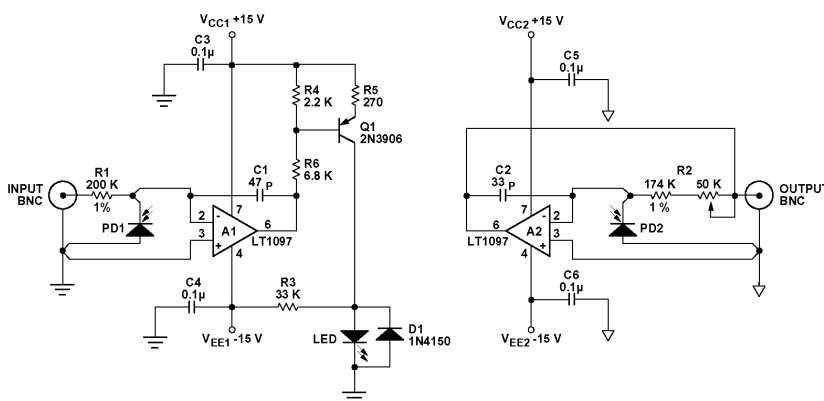
Figure 7.3: Electronic diagram of the optical decoupling

7.2   Standard approach vs force-sensing device

Two clinical trials were carried out both to evaluate the device performance in a surgical environment and to compare the device-assisted to the standard approaches under real conditions of use. To realize these objectives, two sets of measurements in full extension and in 90° flexion were carried out, the first before the femoral cuts were performed and the second after the trial femoral component was placed. After the device insertion, spacers of different thicknesses were introduced to balance the ligament according to the device measurements (Fig.7.4). Then, the device was removed and the surgery proceeded in a standard way. The thickness of the resected condyles was measured for the distal and posterior cuts. Once the trial femoral component was in place, the device was introduced a second time. Spacers were used again to assess the remaining knee imbalance according to the device measurements. The femoral cuts planned by the device measurements, the femoral cuts performed on the basis of standard instrumentation as well as the final imbalance assessment were then compared.

	Patient A		Patient B	
	Extension	Flexion	Extension	Flexion
Balanced knee	3mm	4mm	6mm	3mm
Femoral cuts	3.5mm	1mm	6mm	2mm
Difference	-0.5mm	3mm	0mm	1mm
Final imbalance	-1mm	2mm	0mm	0mm

Table 7.1: Mediolateral difference of the knee gaps
A positive, negative sign corresponds to the medial, lateral side respectively.

The results are summarized in table 7.1. According to the device measurements, the knee of patient A could be balanced with a mediolateral difference in the knee gaps of 3mm in extension and 4mm in flexion. The femoral cuts performed with a standard approach showed a gap difference of 3.5mm in extension and 1mm in flexion. Therefore, the device measurements and the standard approach agreed in extension but not in flexion. However, the surgeon also estimated at that point of the surgery that the knee was not completely balanced and that a ligament release was required. The knee of patient B could be balanced with a mediolateral knee gap difference of 6mm in extension and 3mm in flexion. The femoral cuts had a gap difference of 6mm in extension and 2mm in flexion, showing a complete agreement

(a) Overview of the operating room

(b) Introduction of spacers

Figure 7.4: Clinical trial

Spacers are introduced to balance the knee according to the device measurements

between the device-assisted and the standard approaches. The imbalance assessment with the femoral component in place resulted in values similar to the difference between the device-planned femoral cuts and the femoral cuts effectively performed, thus demonstrating the consistency of the device measurements throughout the surgery.

In addition to these measurements, five dynamic evaluations were performed during knee flexion before the femoral resection. Fig.7.5 shows the variation in medial and lateral forces for patient A as the device spacers were set to balance the knee at 90° flexion. The huge difference of force amplitude in flexion and in extension, and thereby the huge difference in balance, is in agreement with the well-known fact that tibiofemoral gaps ensuring a stable knee are not necessarily the same in flexion and in extension.
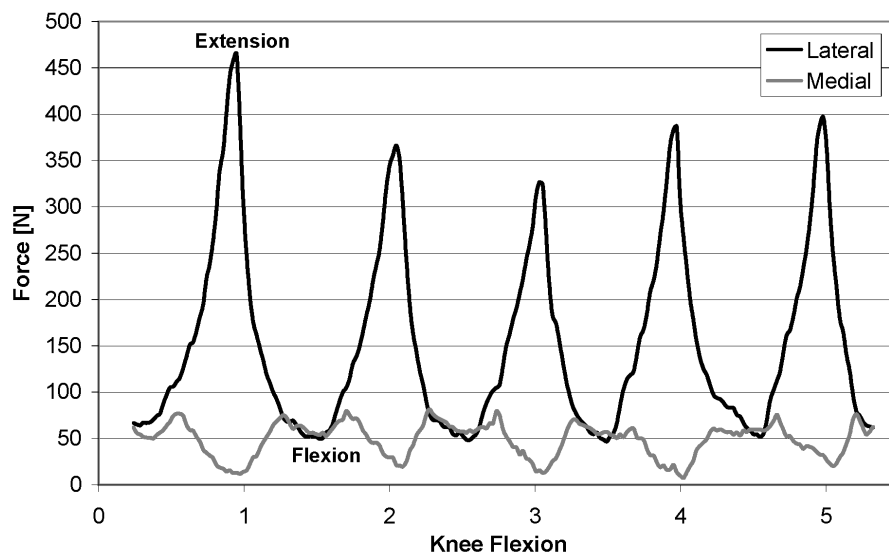
Figure 7.5: Flexion-extension of the knee

In conclusion, these *in-vivo* trials demonstrated that the device measurements are possible, meaningful and consistent with the surgeon's perception in a clinical environment.

Chapter 8

Unicompartmental knee arthroplasty

8.1 Surgical procedure

Unicompartmental Knee Arthroplasty (UKA) is a surgical procedure which consists in replacing either the medial or lateral knee compartment (Fig.8.1). This procedure is indicated when significant degenerative changes exist in only one of the compartments and when the cruciate ligaments are intact. Candidate patients should not be obese, should have good preoperative range of motion (90° flexion), and a deformity below 15° [67]. These strict selection criteria are responsible for the result that only 5-7% of arthritic knee joints are treated with UKA. The theoretical advantages of UKA compared to TKA are a preservation of the intact tissue and bone, a reduction in operating time as well as a better range of motion and improved gait.

UKA was introduced 30 years ago, but frequent and early failures at that time made the treatment controversial. TKA with its encouraging long-term success became the standard procedure. However, in the past few years, a resurgence of interest in the UKA has occurred, particularly with the introduction of minimally invasive techniques. With improved surgical procedures and optimized prostheses, the long-term results with current UKA procedures are now comparable to TKA ones, even though the demanding patient selection may influence the lifetime [68, 69, 70]. Moreover, a knee joint having received a unicompartmental implant can later undergo a TKA, with minimal loss of implant-supporting subchondral bone. Thus, at the point of a TKA, the UKA patient has gained the intervening time over an initial TKA patient.

(a) Prosthetic components   (b) Postoperative X-ray

Figure 8.1: Unicompartmental Knee Arthroplasty
The Oxford Knee from Biomet Europe, Dordrecht, The Netherlands

Aside from the common complications from arthroplasty, the main problem with UKA is the potential for over or undercorrection of the mechanical axis. In the case of overcorrection, excessive loads on the second knee compartment lead to an accelerated degeneration. On the other hand, undercorrection gives abnormal laxity, inducing component loosening or failure. The mechanical axis correction and the joint stability is carried out by inserting thicker or thinner polyethylene meniscal bearing [71, 72]. Ligament release is usually not performed or is minor. In order to avoid overcorrection, which has consequences on the healthy compartment, an undercorrection of the mechanical axis of 2-3° is usually performed. For example, Thornhill [71] recommends to leave some medial tibial opening in extension in the case of medial compartment osteoarthritis. Although this practise is tolerable, it is not optimal. According to Emerson et al. [73], the restoration of normal soft-tissue tension by the insertion of the appropriately sized implant can consistently restore axial alignment within the physiological range. Quantitative measurement of the tibiofemoral condyle contact forces here could help the surgeon to assess the ligamentous balance and consequently to determine the optimal implant size.

8.2 Soft-tissue balancing assistance for UKA

8.2.1 Concept

Since the contralateral knee compartment is not accessible during the surgery, only one sensitive plate can be used. This implies that only half of the parameters required to provide a quantitative evaluation of the knee balance can be measured. Applying and measuring external varus-valgus loads on the leg in addition to the one plate measurements can compensate for the missing information on the healthy side.
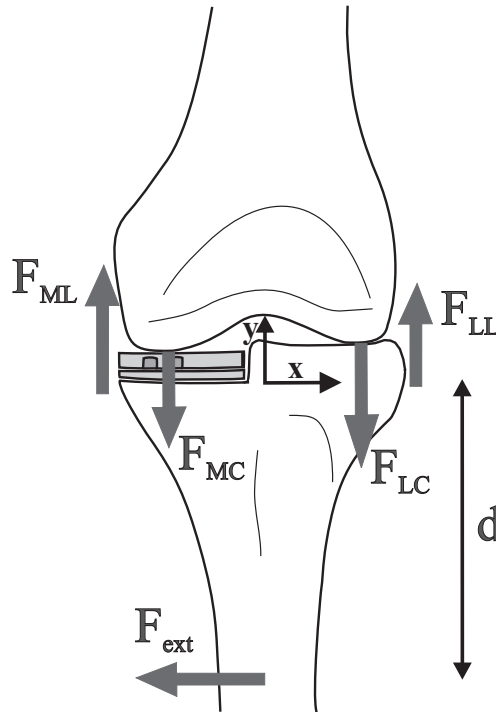
Figure 8.2: Knee joint experiencing external varus-valgus moments

The measurement principle is based on the same simplified planar model of the knee joint presented in section 3.1, except that an external force F_{ext} is applied at the distal part of the tibia at a distance d (Fig.8.2). The forces F_i, $i=\{ML, MC, LC, LL\}$ are the medial ligament, the medial contact, the lateral contact and the lateral ligament forces. To satisfy the equilibrium condition, the sum of the moments must be zero.

$$dF_{ext} + x_{ML}F_{ML} - x_{MC}F_{MC} + x_{LC}F_{LC} - x_{LL}F_{LL} = 0\,, \qquad (8.1)$$

where x_i is the lever arm of the force F_i, $i=\{ML,\ MC,\ LC,\ LL\}$. By renaming and regrouping the amplitude of the different moments, equation (8.1) can be rewritten as:

$$M_{lig} - M_M + M_L + M_{ext} = 0 \,, \tag{8.2}$$

where M_{lig} is the net varus-valgus moment of the collateral ligaments and M_i, $i=\{M,\ L,\ ext\}$, are the moment amplitudes of the medial, lateral and external forces respectively. The amplitude of the contact moments M_M, M_L obviously depend on the external moment M_{ext}. However, if bones are considered as rigid bodies and ligament as springs, the ligament forces and therefore M_{lig} can be assumed constant as long as both condyles are in contact with the tibia. The tension in a spring-ligament would vary only when the joint starts to open, i.e. when one condyle lifts off. Therefore, the net varus-valgus moment of the ligaments is given by:

$$M_{lig} = M_M - M_L - M_{ext} \qquad 0 \le M_{ext} \le M_{ext}^0 \,, \tag{8.3}$$

where M_{ext}^0 corresponds to the moment creating a condyle lift-off. Since this last equation is verifiedvalid for all the values of M_{ext} comprised in the specified range, it is true for the two border values:

$$M_{lig} = M_M - M_L \qquad \text{for } M_{ext} = 0 \tag{8.4}$$

$$M_{lig} = M_M - M_{ext}^0 \qquad \text{for } M_{ext} = M_{ext}^0 \,. \tag{8.5}$$

Equation (8.4) shows that M_{lig} is equivalent to M_{net}, the net varus-valgus moment of the contact forces that characterizes the knee balance (c.f. section 3.1) and equation (8.5) shows that it can be computed by measuring the medial and the external moments at the time of condyle lift-off:

$$M_{net} = M_M \Big|_{M_{ext}=M_{ext}^0} - M_{ext}^0 \,. \tag{8.6}$$

In practise, the medial moment M_M is measured by the sensitive plate and the external moment M_{ext} can be computed from the measurement of the external force amplitude with a dynamometer and the lever arm with a ruler. The experimental issue is then to precisely determine the moment of condyle lift-off without seeing the condyle. According to equation (8.2), a linear relationship exists between the contact moment and the external varus-valgus moment. However, the proportionality factors are not the same before and after condyle lift-off since M_{lig} is constant and M_L non-zero before, whereas M_{lig} varies and M_L is zero after lift-off. The specific external moment M_{ext}^0 at the moment of lift-off can thus be determined by identifying the slope discontinuity in the curve $M_M(M_{ext})$.

8.2.2   In-vitro feasibility study

The delicate point of the proposed method resides in the hypothesis that M_{lig}, the net varus-valgus moment of the collateral ligaments, does not vary before condyle lift-off. In practise, the knee joint is more complex than rigid bodies linked with springs. For instance, the femoral cartilage can be compressed and behaves as a spring-like structure or the relative position between the femur and tibia can slightly vary during loading, thus altering the ligament tension. The goal of this section is therefore to quantify the deviation of the model from the reality in order to estimate if the proposed approach could be used clinically.

If M_{lig} is constant, a partial derivative of equation (8.3) gives

$$\frac{\partial}{\partial M_{ext}} \left(M_M - M_L \right) = 1 \,. \tag{8.7}$$

Consequently, plotting the net varus-valgus moment $M_M - M_L$ in function of the external moment M_{ext} should show a linear relationship with a slope of 1. To experimentally verify that point, the data acquired during the varus-valgus loading experiment of the *in-vitro* study (c.f. section 6.3) were used. For each specimen, the relationship was, as expected, highly linear ($0.99 \leq r^2 \leq 1.00$), such as in the example showed in Fig.8.3. However, the measured slopes ranged from 0.63 to 0.78, the average being 0.69 instead of 1 (Table 8.1). This implies a relative error of the model of 30%, which is obviously not acceptable.

	pilot	knee 1	knee 2	knee 3	knee 4	knee 5	knee 6
slope	0.78	0.72	0.61	0.74	0.66	0.69	0.63

Table 8.1: Slope of the ligament moment vs applied moment

The hypothesis of constant ligament forces before condyle lift-off is therefore too strong. In order to improve the proposed approach, the variation of the net varus-valgus moment of the ligaments M_{lig} as a function of the external moment M_{ext} must be taken into account. An estimate of this variation may be derivable from an intraoperative measurement of the change of the lengths L_M, L_L of the medial and lateral ligaments with the help of a navigation system. Knowing this length variation, the force and thereby the moment variation can be estimated by using a generic or patient-specific ligament stiffness (K_M, K_L). The latter can be determined by comparing
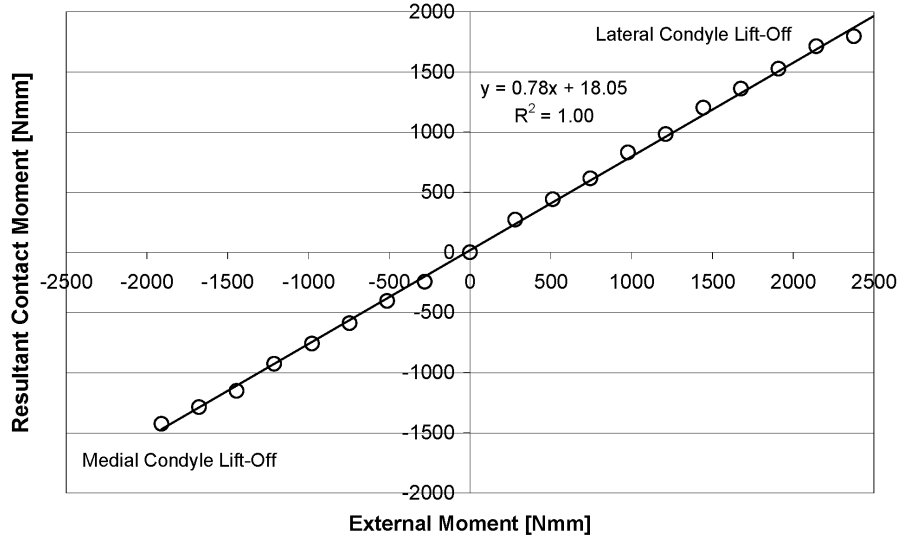
Figure 8.3: Comparison of the contact moments and external moments

contact forces measured by the device and ligament lengths measured by the navigation system in different external loading conditions. With these parameters, the varation of the ligament moment can be computed as follows:

$$M_{lig} \Big|_{M_{ext}=M^0_{ext}} - M_{lig} \Big|_{M_{ext}=0} = x_{ML}K_M\Delta L_M - x_{LL}K_L\Delta L_L \; ; \qquad (8.8)$$

and equation (8.6) can thus be corrected.

$$M_{net} = M_M \Big|_{M_{ext}=M^0_{ext}} - M^0_{ext} - (x_{ML}K_M\Delta L_M - x_{LL}K_L\Delta L_L) \qquad (8.9)$$

In conclusion, substituting the missing information of the healthy side by applying known varus-valgus moments is not sufficient to provide precise stability assessment. Additional measurements, such as the variation of the ligament length, are necessary.

Chapter 9

Conclusion and perspectives

This thesis addressed the issue of the measurement of musculoskeletal forces during orthopaedic surgeries through the development of a force-sensing device for ligament balancing in Total Knee Arthroplasty (TKA). In addition to geometrical parameters given by the standard orthopaedic instrumentation, the measurement of forces involved at the time of surgery can help in improving the placement of implants and/or the adjustment of surrounding soft-tissues to ensure a consistent procedure. During TKA, a good ligament balance must be achieved to ensure a stable and functional prosthetic knee joint. Internal joint forces and moments are therefore of major importance but are nowadays only qualitatively assessed with manipulation or basic instrumentation.

In a first step, three possible designs for a force-sensing device for knee arthroplasty were proposed and studied using finite element analysis. The optimal design consists of two sensitive plates, one for each condyle, a tibial base plate, which is fixed by pins, and a set of lateral and medial spacers, which allow the device thickness to be adapted to the patient-specific tibiofemoral gaps. The entire device fits inside the knee joint after the initial tibial cut with the patella in its anatomical place. The ligament balance assessment can be carried out at the beginning of the surgery, thus offering the possibility to make a better plan for the femoral cuts and the femoral component rotation. Thanks to the top spacer system, additional spacers having the top surface congruent to femoral implants can be easily used to allow measurements and ligament adjustments with the trial components in place. Thus, the main stability assessment made at the beginning of the surgery enables better planning of the femoral cuts, whereas the second at the end of the surgery allows fine-tuning of the ligament balance and correcting eventual deviations from the plan. Each sensitive plate contains three deformable

bridges instrumented with thick-film piezoresistive sensors. This three-point measurement allows determining the amplitude and location of the load applied on a sensitive plate. With these measurements, the net varus-valgus moment, which has been identified as the biomechanical parameter characterizing the knee balance, can be computed. Laboratory experiments showed that the device has an 0.5% full scale accuracy in the range 0-500N and a 1.6N maximal measurement error in the range 0-100N, the expected active range of use. Thus, the accuracy is adequate and the measurement principle and the device design validated.

In a second step, an *in-vitro* study demonstrated the proper *in-situ* functioning of the novel force-sensing device as well as its clinical advantages. For example, patellar eversion, necessary with standard approaches but not with the proposed device, had a significant influence on the mediolateral distribution of the contact forces: one fourth of the patellar load was shifted to the lateral side. Besides the validation of the device design, this *in-vitro* study also addressed two biomechanical issues. The first is the absence of standard interpretation in biomechanical terms of what surgeons intuitively call ligament balancing. Contact pressure, contact forces, tibiofemoral gaps, angular asymmetry, etc., are parameters interchangeably used in literature to describe the ligament balance. To identify which biomechanical parameter the surgeon intraoperatively assesses, the current surgical approach (difference of varus and valgus weights generating a condyle lift-off) was compared theoretically and experimentally to the measurement of contact forces or moments. The weight-based method was similar to the force-based, while the moment-based, proposed as the optimal from the biomechanical point of view, showed a slight lateral imbalance. Surgeons must then be aware that knee stability before and after the insertion of the femoral component may differ even if the ligament forces do not. Instrumentation that bases the ligament imbalance assessment on the measurement of contact forces and moments should therefore be used during the planning of the femoral cuts. The second biomechanical issue is the lack or poor documentation of the effect of ligament release, one of the most used surgical action to correct imbalance, in terms of knee joint forces. Medial contact forces measured after minor and major medial collateral ligament releases were reduced by 20% and 46% in average. The high standard deviations, 19% and 25% respectively, demonstrated the high variability among specimens and therefore the need of an intraoperative monitoring to ensure a patient-specific adjustment of ligament tensions.

In a final step, two *in-vivo* trials confirmed that the device measurements are possible, meaningful and consistent with the surgeon's perception in a clinical environment.

The novel force-sensing device has therefore an appropriate design and performs correctly. In addition to the accurate imbalance assessment based on the measurement of forces and moments, important clinical advantages, such as the possibility to keep the patella in its anatomical place during the measurement or the real-time force monitoring in the delicate phase of ligament release, were demonstrated. The proposed device has thus shown potential to improve the ligament balancing procedure and the lifetime of TKA.

In order to further enhance the device, two ergonomic changes could be implemented. Firstly, the fixation mechanism serving to extend the sensitive area could be replaced by a hinge mechanism at the extremity of the bridge pillars, which would extend the sensitive area to the whole plate while suppressing protuberant parts. Secondly, the data transfer to the computer could be improved by using a multiplexing or a telemetry to reduce or avoid wires. A prototypical telemetric system based on the principle of near-field magnetic induction coupling, commonly used in RFID (Radio Frequency IDentification) applications, was designed and tested by a research partner [47]. The technical feasibility was demonstrated but further work is needed to reduce the size of the electronics to be able to integrate it in the device. In addition to these ergonomic improvements, the functionality of the new instrument can be extended by combining the device with a navigation system. Measuring simultaneously geometrical parameters, such as angles, lengths, axes, and mechanical such as forces and moments enables the use of complex computational knee models, which can act as assistive expert systems. The advantages that such a tool can offer was already perceived during the feasibility study of the adaptation of the force-sensing device for unicompartmental knee arthroplasty. Complete assistive expert systems, which intraoperatively provide an accurate measurement of geometrical and mechanical parameters, a quantitative biomechanical interpretation and finally a precise guidance to achieve the plan will undeniably become an essential tool in the next generation of orthopaedic instrumentation.

The first *in-vivo* trials, which concluded the experimental phase of the thesis, correspond to the starting point of large clinical studies. Thanks to the developed force-sensing device several important biomechanical and clinical issues can be addressed, such as the accuracy and repeatability of the surgeon's performance in soft tissue balancing ; the correlation between intra-

operative ligament imbalance, postoperative knee laxity and postoperative complications ; the lifetime of TKA performed with an assistive expert system compared to standard instrumentation. Up to now, all these important questions could not be studied quantitatively. The new proposed tool has therefore a promising future in research, too.

As has been seen through the development of this force-sensing device for knee arthroplasty, intraoperative measurements of musculoskeletal forces is of major importance and can bring useful help during orthopaedic surgeries. Precise and objective assessment of biomechanical parameters is a valuable complement to the surgeon's perception and the combination of smart surgical instrumentation and human-specific performances should definitely lead to a significant benefit for the patient.

Appendix A

Some basics of solid mechanics

The purpose of this section is not to give an exhaustive course on solid mechanics, but simply to review and introduce the fundamental concepts used in this thesis. More details on solid mechanics can be found in [10].

A.1 Elastic deformation

Two fundamental concepts in mechanics of materials are stress and strain. Stress is the intensity of a force per unit of area and is denoted by σ. Assuming that the stresses are uniformly distributed over a cross section of a body (Fig.A.1), the stress amplitude is expressed by

$$\sigma = \frac{P}{A}, \tag{A.1}$$

where P is the axial force and A the area. By definition, stress is positive when the specimen is tensed and negative when it is compressed.
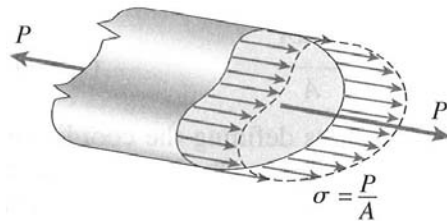

Figure A.1: Definition of stress

Stress σ is the intensity of a force P per unit of area A (picture taken from [10])

A straight bar becomes longer in axial tension and shorter in axial compression. The resulting strain is denoted by ϵ and is defined as the ratio between

this length change (ΔL) and the original length (L),

$$\epsilon = \frac{\Delta L}{L}\,. \tag{A.2}$$

As for the stress, the strain is positive when the bar becomes longer and negative when it becomes shorter.

The relationship between stress and stain is empirical and based on the so-called stress-strain diagram, whose typical example is that of steel (Fig.A.2). In the first part of the diagram, from O to A, the relationship is linear. This area is called the elasticity range of the material and the slope is the modulus of elasticity or Young's modulus. The point A is the elasticity limit. Beyond this point, the stress-strain becomes less steep until, at point B, the curve becomes horizontal. This phenomenon is known as yielding of the material and point B is called the yield point. In the region from B to C, the material becomes perfectly plastic, which means that it deforms without an increase of the applied load. After undergoing the large strains that occur during yielding in the region BC, the material begins to strain harden. During strain hardening, the material undergoes changes in its crystalline structure, resulting in increased resistance of the material to further deformation. Elongation of the test specimen in this area requires an increase in the tensile load, which reaches its maximum value, the ultimate stress, at the point D. Further stretching of the bar is actually accompanied by a reduction in the load and fracture finally occurs at point E.

The relationship between stress and strain in the elastic range for a bar in simple tension or compression can be expressed as

$$\sigma = E\epsilon\,, \tag{A.3}$$

where E designates the Young's modulus. This formula is known as Hooke's law.

In addition to elongation along the axis of loading, the bar reduces its section to keep the volume constant, thus generating lateral strain ϵ'. This lateral strain is proportional to the axial strain ϵ at the same point. The dimensionless ratio ν between these two kinds of strains is a property of the material called Poisson's ratio, which can be expressed as

$$\nu = -\frac{\epsilon'}{\epsilon}\,. \tag{A.4}$$
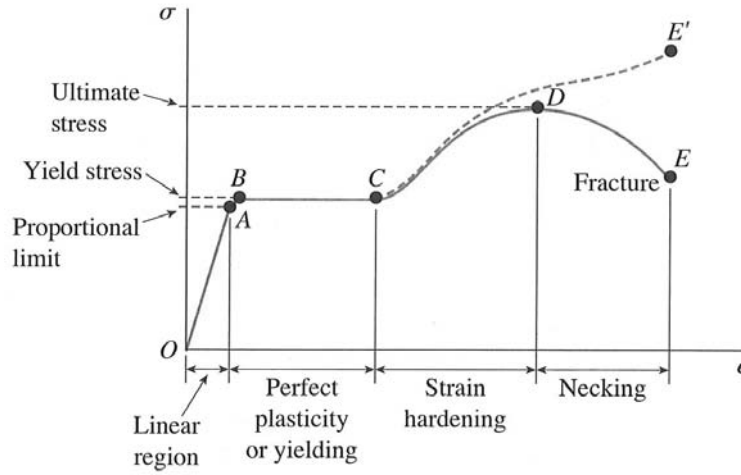
Figure A.2: Stress-strain diagram
Typical structural steel in tension (picture taken from [10])

Taking the lateral strain into account, the triaxial Hooke's law can be written as follows:

$$
\begin{aligned}
\epsilon_1 &= \frac{1}{E}(\sigma_1 - \nu\sigma_2 - \nu\sigma_3) \\
\epsilon_2 &= \frac{1}{E}(\sigma_2 - \nu\sigma_1 - \nu\sigma_3) \\
\epsilon_3 &= \frac{1}{E}(\sigma_3 - \nu\sigma_1 - \nu\sigma_2).
\end{aligned}
\tag{A.5}
$$

In addition to axial loads, tangential loads can act on a specimen's surface. These loads generate shear stresses, which are denoted by τ. Contrary to axial stress which tends to modify the length of a specimen, shear stress tends to change its shape. The corresponding strain is not the relative length variation anymore, but the angle of distortion γ (Fig.A.3).

The shear stress-strain diagram is similar in shape to the tension stress-strain diagram, although it differs in magnitude. A linear relationship, which is called the Hooke's law in shear, also exists close to the origin.

$$
\tau = G\gamma,
\tag{A.6}
$$

where G is the shear modulus.
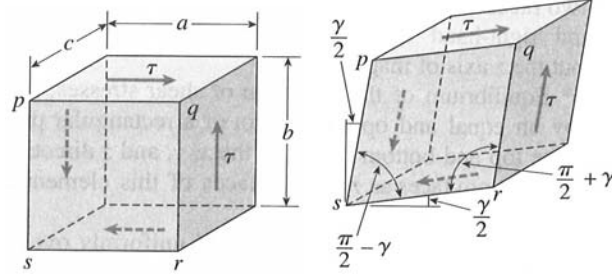
Figure A.3: Shear stress

Element of material subjected to shearing stresses and strains, before and after
deformation (picture taken from [10])

Apparently, 12 shear stress components (2 per face for 6 faces) are required
to completely describe the state of a general three-dimensional stress ele-
ment. However, stresses occurring at opposing faces have opposite signs,
thus reducing the number of significant components to 6. Moreover, in order
to satisfy static equilibrium, the shear stress components are related in the
following way:

$$\tau_{xy} = \tau_{yx} \qquad \tau_{yz} = \tau_{zy} \qquad \tau_{zx} = \tau_{xz} \,, \tag{A.7}$$

where the first subscript is the coordinate normal to the element face and the
second designates the axis parallel to the shear-stress component. Therefore,
only 3 components are significant, or, in other words, independent. This
leads to use the following three equations for a three-dimensional case of
pure shear:

$$
\begin{aligned}
\tau_{xy} &= G\gamma_{xy} \\
\tau_{yz} &= G\gamma_{yz} \\
\tau_{zx} &= G\gamma_{zx} \,.
\end{aligned}
\tag{A.8}
$$

Although the normal and shear stresses were discussed separately, both can
simultaneously occur in a general load state. The set of equations (A.5)
and (A.8) must therefore be used. Considering such a general case, it is
possible to demonstrate that the Young's modulus, the shear modulus and
the Poisson's ratio are related to each other by

$$G = \frac{E}{2(1+\nu)} \,. \tag{A.9}$$

Finally, note that all previous considerations are only valid for homogenous
and isotropic material.

A.2 Stresses in beams

An important and widely used mechanical structure in the domain of force-sensing devices is the bending beam. To establish the stress formula for bending beams, let's consider the Fig.A.4, which presents the side view and the cross section of a beam as well as its deformation resulting from bending moments.
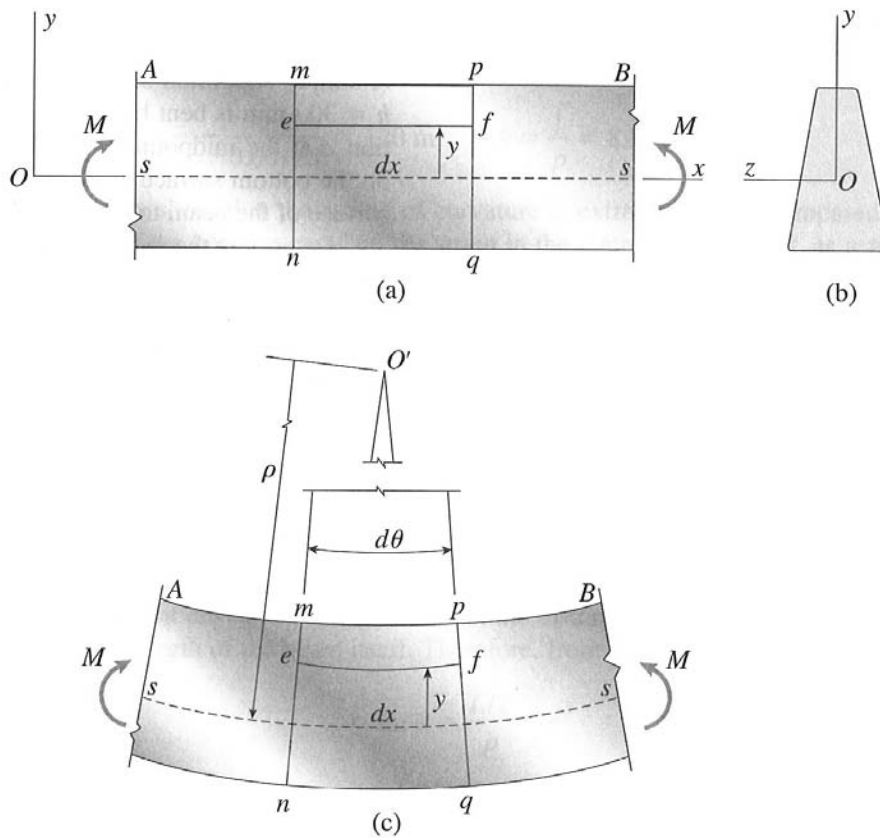

Figure A.4: Deformation of beam in pure bending
a) side view, b) cross section, c) deformed beam (picture taken from [10])

When loads are applied to a beam, its longitudinal axis is deformed into a curve. The curvature (κ) is by definition the inverse of the radius of curvature (ρ), that is

$$\kappa = \frac{1}{\rho}.$$
(A.10)

The neutral axis, the axis along which there is no stress, is represented by a dashed line. Since the distance dx between the planes containing cross sections mn and pq is part of this neutral axis which undergoes no strain, it remains the same before and after deformation, thus allowing us to write

$$\rho d\theta = dx\,, \tag{A.11}$$

giving

$$\kappa = \frac{d\theta}{dx}\,. \tag{A.12}$$

On the other hand, a line ef at a distance y from the neutral axis becomes shorter or longer. Its original length is clearly dx and its length after deformation is

$$(\rho - y)d\theta = dx - \frac{y}{\rho}dx\,. \tag{A.13}$$

The corresponding strain is therefore

$$\epsilon_x = \frac{(dx - \frac{y}{\rho}dx) - dx}{dx} = -\frac{y}{\rho} = -\kappa\rho\,, \tag{A.14}$$

and stress

$$\sigma_x = E\epsilon_x = -E\kappa y\,. \tag{A.15}$$

To express the curvature in mechanical terms, the second equation of equilibrium, which expresses the fact that the sum of the moments should be zero, has to be used. Considering a small part of the beam, the element of force $\sigma_x dA$ acting on an element dA is in the positive direction of the x axis when σ_x is positive and inversely. An infinitesimal moment is therefore generated,

$$dM = -\sigma_x y dA\,, \tag{A.16}$$

thus giving by integration

$$M = -\int_A \sigma_x y dA = \kappa E \int_A y^2 dA = \kappa EI\,, \tag{A.17}$$

where I is the moment of inertia.

$$I = \int_A y^2 dA \tag{A.18}$$

The curvature can hence be expressed by

$$\kappa = \frac{1}{\rho} = \frac{M}{EI}\,. \tag{A.19}$$

Finally, by combining equations (A.15) and (A.19), the flexure formula is obtained:

$$\sigma_x = -\frac{My}{I} \,.$$

(A.20)

This general expression gives the stress for a given cross-section in a specific plane, but designers are more interested in knowing the maximal stresses. These obviously occur at the top and bottom surface of the beam, when y is maximal. In order to give an analytical expression, two specific cases, a rectangular and a circular beam, are now reviewed.

1. Let's consider a rectangular beam with a width b and a height h. If a force is acting in its center, the maximal possible value for y is $h/2$. After integration, the moment of inertia is

$$I = \frac{bh^3}{12} \,,$$

(A.21)

   and the maximal stress amplitude for a rectangular beam is

$$\sigma_x = \frac{6M}{bh^2}$$

(A.22)

2. Let's consider a circular beam with a diameter d and a force acting in its center. The maximal value for y is $d/2$. After integration, the moment of inertia is

$$I = \frac{\pi d^4}{64} \,.$$

(A.23)

   The maximal stress amplitude for a circular beam is

$$\sigma_x = \frac{32M}{\pi d^3}$$

(A.24)

Finally, note that this analysis is valid only for pure bending. Nonuniform bending, which corresponds to bending moment that is not constant along the beam, will produce distortion of the cross section. This distortion has not been taken into account in the previous development. However, detailed investigations show that the normal stresses calculated from the flexure formula are not significantly altered by the shear stresses. Thus, the theory of pure bending for calculating normal stresses in beams subjected to nonuniform bending can be justifiably used.

It has also to be reminded that this analysis does not take into account eventual stress concentrations, making the theory inaccurate near the support of the beam or close to a concentrated load.

Appendix B

Contact pressure and stresses

To evaluate if yielding of a body being in contact with other mechanical parts will occur, a two-step calculation has to be performed:

1. Assess the maximal contact pressure (B.1)

2. Determine if this maximal pressure leads to plastic yielding (B.2)

B.1 Hertzian theory

This typical contact stress problem was solved by Hertz in 1881 for the first time. Even if the Hertzian theory is more than hundred years old, it is still largely used and has been numerous times validated.

The mathematical description that follows is from [74]. A more general approach, which leads to the same final result, can be found in [75].

Let's consider two bodies, which have spherical surfaces of radii R_1, R_2 at the contact point (Fig.B.1). Without pressure between the bodies, the contact point is located in O. The distances from the plane tangent at O of points such as M, N, at a very small distance r from the axes z_1, z_2, can be represented with sufficient accuracy by the formula

$$z_1 = R_1^2 - \sqrt{R_1^2 - r^2} \cong \frac{r^2}{2R_1} \tag{B.1}$$

and the respective distance between these points is

$$z_1 + z_2 = \frac{r^2(R_1 + R_2)}{2R_1 R_2} \ . \tag{B.2}$$
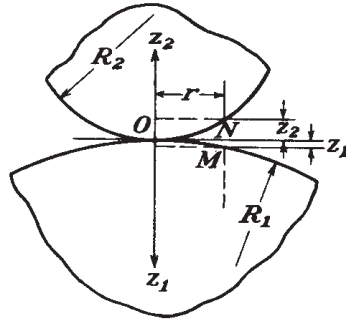
Figure B.1: Two spheres in contact
(picture taken from [74])

In the particular case of contact between a plane and a sphere (Fig.B.2), $1/R_1 = 0$ and the mutual distance becomes

$$z_1 + z_2 = \frac{r^2}{2R_2} \, .$$ (B.3)

In the case of contact between a ball and a spherical seat (Fig.B.2), R_1 is negative and the mutual distance is

$$z_2 - z_1 = \frac{r^2(R_1 - R_2)}{2R_1R_2} \, .$$ (B.4)
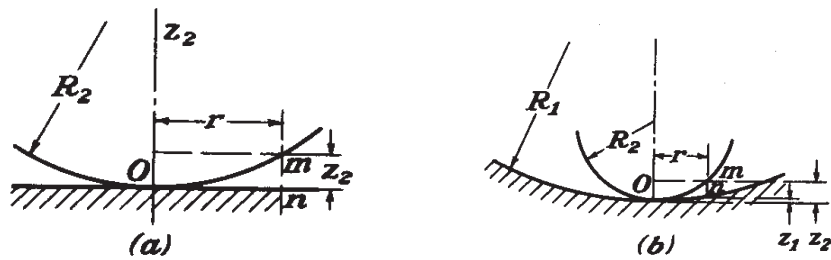
Figure B.2: Different contacts
a) sphere on a plane, b) sphere in spherical socket (picture taken from [74])

Applying a load F on the spheres obviously leads to deformation. This gives a compliance δ corresponding to the movement in the vertical direction of points at a distance r from the loading point, such as M, N. If the

displacements at these points are w_1, w_2, then, for points inside the contact area:

$$(z_1 + w_1) + (z_2 + w_3) = \delta. \tag{B.5}$$

With (B.2), this last equation can be written as:

$$w_1 + w_2 = \delta - \beta r^2, \tag{B.6}$$

where $\beta = \frac{R_1 + R_2}{2R_1 R_2}$.

Assuming that the radii of curvature R_1, R_2 are large in comparison to the radius of the contact surface, the result obtained for semi-infinite bodies in [74] can be applied: the displacement w_1 of a point on the surface of contact of the lower ball is

$$w_1 = \underbrace{\frac{1 - \nu_1^2}{\pi E_1}}_{=K_1} \iint P \, ds \, d\psi = K_1 \iint P \, ds \, d\psi, \tag{B.7}$$

where ν_1, E_1 are the Poisson's and Young's modulus respectively and P the pressure. A similar expression can be written for the upper ball. Thus, (B.6) becomes

$$(K_1 + K_2) \iint P \, ds \, d\psi = \delta - \beta r^2. \tag{B.8}$$

A satisfying assumption is that the distribution of pressure P over the contact area is represented by the ordinates of an hemisphere of radius a, constructed on the surface of contact. If P_{max} is the pressure at the center of the contact area, then

$$P_{max} = ka, \tag{B.9}$$

where k is a constant factor representing the scale factor of our representation of the pressure distribution. After integration, (B.8) becomes

$$(K_1 + K_2) \frac{\pi^2 P_{max}}{4a} (2a^2 - r^2) = \delta - \beta r^2. \tag{B.10}$$

Since this last equation has to be fulfilled for any value of r, it has to be valid for $r = 0$ and $r = a$. Therefore, the following relationships exist for compliance δ and the radius a of the surface of contact:

$$\delta = (K_1 + K_2) P_{max} \frac{\pi^2 a}{2}$$

$$a = (K_1 + K_2) P_{max} \frac{\pi^2}{4\beta}. \tag{B.11}$$

The value of the maximal pressure P_{max} is obtained by equating the sum of the pressures over the contact area to the compressive force F. For the hemispherical pressure distribution, with P_{max}/a being the pressure per unit of ordinates and $2/3\pi a^3$ the hemisphere volume, this gives

$$\frac{P_{max}}{a}\frac{2}{3}\pi a^3 = F\,, \tag{B.12}$$

from which

$$P_{max} = \frac{3F}{2\pi a^2}\,. \tag{B.13}$$

The maximal pressure is thus 1.5 the average pressure of the contact area.

Finally, combining the expressions (B.11) and (B.13) gives the final result

$$
\begin{aligned}
a &= \sqrt[3]{\frac{3\pi}{4}F(K_1 + K_2)\frac{R_1 R_2}{R_1 + R_2}} \\
\delta &= \sqrt[3]{\frac{9\pi^2}{16}F^2(K_1 + K_2)^2\frac{(R_1 + R_2)}{R_1 R_2}} \\
P_{max} &= \frac{1}{\pi}\sqrt[3]{\frac{6}{\pi^2}\frac{F}{(K_1 + K_2)^2}\frac{(R_1 + R_2)^2}{R_1^2 R_2^2}}\,.
\end{aligned} \tag{B.14}
$$

Note that by taking R_1 infinite or negative, the equations are valid for a ball on a plane or in a socket. For a ball in a spherical seat, this gives:

$$P_{max} = \frac{1}{\pi}\sqrt[3]{\frac{6}{\pi^2}\frac{F}{(K_1 + K_2)^2}\frac{(R_1 - R_2)^2}{R_1^2 R_2^2}}\,.$$

B.2   Distortion-energy criterion

Although the maximal pressure in the contact area can be calculated, a criteria to evaluate its effect on the material (elastic, plastic deformation or failure) must be defined. In other words, the correlation between the experienced stress and the yielding point or the ultimate tensile strength of the material should be determined. Unfortunately there is at present time no fundamental rationale for such correlation and the use of empirical relationships, which have been widely proved by experiments, is required. One of the most popular is surely the von Mises or distortion-energy criterion, which is described below [76].

Postulate
Yielding will occur when the distortion-energy per unit volume equals the distortion-energy per unit volume in a uniaxial tension specimen stressed to its yield strength.

The strain energy per unit volume is given by

$$U = \frac{1}{2}\sigma_1\epsilon_1 + \frac{1}{2}\sigma_2\epsilon_2 + \frac{1}{2}\sigma_3\epsilon_3 , \qquad (B.15)$$

where σ_i, ϵ_i are the principal stress and strain components. An expression of the strain energy per unit volume in terms of stress only can be obtained by using the stress-strain relationships,

$$\begin{aligned} \epsilon_1 &= \frac{1}{E}(\sigma_1 - \nu\sigma_2 - \nu\sigma_3) \\ \epsilon_2 &= \frac{1}{E}(\sigma_2 - \nu\sigma_1 - \nu\sigma_3) \qquad (B.16) \\ \epsilon_3 &= \frac{1}{E}(\sigma_3 - \nu\sigma_1 - \nu\sigma_2) , \end{aligned}$$

thus giving

$$U = \frac{1}{2E}\left[\sigma_1^2 + \sigma_2^2 + \sigma_3^2 - 2\nu(\sigma_1\sigma_2 + \sigma_2\sigma_3 + \sigma_3\sigma_1)\right] . \qquad (B.17)$$

The principal stress components can be theoretically separated into two different contributions: the hydrostatic and the distortional stresses (Fig.B.3). By definition, the hydrostatic stress is given by

$$\sigma_h = \frac{\sigma_1 + \sigma_2 + \sigma_3}{3} . \qquad (B.18)$$

On one hand, the hydrostatic stresses cause a change only in volume, not in shape. A cube gets bigger in tension and smaller in compression, but remains a cube. On the other hand, distortional stresses act to deform or distort the material element. There is no change in volume, only in shape. These stresses try to elongate or compress the material more in one direction than in another and are responsible for yielding.
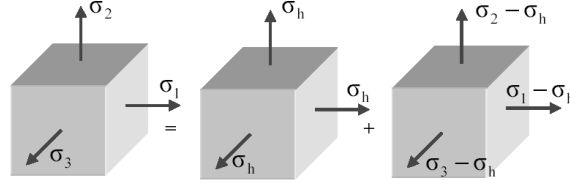
Figure B.3: Hydrostatic and distortional stresses definition

The distortional strain energy is equal to the difference between the total strain energy and the hydrostatic strain energy.

$$
\begin{aligned}
U_d &= U - U_h \\
&= \frac{1}{2E} \left[\sigma_1^2 + \sigma_2^2 + \sigma_3^2 - 2\nu(\sigma_1\sigma_2 + \sigma_2\sigma_3 + \sigma_3\sigma_1) \right] \\
&\quad - \frac{3}{2} \frac{1-2\nu}{E} \left(\frac{\sigma_1 + \sigma_2 + \sigma_3}{3} \right)^2 \\
U_d &= \frac{1+\nu}{3E} [\sigma_1^2 + \sigma_2^2 + \sigma_3^2 - \sigma_1\sigma_2 - \sigma_2\sigma_3 - \sigma_1\sigma_3] \qquad \text{(B.19)}
\end{aligned}
$$

Thus, the distortional strain energy depends only on the effective stress, ususally called the von Mises stress, defined by

$$
\sigma_{eff} = \sqrt{\sigma_1^2 + \sigma_2^2 + \sigma_3^2 - \sigma_1\sigma_2 - \sigma_2\sigma_3 - \sigma_1\sigma_3} \,. \qquad \text{(B.20)}
$$

In a uniaxial tension test ($\sigma_2 = \sigma_3 = 0$), this effective stress is equivalent to the tension stress;

$$
\sigma_{eff} = \sigma_1 \,. \qquad \text{(B.21)}
$$

Therefore, this effective stress is the parameter which should be compared to the tensile strength of the material to determine if yielding may occur or not.

B.3   Conclusion

From the two previous sections, the maximal contact pressure an the effective stress that has to be compared to the tensile strength of material can be computed. However, the link between both parameters still need to be determined. The maximum stresses of two spherical bodies in contact obviously occur in the z axis. These are principal stresses and their expression is

given by [77]

$$\sigma_1 = \sigma_2 = -P_{max} \left[\left(1 - \frac{z}{a} \tan^{-1} \left(\frac{1}{\frac{z}{a}} \right) \right) (1 + \nu) - \frac{1}{2 \left(1 + \left(\frac{z}{a} \right)^2 \right)} \right]$$

$$\sigma_3 = \frac{-P_{max}}{1 + \left(\frac{z}{a} \right)^2}.$$

(B.22)

The corresponding shearing stress are given by

$$\tau_{xy} = \frac{\sigma_1 - \sigma_2}{2} = 0$$

$$\tau_{xz} = \tau_{yz} = \frac{\sigma_1 - \sigma_3}{2} = \frac{\sigma_2 - \sigma_3}{2}.$$

(B.23)

With these expressions, the curve representing the stresses per unit of P_{max} versus the depth in the z axis per unit of radius of contact area a can be drawn (Fig.B.4).
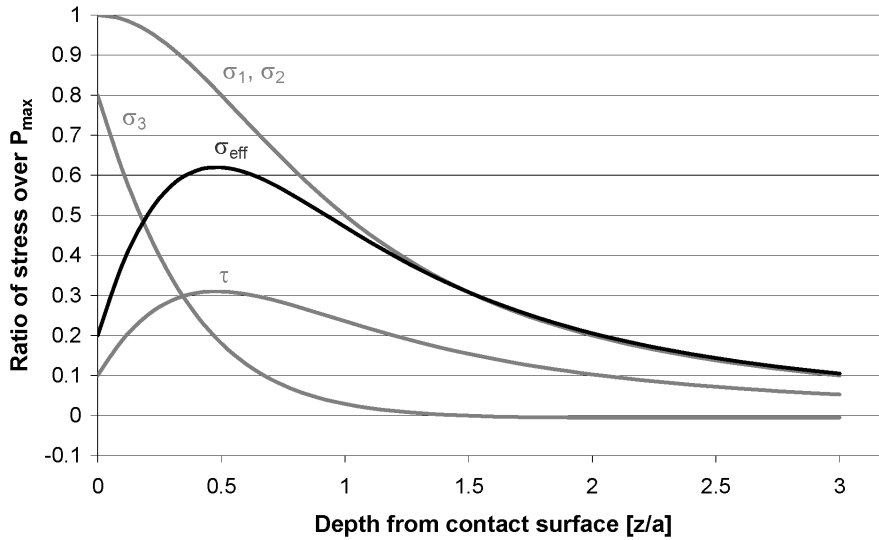

Figure B.4: Principal, von Mises and shearing contact stress

Fig.B.4 shows that the maximal von Mises stress occur just below the surface, at a depth of $0.5a$, and with an amplitude of

$$\sigma_{eff}^{max} = 0.6 P_{max}.$$

(B.24)

Bibliography

[1] Nerlich A.G., Zink A., Szeimies U., Hagedorn H.G., *Ancient Egyptian Prosthesis of the Big Toe*, Lancet, vol. 356, pp. 2176-2179 (2000)

[2] Breasted J.H., *The Edwin Smith Surgical Papyrus*, Chicago: The University of Chicago Press (1930)

[3] Nolte L.P., Ganz R. (Editors), *Computer Assisted Orthopaedic Surgery (CAOS)*, Bern: Hogrefe and Huber Publishers (1999)

[4] Dario P., Carrozza M.C., Marcacci M., D'Attanasio S., Magnami B., Tonet O., Megali G., *A Novel Mechatronic Tool for Computer-Assisted Arthroscopy*, IEEE T Inf Technol B, vol. 4(1), pp. 15-29 (2000)

[5] Allotta B., Belmonte F., Bosio L., Dario P., *Study on a Mechatronic Tool for Drilling in the Osteosynthesis of Long Bones: Tool/Bone Interaction, Modeling and Experiments*, Mechatronics, vol. 6(4), pp. 447-459 (1996)

[6] Klöckner C., Rohlmann A., Bergmann G., *Instrumented Forceps for Measuring Tensile Forces in the Rod of VDS Implant During Correction of Scoliosis*, Biomed Tech, vol. 48(12), pp. 362-364 (2003)

[7] Marieb E.N., *Human Anatomy and Physiology*, 5th Ed., San Francisco: Benjamin Cummings (2001)

[8] Pinskerova V., Iwaki H., Freeman M.A.R., *The Shapes and Relative Movements of the Femur and Tibia at the Knee*, Orthopäde, vol. 29(Suppl.1), pp. S3-S5(2000)

[9] Nordin M., Frankel V.H., *Basic Biomechanics of the Musculoskeletal System*, 2nd Ed., Philadelphia: Lea & Febriger (1989)

[10] Gere J.M., *Mechanics of Material*, 5th SI Ed., Cheltenham: Nelson Thornes (2002)

[11] Gluck T., *Referat über die durch das moderne chirurgische Experiment gewonnenen positiven Resultate, betreffend die Naht und den Ersatz von Defecten höherer Gewebe, sowie über die Verwertung resorbierbarer und lebendiger Tampons in der Chirurgie*, Arch Klin Chir, vol 41, pp. 187-239 (1890)

[12] Ranawat C.S., *History of Total Knee Arthroplasty*, J South Orthop Assoc, vol. 11(4), pp. 218-226 (2002)

[13] Kapandji I.A., *The Physiology of the Joints*, New York: Churchill Livingstone (1976)

[14] Whiteside L.A., *Soft Tissue Balancing*, J Arthroplasty, vol.17(4), Suppl.1, pp. 23-27 (2002)

[15] Insall J., Ranawat C.S., Scott W.N., Walker P., *Total Condylar Knee Replacement: Preliminary Report*, Clin Orthop, vol. 120, pp. 149-154 (1976)

[16] Harner C.D., Vince K.G., Fu F.H., *Techniques in Knee Surgery*, Philadelphia: Lippincott Williams & Wilkins (2001)

[17] Rathjen K.W., *Surgical Treatment. Total Knee Arthroplasty*, Am J Knee Surg, vol. 11(1), pp. 58-63 (1998)

[18] Rand J. A., Trousdale R. T., Ilstrup D. M., Harmsen W. S., *Factors affecting the durability of primary total knee prostheses*, J Bone Joint Surg Am, vol. 85(2), pp. 259-265(2003)

[19] Lotke P.A., Ecker M.L., *Influence of Positioning of Prosthesis in Total Knee Replacement*, J Bone Joint Surg Am, vol. 59(1), pp. 77-79 (1977)

[20] Freeman M.A., Todd R.C., Bamert P., Day W.H., *ICLH Arthroplasty of the Knee: 1968–1977*, J Bone Joint Surg Br, vol. 60-B(3), pp. 339-344 (1978)

[21] Insall J.N., Binazzi R., Soudry M., Mestriner L.A., *Total Knee Arthroplasty*, Clin Orthop, vol. 192, pp.13-22 (1985)

[22] Dorr L.D., Boiardo R.A., *Technical Considerations in Total Knee Arthroplasty*, Clin Orthop, vol. 205, pp. 5-11 (1986)

[23] Moreland J.R., *Mechanisms of Failure in Total Knee Arthroplasty*, Clin Orthop, vol. 226, pp. 49-64 (1988)

[24] Windsor R.E., Scuderi G.R., Moran M.C., Insall J.N., *Mechanisms of Failure of the Femoral and Tibial Components in Total Knee Arthroplasty*, Clin Orthop, vol. 248, pp. 15-19 (1989)

[25] Teeny S.M., Krackow K.A., Hungerford D.S., Jones M., *Primary Total Knee Arthroplasty in Patients with Severe Varus Deformity. A Comparative Study.*, Clin Orthop, vol. 273, pp. 19-31 (1991)

[26] Fehring T.K., Valadie A.L., *Knee Instability after Total Knee Arthroplasty*, Clin Orthop, vol. 299, pp. 157-162 (1994)

[27] Karachalios T., Sarangi P.P., Newman J.H., *Severe Varus and Valgus Deformities Treated by Total Knee Arthroplasty*, J Bone Joint Surg Br, vol. 76(6), pp. 938-942 (1994)

[28] Matsuda S., Miura H., Nagamine R., Urabe K., Harimaya K., Matsunobu T., Iwamoto Y., *Changes in Knee Alignment after Total Knee Arthroplasty*, J Arthroplasty, vol.14(5), pp.566-570 (1999)

[29] Langlotz F., Nolte L.-P., *Computer-Assisted Orthopaedic Surgery: From Theory to the Operating Room*, Tech Orthop, vol. 18, pp. 140-148, 2003.

[30] Jenny J. Y., Boeri C., *Computer-assisted implantation of total knee prostheses: a case-control comparative study with classical instrumentation*, Comp Aided Surg, vol. 6(4), pp. 217-220 (2001)

[31] Kunz M., *Der intraoperative Einsatz von bildfreien, computergestützten Systemen in der Kniechirurgie zur Wiederherstellung der natürlichen Kinematik*, Ph.D. Thesis, Maurice E. Müller-Institut für Biomechanik, University of Bern, Switzerland (2003)

[32] Stulberg S. D., *How accurate is current TKR instrumentation*, Clin Orthop, vol. 416, pp. 177-184 (2003)

[33] Decking R., Markmann Y., Fuchs J., Puhl W., Scharf H.P., *Leg axis after computer-navigated total knee arthroplasty*, J Arthroplasty, vol. 20(3), pp. 282-288 (2005)

[34] Haaker R.G., Stockheim M., Kamp M., Proff G., Breitenfelder J., Ottersbach A., *Computer-assisted navigation increases precision of component placement in total knee arthroplasty*, Clin Orthop, vol. 433, pp. 152-159 (2005)

[35] Attfield S. F., Warren-Forward M. , Wilton T., Sambatakakis A., *Measurement of soft tissue imbalance in total knee arthroplasty using electronic instrumentation*, Med Eng Phys, vol. 16(6), pp. 501-505 (1994)

[36] Wallace A. L., Harris M. L., Walsch W. R., Bruce W. J., *Intraoperative assessment of tibiofemoral contact stresses in total knee arthroplasty*, J Arthroplasty, vol. 13(8), pp. 923-927 (1996)

[37] Wasielewski R.C., Galat D.D., Komistek R.D., *An intraoperative pressure-measuring device used in total knee arthroplasties and its kinematics correlations*, Clin Orthop, vol. 427, pp. 171-178 (2004)

[38] Wasielewski R.C., Galat D.D., Komistek R.D., *Correlation of compartment pressure data from an intraoperative sensing device with postoperative fluoroscopic kinematic results in TKA patients*, J Biomech, vol. 38(2), pp. 333-339 (2005)

[39] Takahashi T., Wada Y., Yamamoto H., *Soft-tissue balancing with pressure distribution during total knee arthroplasty*, J Bone Joint Surg, vol. 79(2), pp. 235-239 (1997)

[40] D'Lima D. D., Patil S., Steklov N., Colwell C. W., *In vitro measurement of dynamic soft-tissue balance during total knee arthroplasty with an instrumented tibial prosthesis*, in Trans. 50th annual meeting of Orthopaedic Research Society, San Francisco, pp. 301 (2004)

[41] Morris B. A., D'Lima D. D., Slamin J., Kovacevic N., Arms S. W., Townsend C. P., Colwell C. W., *E-Knee: evolution of the electronic knee prosthesis*, J Bone Joint Surg Am, vol. 83 Suppl 2(Pt 1), pp. 62-66(2001)

[42] Kauffman K. R., Kovacevic N., Irby S. E., Colwell C. W., *Instrumented implant for measuring tibiofemoral forces*, J Biomech, vol. 29(5), pp. 667-671 (1996)

[43] Davy D. T., Kotzar G., Berilla J., Brown R.H., *Telemetrized orthopaedic implant work at Case Western Reserve University*, in Implantable Telemetry in Orthopaedics, Bergmann G., Graichen F., Rohlmann A., Ed. Berlin: Forschungsvermittlung der Freien Univ., pp. 205-219 (1990)

[44] Winemaker M.J., *Perfect balance in total knee arthroplasty: the elusive compromise*, J Arthroplasty, vol. 17(1), pp. 2-10 (2002)

[45] Ritschl P., Machacek F. Jr., Fuiko R., *Computer assisted ligament balancing in TKR using the Galileo system*, 3rd Annual Meeting of CAOS-International Proceedings, pp. 304-305, June 2003

[46] Marmignon C., Leimnei A., Cinquin P., *Robotized distraction device for knee replacement*, Proceedings of Computer Assisted Radiology and Surgery, pp. 638-643 (2004)

[47] Kauert D., *A wireless telemetric system in total knee arthropplasty*, Diploma Thesis, Division of Microtechnology, University of Applied Sciences, Biel, Switzerland (2004)

[48] Grimaldi C., Ryser P., Straessler S., *Gauge factor enhancement driven by heterogeneity in thick-film resistors*, J Appl Phys, vol. 90(1), pp. 322-27 (2001)

[49] Grimaldi C., Ryser P., Stässler S., *Piezoresistive anisotropy of thick-film resistors*, J Eur Ceram Soc, vol. 24(6), pp. 1893-96 (1992)

[50] Prudenziati M., Morten B., *The state of the art in thick-film sensors*, Microelectr J , vol. 23, pp. 133-41 (1992)

[51] White N.M., Turner J.D., *Thick-film sensors: past, present and future*, Meas Sci Technol, vol. 8, pp. 1-20 (1997)

[52] White N.M., *Study of the piezoresistive effect in thick-film resistors and its application to load transduction*, Ph.D. thesis, Faculty of Engineering & Applied Science, University of Southampton, United Kingdom (1988)

[53] White N.M., Brignell J.E., *A planar thick-film load cell*, Sensor Actuator A, vol. 26, pp. 313-19 (1991)

[54] Arshak K.I., Ansari F., Collins D., *Analysis of thick film strain resistors on stainless steel and ceramic substrates*, Int J Electronics, vol. 76(2), pp. 365-376 (1994)

[55] Fraigi L., Lupi D., Malatto L., *A thick-film pressure for cars propelled by natural gas*, Sensor Actuator A, vol. 42, pp. 439-41 (1994)

[56] Jacq C., Maeder Th., Ryser P., *High-strain response of piezoresistive thick-film resistors on titanium alloy substrates*, J Eur Ceram Soc, Vol. 24, pp. 1897-1900 (2004)

[57] Hrovat M., Smetana W., Belavic D., Homolka H., Reicher R., Zarnik M.S., *An investigation of thick-film materials on steel substrates for possible sensor applications*, Proceedings, IMAPS Poland, Polanczyk, Poland, pp. 199-202 (2001)

[58] Hrovat M., Belavič D., Benčan A., Bernard J., Holc J., Cilenšek J., Smetana W., Homolkac H., Reicher R., Golonka L., Dziedzic A., Kita J., *Thick-film resistors on various substrates as sensing elements for strain-gauge applications*, Sensor Actuator A, Vol. 107, pp. 261-72 (2003)

[59] Maeder T., Grimaldi C., Ryser P., *Properties of thick-film resistors on dielectric and metal substrates for piezoresistive sensors*, Proceedings, IMAPS Poland, Podlesice, pp. 219-222 (2003)

[60] Dürselen L., Claes L., Kiefer H., *The influence of muscle forces and external loads on cruciate ligament strain*, The American Journal of Sports Medicine, Vol. 19, pp. 381-383 (1995)

[61] Lüring C., Hüfner T., Kendoff D., Perlick L., Bäthis H., Grifka J., *Influence of everted and subluxed patella in ligament balancing*, Proceedings, CAOS-International, Helsinki, Finland, pp. 289-292 (2005)

[62] Röstlund T., Carlsson L., Albrektsson B., Albrektsson T., *Morphometrical studies of human femoral condyles*, Journal of Biomedical Engineering, Vol. 11, pp. 442-448 (1989)

[63] Krackow K.A., Mihalko W.M., *The effect of medial release on flexion and extension gaps in cadaveric knees*, The American Journal of Knee Surgery, Vol. 12, pp. 222-228 (1999)

[64] Mihalko W.M., Whiteside L.A., Krackow K.A., *Comparison of ligament-balancing techniques during total knee arthroplasty*, The Journal of Bone and Joint Surgery, Vol. 85-A (Suppl. 4), pp. 132-135 (2003)

[65] Baldini A., Scuderi G.R., Aglietti P., Chalnick D., Insall J.N., *Flexion-extension gap changes during total knee arthroplasty*, The Journal of Knee Surgery, Vol. 17(2), pp. 69-72 (2004)

[66] International Electrotechnical Commission, *International standard on medical electrical equipment*, IEC 60601-1, Geneva, Switzerland

[67] Kozinn S.C., Scott R., *Current concepts review: unicondylar knee arthroplasty*, J Bone JOint Surg Am, vol. 71-A, pp. 145-50 (1989)

[68] Murray D.W., Goodfellow J.W., O'Connor J.J., *The Oxford medial unicompartmental arthroplasty: a ten-year survival study*, J Bone Joint Surg Br, vol. 80-B(6), pp. 983-9 (1998)

[69] Berger R.A., Nedeff D.D., Barden R.M., Sheinkop M.M., Jacobs J.J., Rosenberg A.G., Galante J.O., *Unicompartmental knee arthroplasty: clinical experience at 6- to 10-year followup*, Clin Orthop, vol. 367, pp. 50-60 (1999)

[70] Vince K.G., Cyran L.T., *Unicompartmental knee arthroplasty: New indications, more complications?*, J Arthroplasty, vol. 19(4) Suppl 1, pp. 9-16 (2004)

[71] Thornhill T.S., *Unicompartmental knee arthroplasty*, Clin Orthop, vol. 205, pp. 121-31 (1986)

[72] Goodfellow J.W., Kershaw C.J., D'a Benson M.K., O'Connor J.J., *The Oxford knee for unicompartmental osteoarthritis*, J Bone Joint Surg Br, vol. 70-B(5), pp. 692-701, (1988)

[73] Emerson R.H. Jr, Head W.C., Peters P.C. Jr, *Soft-tissue balance and alignement in medial unicompartmental knee arthroplasty*, J Bone Joint Surg Br, vol. 74-B(6), pp. 807-10 (1992)

[74] Timoshenko S.P., Goodier J.N., *Theory of Elasticity*, Auckland: McGraw Hill (1988)

[75] Whitehouse D.J., *Handbook of Surface Metrology*, Bristol: Institute of Physics Publishing (1994)

[76] Dieter G.E., *Mechanical Metallurgy*, London: McGraw Hill (1988)

[77] Shigley J.E., Mischke C.R., *Mechanical Engineering Design*, 5th Ed., New York: McGraw Hill (1989)

Curriculum Vitae

Name	DENIS CROTTET
Date of birth	12th August 1976, Fribourg, Switzerland
Nationality	Swiss
Marital status	Married

EDUCATION

2001-2005   **Ph.D. in Biomedical Engineering & Microtechnique**
Laboratoire de Systèmes Robotiques, EPF Lausanne

1996-2001   **M.Sc. in Physics**
Department of Physics, EPF Lausanne

1992-1996   **High school, scientific section**
Collège Sainte-Croix, Fribourg

PROFESSIONNAL EXPERIENCES/PROJECTS

2001-2005   **MEM Research Center for Orthopaedic Surgery**, Bern
"A FORCE-SENSING DEVICE FOR TKA": Development of a force-sensing device to help the surgeon balance soft-tissues during total knee arthroplasty.

2000-2001   **Institut de Physique Expérimentale**, EPF Lausanne
"ANTENNAE COMPATIBLE FOR ENDOVASCULAR MRI": Development of an endovascular antenna able to provide high resolution magnetic resonance images for diagnosis of vascular diseases.

1999-2000   **CFG Microelectronics**, Morges
Summer internship followed by a part-time work
"ORGANIC LIGHT EMITTING DIODES": Identification of the lifetime-limiting parameters of organic light emitting diodes.

JOURNAL ARTICLES

1. Crottet D., Kowal J., Sarfert S.A., Maeder T., Bleuler H., Nolte L.P., Dürselen L., *Ligament Balancing in TKA: Evaluation of a Force-Sensing Device and the Influence of Patellar Eversion and Ligament Release*, Journal of Biomechanics, submitted

2. Crottet D., Maeder T., Fritschy D., Bleuler H., Nolte L.P., Pappas I.P., *Development of a Force Amplitude- and Location-Sensing Device Designed to Improve the Ligament Balancing Procedure in TKA*, IEEE Transactions on Biomedical Engineering, vol. 52(9), pp. 1609-1611, September 2005

3. Crottet D., Meuli R., Wicky S., van der Klink J.J., *Reciprocity and Sensitivity of Opposed-Solenoid Endovascular MRI Probes*, Journal of Magnetic Resonance, vol. 159, pp. 219-225, December 2002

CONFERENCE ABSTRACTS

1. Crottet D., Kowal J., Sarfert S.A., Bleuler H., Nolte L.P., Dürselen L., *In-Situ Evaluation of a Force-Measuring Device for Assistance in Ligament Balancing during Knee Arthroplasty*, 5th Annual Meeting of the International Society for Computer Aided Orthopaedic Surgery, 147-8, Helsinki, Finland, June 2005

2. Crottet D., Maeder T., Sarfert S., Fritschy D., Bleuler H., Nolte L.P., Pappas I.P., *In-vitro Evaluation of a Force-Sensing Device for Ligament Balancing in TKA*, 51st Annual Meeting of the Orthopaedic Research Society, Washington, USA, February 2005

3. Crottet D., Maeder T., Fritschy D., Bleuler H., Nolte L.P., Pappas I.P., *In-vitro Validation of a Device Measuring the Tibio-femoral Contact Forces and Moments for Assistance during Ligament Balancing in TKA*, 17th Annual Symposium of the International Society for Technology in Arthroplasty, Rome, Italy, September 2004

4. Crottet D., Maeder T., Fritschy D., Bleuler H., Nolte L.P., Pappas I.P., *A Force-Sensing Device for Ligament Balancing in Total Knee Arthroplasty*, 4th Annual Meeting of the International Society for Computer Aided Orthopaedic Surgery, 147-8, Chicago, USA, June 2004

PATENT

1. D. Crottet, I.P. Pappas, T. Maeder, C. Jacq, H. Bleuler, *Device for Measuring Tibio-Femoral Force Amplitudes and Force Locations in Total Knee Arthroplasty*, international patent application, PCT/CH04/000361, June 2004.

AWARDS

1. 2005 Research Award of the Swiss Society of Biomedical Engineering

2. 2004 Best Poster Award of the 4th Annual Meeting of the International Society for Computer Aided Orthopaedic Surgery